MENDELOVA UNIVERZITA V BRNĚ
AGRONOMICKÁ FAKULTA

DISERTAČNÍ PRÁCE

BRNO 2017 **STANISLAV JURÁŇ**

Mendel University in Brno
Faculty of Agronomy
Department of Plant Biology

Ecophysiological control of BVOC emissions in ozone polluted forest ecosystems

Ph.D. thesis

Supervisor: *Written by:*
prof. RNDr. Ing. Michal V. Marek, DrSc.   Ing. Stanislav Juráň

Scientific advisor:
doc. Mgr. Otmar Urban, Ph.D.

Consultants:
Dr. Silvano Fares, Ph.D.
doc. RNDr. Pavel Cudlín, CSc.
Dr. Elena Paoletti, Ph.D.

Brno 2017

Čestné prohlášení

Prohlašuji, že jsem práci Ecophysiological control of BVOC emissions in ozone polluted forest ecosystems vypracoval samostatně a veškeré použité prameny a informace uvádím v seznamu použité literatury. Souhlasím, aby moje práce byla zveřejněna v souladu s § 47b zákona č. 111/1998 Sb., o vysokých školách ve znění pozdějších předpisů a v souladu s platnou *Směrnicí o zveřejňování vysokoškolských závěrečných prací.*

Jsem si vědom, že se na moji práci vztahuje zákon č. 121/2000 Sb., autorský zákon, a že Mendelova univerzita v Brně má právo na uzavření licenční smlouvy a užití této práce jako školního díla podle § 60 odst. 1 autorského zákona.

Dále se zavazuji, že před sepsáním licenční smlouvy o využití díla jinou osobou (subjektem) si vyžádám písemné stanovisko univerzity, že předmětná licenční smlouva není v rozporu s oprávněnými zájmy univerzity, a zavazuji se uhradit případný příspěvek na úhradu nákladů spojených se vznikem díla, a to až do jejich skutečné výše.

V Brně dne:……………………..

………………………………………………..
podpis

ACKNOWLEDGEMENT

TABLE OF CONTENTS

Abstrakt

Biogenní volatilní organické látky (BVOC) jsou nedílnou součástí atmosféry a významně se podílejí na interakcích mezi ní a biosférou. Působením různých stresorů dochází v rostlinných pletivech k vyšší produkci těchto látek, které mají řadu ochranných funkcí. Vyšší emise BVOC však mohou zároveň vést k tvorbě troposférického ozonu a to zejména při zvýšené koncentraci oxidů dusíku a zvýšené intenzitě ultrafialové radiace. BVOC mohou rovněž přispívat k tvorbě sekundárního organického aerosolu. Troposférický ozon působí jako silné oxidační činidlo a rozkládá BVOC na odlišné produkty. Vlivem globální změny se zvyšuje míra a četnost výskytu stresorů působících na lesní porosty, což vede k vyšším emisím BVOC. Po chemické stránce jsou BVOC velmi heterogenní skupinou. Nejvýznamnější sloučeniny představují monoterpeny a isopren. Cílem práce bylo (1) zvládnutí metod detekce BVOC v polních podmínkách, (2) provedení polních experimentů na ekosystémových stanicích Castelporziano u Říma, Itálie s dominujícím porostem dubu cesmínového a Bílý Kříž, Česká republika s porostem smrku ztepilého a (3) kvantifikovat toky BVOC za různých synoptických situací a s ohledem na přítomnost troposférického ozonu. K měření BVOC byla použita analytická technika „proton-transfer-reaction" spojená s hmotnostním spektrometrem typu „time-of-flight" (PTR-TOF-MS) a kvadrupolem (PTR-MS). K získání denních a sezónních toků různých monoterpenů byl využit Inverzní Lagrangianův Transportní Model. Bylo prokázáno, že rozdílný základní emisní faktor pro slunné a stinné jehlice vede ke zpřesnění modelovaných emisí modelem MEGAN (Model of Emissions of Gases and Aerosols from Nature). Byla kvantifikována ztráta uhlíku díky emisím BVOC oproti GPP (gross primary production) ve výši až 1,5 %.

Klíčová slova

PTR-MS, modelování, toky, smrk ztepilý, dub cesmínový, monoterpeny, isopren, ozon

Abstract

Biogenic volatile organic compounds (BVOCs) are important constituents of the atmosphere and substantially contribute to biosphere-atmosphere interactions. Occurrence of various stressors induces their production in plant tissue, which might be plant-protective. Higher BVOC emissions might lead to tropospheric ozone production under the presence of nitrogen oxides and high intensities of ultraviolet radiation. BVOCs contribute to secondary organic aerosol formation. Tropospheric ozone as a powerful oxidizing agent cleaves BVOCs into other compounds. Frequency and severity of stressors occurrence is enhanced under the climate change and thus BVOCs are emitted in higher quantities. Chemically are BVOCs heterogeneous group with most important compounds being monoterpenes and isoprene. The aim of the thesis was (1) to manage BVOC detection methods in field conditions, (2) to conduct field experiments at Castelporziano experimental station nearby Rome, Italy with dominating Holm oak forest and Bílý Kříž, Czech Republic with dominating Norway spruce forest, and (3) to quantify BVOC fluxes under the presence of tropospheric ozone. Spectrometers with „time-of-flight" (PTR-TOF-MS) and quadrupole (PTR-MS) have been used for measurements. To get fluxes of various monoterpenes, Inverse Lagrangian Transport Model has been deployed. It was proven, that distinguished basal emission factor for sun and shaded needles leads for better prediction by MEGAN model. Carbon loss due to BVOC emissions was quantified to be up to 1.5 % of GPP.

Key words

PTR-MS, modelling, fluxes, Norway spruce, Holm oak, monoterpenes, isoprene, ozone

Souhrn

Biogenní volatilní organické látky (BVOC) jsou nedílnou součástí atmosféry a významně se podílejí na interakcích mezi ní a biosférou. Působením různých stresorů dochází v rostlinných pletivech k vyšší produkci těchto látek, které mají řadu ochranných funkcí. Vyšší emise BVOC však mohou zároveň vést k tvorbě troposférického ozonu a to zejména při zvýšené koncentraci oxidů dusíku a zvýšené intenzitě ultrafialové radiace. BVOC mohou přispívat k tvorbě sekundárního organického aerosolu. Troposférický ozon působí jako silné oxidační činidlo a rozkládá BVOC na odlišné produkty. Vlivem globální změny se zvyšuje míra a četnost výskytu stresorů působících na lesní porosty, což vede k vyšším emisím BVOC. Po chemické stránce jsou BVOC velmi heterogenní skupinou s nejvýznamnějšími sloučeninami monoterpeny a isoprenem. Cílem práce je (1) zvládnutí metod detekce BVOC v polních podmínkách, (2) provedení polních experimentů na ekosystémových stanicích Bílý Kříž, Česká republika s porostem smrku ztepilého a Castelporziano u Říma, Itálie s dominujícím porostem dubu cesmínového, (3) vymodelovat toky BVOC pomocí Inverzního Lagrangianova Transportního Modelu a modelu MEGAN a (4) kvantifikovat toky troposférického ozonu v porostu na Bílém Kříži. K měření BVOC byla použita technika vířivé kovariance spolu s technikou „proton-transfer-reaction" spojená s hmotnostním spektrometrem typu „time-of-flight" (PTR-TOF-MS) či kvadrupolem (PTR-MS). K získání denních toků různých monoterpenů a ozonu byl využit Inverzní Lagrangianův Transportní Model (ILTM). K získání sezonních toků monoterpenů model Model of Emissions of Gases and Aerosols from Nature (MEGAN).

Na Bílém Kříži byly pozorovány nejvyšší toky monoterpenů a isoprenu spolu s 2-methyl-3-buten-2-olem (MBO). Tok MBO byl identifikován v porostu smrku ztepilého vůbec poprvé, což naznačuje výskyt různých chemotypů smrku ztepilého. Toky oxidovaných BVOC vykazovaly vysoký obousměrný tok. Překvapením byl vysoký tok toluenu a benzenu, který se akumuloval během smrskávající se hraniční vrstvy atmosféry a při východu slunce byl znovu transportován z lesa. Měřením a pomocí HYSPLIT modelu byl identifikován potenciální zdroj toluenu nacházející se v Ostravě a přilehlé části Polska v okolí Katowic, kde se vyskytuje těžký metalurgický průmysl. Navíc v odpoledních hodinách byl pozorován malý tok toluenu, který by mohl pocházet primárně z lesa.

Byla vypočítána ztráta uhlíku ve formě BVOC oproti množství uhlíku fixovanému fotosyntézou, která dosahovala maximálních hodnot 1,5 %. Ztrátě dominovaly monoterpeny a methanol. Díky PCA analýze byly zjištěny závislosti toků různých monoterpenů na přírodních parametrech. Většina monoterpenů byla závislá na záření dopadajícího na povrch půdy, kromě Δ-3-karenu, který se choval opačným způsobem, což ukazuje na vysoký vliv rozkládajícího se jehličí na celkový tok.

Model MEGAN byl parametrizován pomocí změřených základních emisních faktorů, kdy byly použity pro slunné a stinné jehlice zvlášť, či dohromady jen pro slunné jehlice. Porovnáním měřených a modelovaných toků bylo zjištěno, že rozdělením základních emisních faktorů na slunné a stinné jehlice vykázal model větší přesnost. Ty byly použity v modelu MEGAN pro vymodelování toků monoterpenů pro pět po sobě jdoucích roků, kde byla pozorována velmi vysoká míra variability toků. Nejvyšší vliv na velikost toků měly vysoké teploty vzduchu v létě. Vyšší teploty v zimě měly jen okrajový vliv díky exponenciální závislosti toků na teplotě.

Koncentrační profily ozonu pro různé podmínky počasí, modelované toky ozonu pomocí ILTM modelu a koncentrační závislost NO a NO_2 na ozonu byly měřeny a modelovány. Koncentrace ozonu byly nejvyšší v létě a nejnižší v zimě. Noční toky ozonu do ekosystému vykazovaly stomatální i nestomatální depozici.

V Castelporzianu u Říma proběhly dvě polní kampaně pokrývající odlišné klimatické periody. Byla použita technika PTR-MS s a bez vířivé kovariance během léta a v zimě, respektive. Les dubu cesmínového se ukázal být především emitorem monoterpenů; isopren byl pozorován v mnohem menším měřítku. Byl otestován ILTM model s relativně dobrou korelací s měřenými toky v případě monoterpenů.

Díky blízkosti mezinárodního letiště Leonardo da Vinci a města Řím byly pozorovány vysoké koncentrace benzenu a toluenu pocházející z těchto směrů. Spočítáním poměru toluenu k benzenu byl zjištěn jejich původ v procesech spalování, pouze malá část pocházela z emisí z přečerpávání pohonných hmot na letišti.

1 INTRODUCTION

Discoveries of a blue haze above unpolluted forests by Fritz Went in 1960 have compelled researchers to ask what are the plants emitting, how much is being emitted and what is the impact of those emissions? Later a burden of tropospheric ozone pollution above suburban areas has been observed (Rasmussen 1972; Chameides et al., 1988). Such important questions formed a highly interdisciplinary field of research: Biogenic Volatile Organic Compounds (BVOCs) in biosphere-atmosphere interactions. Since the time when BVOCs were first identified, some of them, such as terpenes, were possible to detect with its own smell. An era of not-yet-ended modelling and quantification of BVOCs to various inventories has started. Worldwide emissions are currently estimated to be 1 Pg C yr^{-1} (Guenther et al. 2012). Most of the research is focused on C5 volatile hydrocarbon – isoprene and it sources, distribution among plant taxa followed by emission algorithms. Nowadays it is known that multiple BVOCs are contributing to a very complex mixture in the chemosphere and form atmospheric dynamics. By its oxidation and condensation, a secondary organic aerosol is formed with a subsequent cloud condensation nuclei formation influencing the climate and solar radiation balance (Kulmala et al., 2004).

Trees are traditionally thought to be the highest emitters due to their abundance and a presence of highly constitutively emitting species. Apart from this, a large group of species emits BVOCs by presence of biotic and abiotic stressors, suggesting strong biological control over the emission spectra. Biosynthesis of BVOCs requires a lot of energy and leads to a carbon loss. On the other hand, it enables enhanced thermotolerance (Sharkey and Singsaas, 1995) and increased resistance of plants to atmospheric oxidants (Loreto et al., 2001). In addition, BVOCs are responsible for biotic stress signalling and attracting of pollinators leading to increased yields. Furthermore, molecular mechanisms and biochemical pathways of synthesis/degradation of some BVOCs have been identified including isoprene and terpene synthases and shikimate biochemical pathway, which produces biogenic benzenoids (Misztal et al., 2015).

Due to the rapid development of cutting-edge sensors, such as proton-transfer-reaction mass spectrometers coupled with the eddy covariance technique, flux measurements of the whole spectra of BVOCs can be done at ecosystem level. Those measurements can be up-scaled by models, which are verified back by flux and cuvette measurements, or from the top by large-scale measurements derived from satellites. That state-of-the-art information is applied by policy professionals in order to prevent tropospheric ozone formation and secure human welfare and health. The aims of this thesis are to find out and quantify the amount of VOC emitted by two distinct ecosystems: Norway spruce forest (I) at Bílý Kříž, Czech Republic and Holm oak forest (II) at Castelporziano, Italy, which are known to be highly polluted by tropospheric ozone. Next, models are applied to test whether basal emission factors used separately for sun and shaded leaves or only for sun leaves fit measured data better with regards to monoterpenes. The hypothesis that both experimental forests are influenced by anthropogenic volatile organic compounds (AVOCs) is tested and various sources are identified. To get VOC fluxes, various approaches are utilized, including the eddy covariance technique and Inverse Lagrangian Transport Model.

2 LITERARY OVERVIEW

2.1 Sources of volatile organic compounds

Volatile organic compounds (VOCs) emitted by plants and animals are called biogenic (BVOCs), whereas those coming from anthropogenic sources are called anthropogenic volatile organic compounds (AVOCs). Both, VOCs and AVOCs affect the physical and chemical properties of the atmosphere. Global estimates of BVOCs production from plants range between 1 000 and 1 500 Tg C yr^{-1} (Guenther et al., 2012). However, the advanced model MEGAN v. 2.1 (Model of Emissions of Gases and Aerosols from Nature) combined with Modern-Era Retrospective Analysis for Research and Applications estimated a global BVOC value of just 760 Tg C yr^{-1}, consisting of 70% isoprene, 11% monoterpenes, 6% methanol, 3% acetone, 2.5% sesquiterpenes, and other BVOCs less than 2% (Sindelarova et al., 2014). The main sources of BVOC emissions are plants, in particular trees, which emit different compositions of BVOCs. BVOC emissions differ among species as well as among different annual periods. Plant emissions are usually higher in stress then under physiologically friendly conditions (Steinbrecher et al., 2009). BVOCs contribute to the formation of tropospheric ozone in the presence of high NOx (NO + NO_2) concentration and high radiation intensities resulting in a substantial damage to terrestrial ecosystems (Paoletti et al., 2007).

BVOCs production can be constitutive, which means, that the synthesis and emission are continuous − genetically given, although emission rates are oscillating. On the other hand, emissions and BVOCs production can be induced by various factors such as light and temperature, which are the most common stressors occurring in forest ecosystems. Other stresses inducing emission are mechanical wounding caused by wind or damage of cells caused by pollutants, pathogens or herbivores (Arneth and Niinemets, 2010). After BVOCs are released, they could be oxidized by ozone, could be cleaved via radical reactions, could react with NOx, and could react among each other. I will focus on reaction with ozone and OH radical, since those two are dominating the VOC removal. Their lifetime in the

atmosphere is therefore limited, which makes it very difficult to accurately estimate their real concentrations, fluxes and bi-directional exchanges (Atkinson a Aschmann, 1993; Atkinson 2000). Therefore, deeper analyses are necessary in order to understand the whole exchange and reactions in the specific case studies. In order to estimate total BVOC emission on the global scale, correct modelling of these fluxes is necessary.

BVOCs emissions are very important especially in urban environments, where they react with the broad range of compounds written above and can form secondary organic aerosols (SOA). Great interest is given on Mediterranean areas, where during summer high temperatures occur. These high temperatures, together with the scarce precipitation, cause high rates of BVOC and ozone emissions and formations in Mediterranean forests. In urban areas they react with AVOCs that originate from various sources like fossil fuel combustion and transport, storage processes, and an application of adhesives, paints, protective coatings and solvents (e.g. Watson et al., 1991; Wei et al., 2010).

Many measurements have shown that monoterpenes and isoprene are major emitted compounds. In past decades scientific research has been mainly focused on the tropical zone and the Mediterranean, contrary to the temperate zone, where knowledge is relatively scarce. In urban and sub-urban areas of the Mediterranean, a high risk of tropospheric ozone formation occurs due to high temperature, high radiation and high NOx together with high BVOC emissions. Therefore, this work is focused mainly on a temperate Norway spruce forest (I) and Mediterranean sub-urban Holm oak forest (II). For a better understanding of emission potentials, the MEGAN model was applied, although models generally suffer from many uncertainties (Helmig et al., 1999).

2.2 Terpenes

Terpenes are secondary metabolites, which are defined as bioactive plant compounds with a restrictive occurrence in taxonomic groups and are not essential for cells or organisms to live, but provide the survival of the organism in the ecosystem (Verpoorte and Alfermann 2000). Terpenes are derived from isoprenoid biosynthetic pathways and are classified according to the number of C5 blocks: hemiterpenes (C5), monoterpenes (C10), homoterpenes (C11, C16), sesquiterpenes (C15), diterpenes (C20), triterpenes/steroids (C30) and tetraterpenes/carotenoids (C40). Only terpenes with a C-chain shorter than 15C are volatile.

More than 1 700 BVOCs were described, emitted by 90 different plant families (Knudsen and Gershenzon, 2006). Isoprene and terpenes are the most common and most important volatiles emitted by plants, since their emissions into the atmosphere substantially contribute to atmospheric chemistry and global climate (Peñuelas and Staudt, 2010).

Isoprene can be synthetized in plants by two independent biochemical pathways, which synthetize isopentenyl diphosphate or its isomer dimethylallyl diphosphate. One is the conventional mevalonate pathway in cytosol and perhaps in peroxisomes as well (Sapir-Mir et al., 2008) and in membranes of endoplasmatic reticulum (Vranová et al., 2012). The pathway starts with two acetyl-coenzymes A and undergoes other biochemical steps to form mevalonate and finally isopentenyl diphosphate. A non-mevalonate pathway, also called the 2-C-methyl-D-erythritol-4-phosphate pathway (MEP), occurs in plastids uses pyruvate and glyceraldehyde-3-fosfate to form 1-deoxy-D-xylulose-5-phosphate. Other steps are various types of erythritols, from which 1-hydroxy-2-methyl-2-butenyl-4-diphosphate is formed as a step between the isopentenyl diphosphate. Two subsequent steps under the control of two enzymes are needed to form isopentenyl diphosphate and finally after isomerisation to dimethylallyl diphosphate, from which head to tail condensation isoprene is formed. In higher plants, mevalonate pathways synthetize sterols and terpenes are formed mostly in plastids via MEP (Eisenreich et al., 2001). Compartmental separation is not absolute; at least one of the intermediates can be transferred to other pathways (Thiel

and Adam, 2002). Complementarity between these two pathways has been observed in the formation of isoprenoid units for sesquiterpene synthesis in *Matricaria recutita* (Adam and Zapp, 1998).

2.2.1 Isoprene

Isoprene is the most abundant terpene, since its emissions are the largest world-wide. Chemically it is 2-methyl-1,3-butadiene with conjugated double bonds, that are responsible for the high reactivity of the molecule. The ability to emit isoprene is wide-spread among different plant species; mosses (Hanson et al., 1999), ferns (Tingey et al., 1987), gymnosperms and angiosperms have exhibited this ability. All of them have families, which emit and do not. Among angiosperms and gymnosperms, the ability to emit has been evolved phylogenetically independently multiple times (Harley et al., 1999) as a response to environmental constrain. Till now, the phylogeny of isoprene emissions is still not clear. More than 1 200 plant species spread all over the globe emit isoprene, as reported by Hewitt et al. (2016) in the Lancaster University database available at http://www.es.lancs.ac.uk/cnhgroup/iso-emissions.pdf. However, some conclusions could be done. Only C3 plants emit isoprene in considerable amounts, while C4 and CAM (C*rassulacean* acid metabolism) plants do not have this ability. Only perennial plants emit isoprene, annual do not. Such behaviour was found in both dicotyledon and monocotyledon plants, if they have the annual and perennial families. Emissions are found in deciduous perennials rather than in evergreen perennials of temperate regions.

Emissions are found especially in fast-growing plants, such as willows, poplars or reeds (*Arundo donax*) in both dicots and monocots (Loreto et al., 2014). A nice example are oaks, where *Quercus rubra* and *Q. robur*, more hygrophilous oaks, emit isoprene in great amounts, whereas slow-growing oaks *Q. ilex* or *Q. suber* do not emit isoprene in great amounts, but rather monoterpenes (Dani et al., 2014).

Isoprene strongly impacts atmospheric chemistry, since it reacts rapidly with the main oxidative compound – OH radical, which is leading to the formation of highly reactive products (Atkinson 2000).

2.2.1.1 Temperature and light dependence

According to Guenther et al. (1993), isoprene synthesis is considered as a light dependent; although some exceptions can be found. Onset of isoprene emission per unit leaf area (hereafter referred as emission) from *Q. pubescens* can be driven by temperature, while evening emission decline can be correlated with the intensity of photosynthetically active radiation (PAR). In between, uncoupling of temperature and light was observed with emission decline in the early afternoon at temperature stress and stabile light. Moreover, isoprene emissions are increasing exponentially with net CO_2 assimilation (Genard-Zielinski et al., 2015). Discrepancy during the drought period between measured fluxes of isoprene and fluxes predicted with the MEGAN model occurred at a forest dominated by oaks in the USA, suggesting that not only light intensity controls the isoprene emissions. During non-stressed conditions, correlation between PAR intensity and isoprene emission was observed (Potosnak et al., 2014).

2.2.1.2 Oxidation of isoprene by OH radicals

Isoprene as a conjugated diene is highly reactive, which results in a short atmospheric lifetime. Isoprene is cleaved by various oxidants, from which the highest oxidation activity evince OH radical, that is formed mainly by ozone photolysis and the reaction of the resulting excited oxygen with water vapour. The lifetime of isoprene is limited to approximately 1.7 h (Karl et al., 2006). The impact of isoprene on atmospheric chemistry is important due to a large abundancy and presence of other oxidative compounds in the atmosphere. Firstly, OH radical attacks isoprene and forms the first generation of stable oxidation products. At this point other isoprene oxidative compounds are not involved. Methyl vinyl ketone (MVK), methacrolein (MACR) and formaldehyde (CH_2O) are formed in the presence of a sufficient amount of NO_x (Miyoshi et al., 1994). Another two minor products were detected in a reaction chamber by a proton-transfer-reaction-mass-spectrometer with time of flight (PTR-TOF-MS): 3-methylfuran and summary formula C_5H_8O, which might be attributed to 2-methylbut-3-enal. Photolysis and reaction of the first generation products are not significant during the first hour of isoprene oxidation by OH radicals (Brégonzio-Rozier et al., 2015).

Higher generation products, as a result of continuous flow of OH radicals, were formed consequently. Among these compounds, methylglyoxal, glycoladehyde, hydroxyacetone, peroxyacetyl nitrate and peroxymethacryloyl nitrate dominated. By adding OH to one of the isoprene double bonds, unsaturated C5 oxidation products can be formed. Additionally, the oxidation of hydroxyalkyl radical occurs (Brégonzio-Rozier et al., 2015).

The molecular formula $C_5H_6O_2$, formed as a second generation product of isoprene oxidation, can be linked with methylbutandial, and $C_4H_6O_2$ is assumed to be 3-oxobutanal (Paulot et al., 2009) or hydroxymethyl vinyl ketone (Galloway et al., 2011).

Isoprene OH oxidation is dependent on the NOx concentration. This is partly because of the NOx dependence on HOx (OH + HO$_2$) radical concentration. The fate of peroxy radicals depends on NOx in a nonlinear way. At low NOx concentrations the last step is the reaction of themselves and the HO$_2$ radicals. When high NOx concentration occurs, nitric acid is formed after the conversion of NO to NO$_2$, as shown below. Consequently, HOx concentration depends nonlinearly on the NOx concentration (Cantrell et al., 1992).

2.2.1.3 Isoprene photooxidation

A substantial amount of ozone is produced as a result of isoprene or other VOCs oxidation. In the presence of enough NOx, isoprene (ISOP) is oxidized and ozone is produced. At the same time MVK and MACR are produced. Therefore, ozone production is possibly directly related to MVK and MACR production.

According to Tuazon and Atkinson (1990) the crucial reactions are:

$$OH + ISOP \longrightarrow ISOP\text{-}O_2$$

$$ISOP\text{-}O_2 + NO \longrightarrow ISOPONO_2$$

$$\longrightarrow ISOP\text{-}O + NO_2$$

$$ISOP\text{-}O + O_2 \longrightarrow MVK\,(+\,CH_2O) + HO_2$$

$$\longrightarrow MACR\,(+CH_2O) + HO_2$$

$$HO_2 + NO \longrightarrow NO_2 + OH\cdot$$
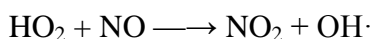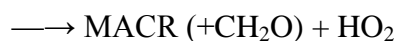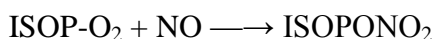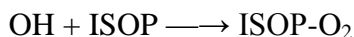
The oxidation of NO to NO_2 is equal to the ozone production, caused by the fast photooxidation of NO_2 to O_3 under sunlit conditions. Five molecules of ozone are produced from the MVK formed from isoprene (Biesenthal and Shepson, 1997).

2.2.1.4 First generation products of isoprene oxidation

As mentioned before, isoprene is removed with the reaction of OH radicals during the day, whereas in the night it is removed with ozone or NO_3 radicals (Brown et al., 2009). More than 50% of carbon assimilated in photosynthesis is used for synthesis of MVK, MACR and CH_2O. Many studies have reported the ratio of isoprene and its oxidation products to investigate the magnitude and location of isoprene sources (Karl et al., 2007). The MVK/MACR ratio is used as a direct state of isoprene oxidation and allows an estimation of how isoprene contributes to ozone formation (Biesenthal et al., 1997).

When using different ratios, e.g. MVK/isoprene plotted against MACR/isoprene, the photochemical age of isoprene can be estimated (Fig. 1; Cheung et al., 2014), especially when using daytime data, when isoprene is highly oxidized (Roberts et al., 2006).
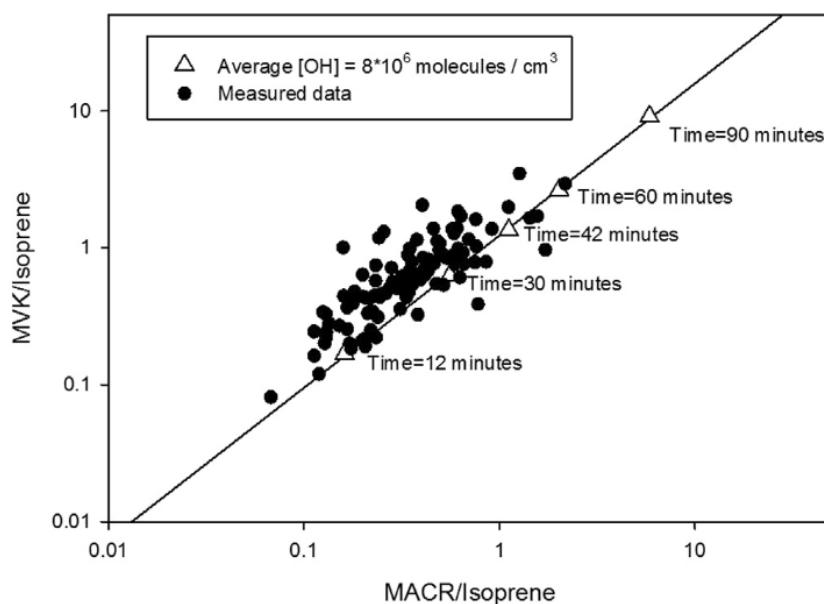
Fig. 1: Expressed time rate in a NOx rich environment of isoprene oxidation by OH radicals. MVK – methyl vinyl ketone, MACR – methacrolein. Adapted after Cheung et al. (2014).

However, these oxidation products might originate from primary anthropogenic sources, such as automobile exhaust, which should be accounted for when investigating in peri-urban locations (Biesenthal and Shepson, 1997).

Another isoprene oxidation product, formaldehyde, can also be released directly by vegetation under stress conditions (Brilli et al., 2012), as reported for a Ponderosa pine forest (DiGangi et al., 2011). Biosynthesis of formaldehyde still remains unclear. Whether directly released by vegetation or a product of the oxidation of isoprene, it can be accepted by the vegetation during warm middays with bright radiation and with high NOx ambient concentration. The cycling of HOx radicals is stimulated during such conditions and isoprene release is high (Brilli et al., 2014).

2.2.2 Monoterpenes

One of the most diverse terpenes consisting of two isoprene units with the molecular formula $C_{10}H_{16}$ and the relative molecular weight 136.24. Structure differences in one or two rings are leading to reactivity change (Fig. 2; Mohd Zul Helmi Rozaini 2012).

α-pinene   β-pinene   Δ³-carene   d-limonene   camphene   myrcene   α-terpinene

β-phellandrene   sabinene   ρ-cymene   ocimene   α-thujene   terpinolene   γ-terpinene

Fig. 2: Structure of selected monoterpenes. Adapted after Mohd Zul Helmi Rozaini 2012.

2.2.2.1 Temperature and light dependence

Temperature and light intensity are the most important environmental drivers of MT emission rate. In most current models of 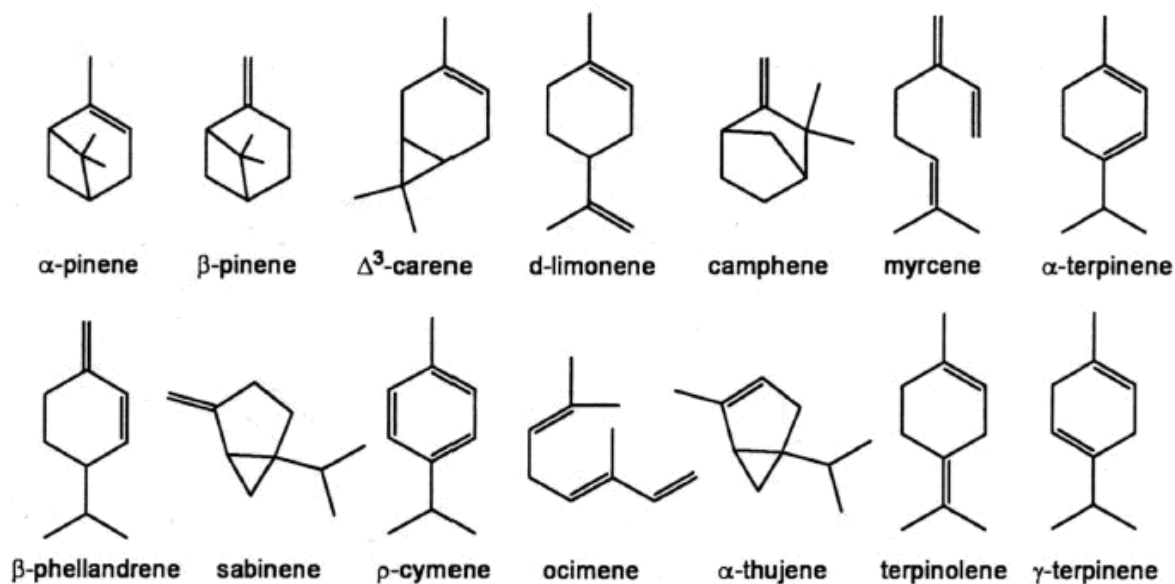BVOC emissions, isoprene emissions are regarded as light and temperature dependent, while MT emissions are regarded as only temperature dependent (Guenther et al., 1993). Recently, many exceptions were found, highlighting the huge variety of MTs emitted. Moreover, more species were studied and their emissions were examined under various environmental conditions.

Noticeable results were found for high arctic ecosystems, where emissions were observed only at daytime, when temperature and radiation rise. In low arctic ecosystems, it was found, that α-thujene, α-fenchene, α-phellandrene, β-pinene, 3-carene, α-terpinene and fenchol were emitted only at sufficient light intensities. In addition, α-fenchene, 3-carene and α-terpinene were correlated with chamber temperature and α–pinene, camphene and limonene were not affected by the light manipulation. On the other hand, the emissions were very low during night-time in high arctic ecosystems, even though the PAR intensity was still high and the temperature was enough for MTs release. Moreover in subarctic regions, the night-time emissions of isoprene were found, suggesting the presence of isoprene storage pools rather than *de novo* synthesis (Lindwall et al., 2015).

The light-dependent MT emissions were shown for dominant Japanese coniferous tree species by Bao et al. (2008). Later Nishimura et al. (2015) confirmed this finding by chamber measurements and proposed a new empirical equation estimating MT emissions.

2.2.2.2 Monoterpenes oxidation products

The main oxidation products of α-pinene, β-pinene, limonene and linalool are pinonaldehyde (*cis*-3-acetyl-2,2-dimethylcyclobutylethanal), nopinone (6,6-dimethylbicyclo[3.1.1]-heptan-2-one), 3-isopropenyl-6-oxoheptanal (IPOH) and 5-methyl-5-vinyltetrahydrofuran-2-ol (MVT). The main oxidizing agent is OH radical, whereas NO_3 and ozone are much less responsible for MT oxidation. Not too much is known about the fate of the above mentioned oxidized MTs. Pinonaldehyde is oxidized by OH radicals or NO_3, with the reaction speed factor of about 2 between each other. The reaction speed of pinonaldehyde with ozone is much lower, as expected for the reaction of aldehydes with ozone (Glasius et al., 1997). The reaction of nopinone with OH radicals is very fast,

whereas with NO_3 is very slow and with ozone is below a measurable rate (Atkinson and Aschmann, 1993). The reaction of OH with IPOH or MVT is fast.

The consequent reaction of pinonaldehyde and OH leads to norpinonaldehyde (*cis*-3-acetyl-2,2-dimethylcyclobutylmethanal), methylglyoxal and acetone formation (Calogirou et al., 1999). Norpinonaldehyde was observed as a reaction product of α–pinene and ozone, together with dimethylbicylco[3.1.1]heptan-2,3-dione and 6,6-dimethyl-3-hydroxybicylco[3.1.1]heptan-2-one (Barton et al., 1989).

Nopinone and OH radical reaction results in a formation of 6,6-dimethylbicyclo-[3.1.1]heptan-2,3-dione, 3,7-dihydroxy-6,6-dimethylbicyclo[3.1.1]heptan-2-one, 6,6-dimethyl-3-hydroxybicyclo[3.1.1]heptan-2-one and acetone as its hydrazone (Calogirou et al., 1999).

The reaction between IPOH and OH results in 2-isopropenyl-5-oxo-hexanal. While the reaction between MVT and OH results in 4-oxopentanal, 5-methyl-5-vinyltetrahydrofuran-2-one and 5-methyl-4-oxo-5-vinyltetrahydrofuran-2-ol in small amounts (Calogirou et al., 1999). Thus, the typical atmospheric lifetime can be calculated by applying reaction speeds, as shown in Table 1 (adapted after Calogirou et al., 1999), where typical day time or night time concentration values were used.

Table 1: Lifetime of atmospheric oxidants. ppbv = parts per billion per volume, pptv = parts per trillion per volume, IPOH = 3-isopropenyl-6-oxoheptanal, MVT = 5-methyl-5-vinyltetrahydrofuran-2-ol. Adapted after Calogirou et al. (1999).

Oxidant	Concentration	Pinonaldehyde	Nopinone	IPOH	MVT
OH	0.08 pptv	2 hours	9 hours	1 hour	2 hours
NO_3	5 pptv	2 days	47 days	8 hours	5 days
O_3	30 ppbv	176 days	8 years	2 days	4 days

Reactions with OH radicals seem to be dominant, while reactions with ozone seem to be negligible, as opposed to isoprene oxidation. Considering the atmospheric oxidizing agent mixture shown in Table 1., the lifetime of pinonaldehyde, IPOH and MVT is 1–2 hours, whereas nopinone persists for 9 hours. The degradation products of monoterpenes are still poorly understood, only a few authors have conducted field measurements and it is almost certain, that more products will be revealed in the future (Calogirou et al., 1999).

Ozonolysis of monoterpenes under the control of the Criegee mechanism adds ozone to the double bond and forms molozonide, a transient form of ozone cleavage. Depending on the monoterpene structure, especially the proximity of the methyl groups to the double bond (camphene and sabinene) or the location of the endo and exocyclic double bond, distinct conformations of molozonides occur. This was verified; even the relative free Gibbs energies differences were not significant. Formation of exoconformers for α-pinene, β–pinene and camphene were more than 97%, whereas for sabinene exo and endoconformers compete (Oliveira and Bauerfeldt, 2015).

Only a few studies were published concerning the photolysis of monoterpenes. The lifetime was calculated to 3.3 hours for pinonaldehyde in July and 22 hours in January, both during clear sky conditions (Hallquist et al., 1999). Different reaction constants among MTs with OH, NO_3 radicals and ozone are shown in Table 2 (National Research Council, 1992). Among others, R-limone has the fastest reactivity with ozone of all MTs.

Table 2: Gas-phase reaction constants (cm^3 molecule^{-1} s^{-1}) for room temperature of chosen BVOCs with OH, NO_3 radicals and ozone. Adapted after National Research Council, 1992.

BVOC	Rate constant for reaction with		
	OH	NO_3	O_3
Isoprene	1.0×10^{-10}	5.9×10^{-13}	1.4×10^{-17}
Camphene	5.3×10^{-11}	6.5×10^{-13}	9.0×10^{-19}
2-carene	8.0×10^{-11}	1.9×10^{-11}	2.4×10^{-16}
Δ-3-carene	8.8×10^{-11}	1.0×10^{-11}	3.8×10^{-17}
R-limonene	1.7×10^{-10}	1.3×10^{-11}	2.1×10^{-16}
Myrcene	2.2×10^{-10}	1.1×10^{-11}	4.9×10^{-16}
Ocimene	2.5×10^{-10}	2.2×10^{-11}	5.6×10^{-16}
α-pinene	5.4×10^{-11}	5.8×10^{-12}	8.7×10^{-17}
β-pinene	7.9×10^{-11}	2.4×10^{-12}	1.5×10^{-17}
α-phellandrene	3.1×10^{-10}	8.5×10^{-11}	1.9×10^{-15}

2.3 BVOCs in relation to carbon fluxes

Respiration is not the only important loss of carbon to the atmosphere. BVOCs represent a small, but highly reactive part of assimilated carbon, which is released back to the atmosphere. Generally, isoprenoids are emitted at low rates, when compared to CO_2 fluxes, ranging between 1 and 100 nmol m^{-2} s^{-1} (Loreto and Schnitzler, 2010). Emissions reach 2–5% of the carbon fixed by photosynthesis during physiologically convenient conditions. When plants are stressed, the carbon loss could increase up to 10–50% and might even exceed the amount of carbon fixed by photosynthesis. This is caused by almost the same rate of isoprene emissions, but very different photosynthesis speed during stress conditions (Brilli et al., 2007).

At ecosystem scale, it has been documented in the case of ponderosa pine forest, that carbon losses occupy as much as 4% (mean value) of CO_2 NEE (net ecosystem exchange), ranging from 2–7.9%, which represents a mean of 9.4 (range 6.2–12.5) g C m^{-2} yr^{-1}. In

summer in daylight hours, most of the carbon loss was dominated by methanol (32.9%) and 2-methyl-3-buten-2-ol (MBO) (32%) followed by monoterpenes (12.7%), ethanol (7.4%), methyl chavicol (5.1%), acetone (4.3%), sesquiterpenes (3.3%) and acetaldehyde (2.3%) (Bouvier-Brown et al., 2012).

Sesquiterpenes represent 2.4% of total BVOCs carbon emissions (Sindelarova et al., 2014) but can contribute up to 70%, specifically in citrus orchards (Ciccioli et al., 1999).

Bouvier-Brown et al. (2012) found that omitting carbon fluxes of BVOCs to the NEE-based carbon balance causes errors similar to the potential systematic errors associated with eddy covariance measurements.

2.4 Secondary organic aerosol

Organic aerosols account for 20–90% of the aerosol mass in the lower troposphere and are a major component of fine particle pollution (P.M. 2.5). Primary aerosols are emitted from biomass burning, combustion processes, dust, soil suspensions, volcanic eruptions or sea salt. Whereas, secondary organic aerosols (SOA) are formed by gas-particle conversion in the atmosphere, such as nucleation, condensation and multiphase chemical reaction, from which many controlling factors still remain highly uncertain. Aerosols scatter and absorb the solar radiation and influence cloud formation. Participation in various chemical reactions in the atmosphere influences the distribution of atmospheric trace gases (Andreae and Crutzen, 1997). They contribute to respiratory and cardiovascular maladies (Harrison and Yin, 2000). They are formed by a variety of AVOCs.

In case of biogenic origin, formation starts by oxidation of isoprene or monoterpenes. In case of isoprene oxidation at high NO_2 chemistry, SOA is formed when acyl peroxynitrate and ethacryloyl peroxynitrate undergo a photochemical reaction with MACR (Chan et al., 2010). Reactions towards SOA produce compounds with decreasing volatility with subsequent partitioning into condensed phase. However, reactions of semi volatile organics (which exist in both gas and particle phases) could lead to the formation of particles and the final SOA is formed by a reaction of organics in the condensed phase (Robinson et al., 2007).

SOA yields are decreasing substantially as NOx increase, including oxidation of small hydrocarbons up to 10, isoprene, monoterpenes and simple aromatics. An exception is the formation of benzene photooxidation (Martín-Reviejo and Wirtz, 2005) and limonene ozonolysis (Zhang et al., 2006), which is independent of NOx concentration. In the case of sesquiterpenes (longifolene and aromadendrene) the situation is the opposite: higher NOx concentrations trigger SOA formation (Ng et al., 2007).

The latest observations have shed light on SOA formation from BVOCs under the presence of sulphuric acid and ammonia. A huge burst of extremely low volatile organic compounds was observed after two days (Bianchi et al., 2016). It is thought that particle formation is always initiated by the presence of sulphuric acid. However, a direct formation of SOA from α-pinene in the absence of sulphuric acid has been observed using a cloud chamber in Conseil Européen pour la Recherche Nucléaire (CERN) (Kirkby et al., 2016). Examples of BVOCs oxidation towards SOA are given by many authors, autoxidation (Crounse et al., 2013), particle surface acceleration (Barsanti and Pankow, 2004) and/or α-pinene oxidation (Ehn et al., 2014).

2.5 Tropospheric ozone

Tropospheric ozone has been suggested as the most dangerous secondary phytotoxic organic pollutant causing injuries of plants and thus economical losses in forest and agricultural ecosystems (Paoletti et al., 2007). It is considered as a powerful oxidizing agent, which initiates the chemical removal of many hydrocarbons, as it was discussed above. Since preindustrial time, its concentration has grown exponentially (Fig. 3; Marenco et al., 1994). Apart from the detrimental effect on plants, ozone causes respiratory diseases and premature mortality (WHO, 2013). Ozone phytotoxic dose is expressed as AOT40 (Accumulated exposure Over a Threshold of 40 ppbv), even among the scientists it is suggested to express the real flux of ozone into the stomata and thus quantify real ozone exposure (Matyssek et al., 2007; Emberson et al., 2000). The flux-based index POD_Y (Phytotoxic Ozone Dose above a flux threshold Y in nmol m^{-2} s^{-1}) has been established. This index takes into account solar radiation, temperature, vapour pressure deficit, soil water potential, atmospheric ozone concentration and plant phenology stage (CLRTAP,

2015; Pleijel et al., 2007). Some studies suggest linear and some suggest non-lineal correlations between AOT40 and real flux, depending on climate, canopy position, tree age etc. (Matyssek et al., 2004). Measurements of beech tree transpiration and ozone uptake derived by xylem sap flow measurements were conducted at Kranzberg forest (Germany) for the entire growing season. Twice ambient ozone uptake was 20% smaller than ozone exposure, caused by stomata uptake limitation. European beech (*Fagus sylvatica*) stem productivity also declined substantially (Matyssek et al., 2015).

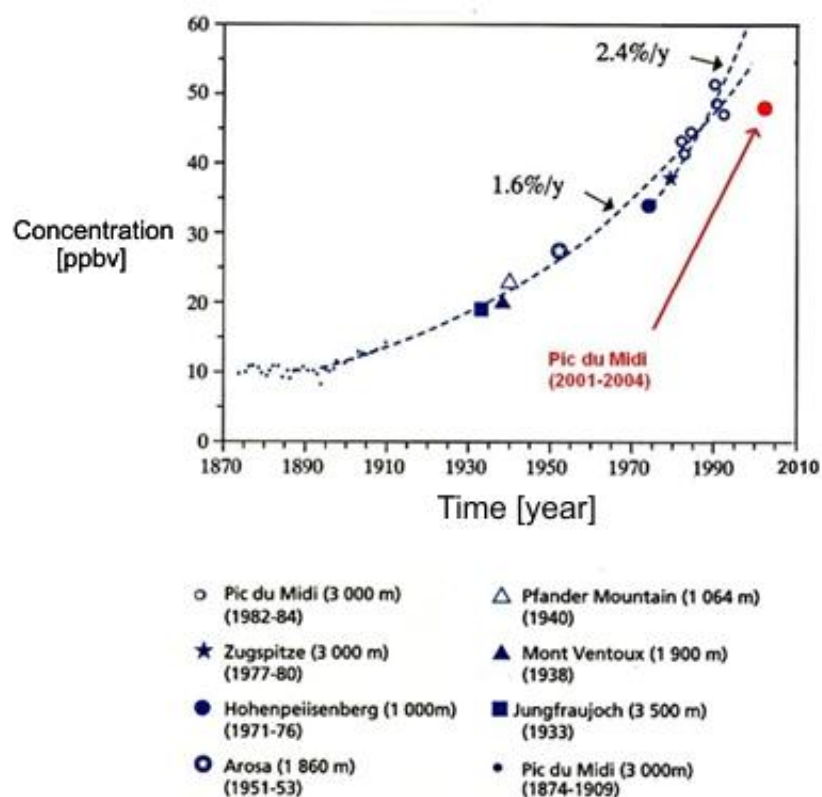Fig. 3: Evolution of ozone in free troposphere over Western Europe. Ozone concentration values are means derived from years in brackets. Trend of ozone growth per year is shown in %. Data are fitted with exponential equation. Adapted after Marenco et al. (1994).

Whole tree ozone uptake based on sap-flow measurements manifested a great difference among tree species. Deciduous tree species had no significantly higher ozone

uptake than evergreens (Wang et al., 2012). On the other hand, Wieser et al. (2003) showed higher ozone uptake by Norway spruce (*Picea abies*) forests than manifested by deciduous trees. Moreover, ozone causes loses of stem increment in European beech and Norway spruce trees. In the case of Switzerland and data taken from the period 1991–2011, growth reduction of deciduous trees was 18.5% and of coniferous trees 6.6% for coniferous trees (Braun et al., 2014). Long-term exposure to the critical values could change the biomass allocation pattern, as shown in ozone fumigated Norway spruce trees, where trees started to be corn-shaped. Norway spruce invests more in higher parts of the canopy and is more vulnerable to a broad range of disturbances. Diameter growth reduction at the reference height of 1.3 m was observed (Pretzsch et al., 2010). Predictions for the future (2040–2059) are not positive, since it is estimated that in the case of Norway spruce forests, values of POD1 will not decrease to a non-critical level (Klingberg et al., 2014).

Precursor substances of ozone formation are increasing and together with temperature rise results in the elevation of ground ozone concentration. Especially in Asia it has a serious air pollution problem with rising of global background concentrations together with local peak concentrations. Only in Europe, North America and Japan is ozone widely monitored, whereas developing countries, which evince higher ozone concentrations, have limited or no continuous ozone monitoring networks. From the long-term observations in the northern hemisphere it is obvious that the ozone concentration has doubled since the pre-industrial time (Paoletti, 2007).

2.5.1 Stomatal and non-stomatal flux

The model developed by Nowak et al. (2000) estimated the change of dry ozone uptake together with the change of urban tree cover. During the day ozone removal by the trees was significantly higher than ozone removal by the reaction with VOCs. At night time the ozone concentration increased due to reduced wind speed and scarce reaction with NO_x, which is driven photochemically. The positive effect of trees removing ozone in cities should be taken into account when planning built-up areas.

As already mentioned, ozone can react via various reactions, depending on many parameters (monoterpene structure, NOx presence, air temperature, air pressure), thus

estimating different ozone sinks for each locality could help secure human welfare and health. Many experiments have been conducted in open-top chambers or enclosures under standard conditions. However, the particular conditions in chambers differ (high air turbulence, enhanced temperature) and could influence plant traits (Nussbaum and Fuhrer, 2000) compared to field grown plants. It is sufficient to determine driving parameters of ozone loss, but those studies are done mostly on seedlings so that the effect of long-term exposure on mature trees could be markedly different, as it was discussed in various studies (Kolb and Matyssek, 2001). Similar sensitivity of tree growth for adult and juvenile trees to ozone stress was recorded for climax and pioneer stages, even though the response mechanisms differ (Matyssek et al., 2010). On the other hand, leaf physiological parameters are changing with leaf age and tree size. Due to hydraulic constraints, stomatal conductance declines with tree age (Ryan et al., 2006).

As a consequence of higher stomatal flux, depressing of stomatal conductance occurs in angiosperms, which is reducing the stomatal ozone influx. Contrary to that gymnosperms were not affected. The data were calculated in meta-analytic review by Wittig et al. (2007), who compared ozone datasets from pre-industrial evolution till current time for forests of northern temperate zone. Modelling studies are trying to integrate the stomatal narrowing into ozone models, assuming, that stomatal conductance is decreasing with cumulative ozone flux or exposure (Felzer et al., 2004), which could consequently lead to lower ozone stomatal flux. Seasonal leaf senescence and stomatal regulation through ozone impact was observed, when stomatal narrowing was diminished in autumn. Thus showing that the response of stomatal ozone induced narrowing is more complex. Stomatal conductance monotonically decreases with cumulative ozone flux or exposure, and it is taken into account in current global models (Hoshika et al., 2015).

Allocation of ozone into different sinks in a Mediterranean holm oak (*Q. ilex*) forest was calculated from eddy covariance data measured for ozone and evapotranspiration above and below the canopy. Results suggested that stomata represent the major ozone sink, especially in winter, for the rest of the year stomata flux explained less than 60% of total ozone flux. Cuticular sink was estimated as 30% and reactions with VOCs were at the monitored period negligible (Fares et al., 2014). Moreover, it was measured and calculated,

that the forest acted as an ozone sink in both the warm and cold periods of the Mediterranean climate, and it was concluded that both models based on the Ball-Berry and Jarvis approach are well parametrized for the stomatal conductance predictions (Fares et al., 2013a).

On the contrary, non-stomatal ozone sink represented a major ozone removal pathway at a citrus orchard, with the highest deposition occurring close to ground due to chemical reactions with NO and BVOCs. Significant reaction of ozone with NO was caused by its huge release from soil caused by fertilization (Fares et al., 2012).

Stomatal ozone deposition in field conditions is responsible for the reduction of carbon assimilation, which was shown in the case of a ponderosa pine (*Pinus ponderosa*) forest and citrus orchard (Fares et al., 2013b).

A young Norway spruce forest at Bílý Kříž experienced ozone exposure concentrations at 15 m above ground of 44.7 ppbv and 45.6 ppbv in July and August 2008, respectively. That corresponds with a deposition velocity ranging from 0–1.25 cm s^{-1} and an ozone flux into the forest peeking around -18 nmol m^{-2} s^{-1}, as calculated by the model developed by Emberson et al. (2000). During that summer period, forest was a net ozone sink of 9.4 kg ha^{-1} of ozone with 47.5% of that being accepted by stomata. Ozone deposition velocity peeked around noon, while ozone concentration in the afternoon. Stomatal ozone uptake over a threshold of 1 nmol m^{-2} s^{-1} exceeds the threshold of 8 mmol m^{-2} per leaf area, which is suggested by CLRTAP, 2015 for Norway spruce protection. A year later (2009), ozone exposure was 14.1 mmol m^{-2} per leaf area with a AOT40 value of 11 562 ppb h, which is 131% of the critical level 5 000 ppb h (Zapletal et al., 2012). Moreover, stomatal uptake was responsible for a significant decrease of net ecosystem production (NEP) under the high intensity of solar radiation (Zapletal et al., 2011).

Prediction into the year 2030 was conducted by Zapletal et al. (2012), who calculated AOT40 to be 13 659 ppb h. Contrary to that, POD$_1$ should decrease to 11.9 mmol m^{-2} per leaf area caused by limited stomatal uptake by the presence of higher vapour pressure deficit.

Similar research was done by Vlasáková-Matoušková and Hůnová, (2015) at Jizerske Mountains, Czech Republic in a European beech (*Fagus sylvatica*) forest too. Authors found that AOT40 was exceeded at four of six sites and visible leaf injuries were correlated with higher ozone levels. Accumulated stomatal fluxes ranged between 13.4 and 22.3 mmol m^{-2} per leaf area, which is an even higher value than at Bílý Kříž.

2.5.2 BVOCs as ozone protectors

Can ozone scavenge the monoterpenes and isoprene and thus protect a plant from ozone stomata influx and injuries? In the whole-plant enclosure system it was shown in the case of holm oak (MT emitter) and black poplar (*Populus nigra*, isoprene emitter), that the cuticle ozone reaction was negligible. In the case of the poplar, the gas-phase reaction of ozone with isoprene was negligible too, but monoterpenes holm oak emissions were associated with reduced ozone uptake and thus can have a significant protection mechanism (Fares et al., 2008). Another study has revealed a noticeable increase of nocturnal stomatal conductance under high night ozone exposure, which could lead to larger ozone night flux and detrimental effects on leaf function (Vitale et al., 2008). A further study investigated the increased emissions with irradiation and consequent ozone decrease that was measured at a *Cryptomeria japonica* whole-tree enclosure system (Matsumoto, 2014).

2.5.3 Ozone in urban areas

Ozone is transported from the stratosphere to the troposphere. Photochemical reactions in the troposphere between the BVOCs and NOx take place in the presence of sunlight, especially in the cities, where levels of NOx pollution are high. If no VOCs were in the atmosphere, the levels of ozone would be determined by the photostationary state of NOx. As mentioned above, ozone can be produced by various reactions, which strongly depends on the VOCs/NOx ratio. This ratio is divided to (I) VOC limited zone (VOC/NOx < 4), (II) optimum ozone production zone (15 > VOC/NOx > 4) and (III) NOx limited zone (VOC/NOx > 15), as shown in Fig. 4 (National Research Council, 1992). In urban areas a VOC limited zone with a high concentration of NOx from car exhaust is often observed, whereas in rural areas ozone production is limited by low NOx concentration. Optimum ozone production conditions are found at the transition zones between the NOx polluted

and NOx limited zones, which are mostly in peri-urban locations (Finlayson and Pitts, 1999).

The ozone isopleth diagram is sensitive not only to ambient concentrations of VOC and NOx, but also to the composition of VOCs, especially for low VOC/NOx ratios. Isopleths were originally derived from aircraft measurements above a city, when 390 ppbv peek ozone concentration occurs and VOC composition and concentration was taken as a city average (Jeffries et al., 1989). For example, VOC concentration of 1 ppmv and NOx concentration of 100 ppbv, changes peek ozone concentration from 300 ppbv for the base case (city average VOC) to 280 ppbv in case of VOCs being composed of lower aldehydes. At 500 ppbv of VOC and NOx of 100 ppbv the change is from 160 ppbv to 120 ppbv of ozone. That is due to higher efficiency of aldehydes to create radicals during sunlight conditions. Similar findings of VOC speciation were published by Dodge (1990).

Moreover, diagram (Fig. 4) was calculated for one day simulation at a specific location, thus not reflecting week long episodes of high ozone concentration at downwind areas. The VOC/NOx ratios varied hour by hour and in space from ground to aloft, reflecting current emissions and those from previous days. In local and global models the variability of isopleths is thus accounted and assessment to reduce ozone pollution should be tailor-made for the particular location.
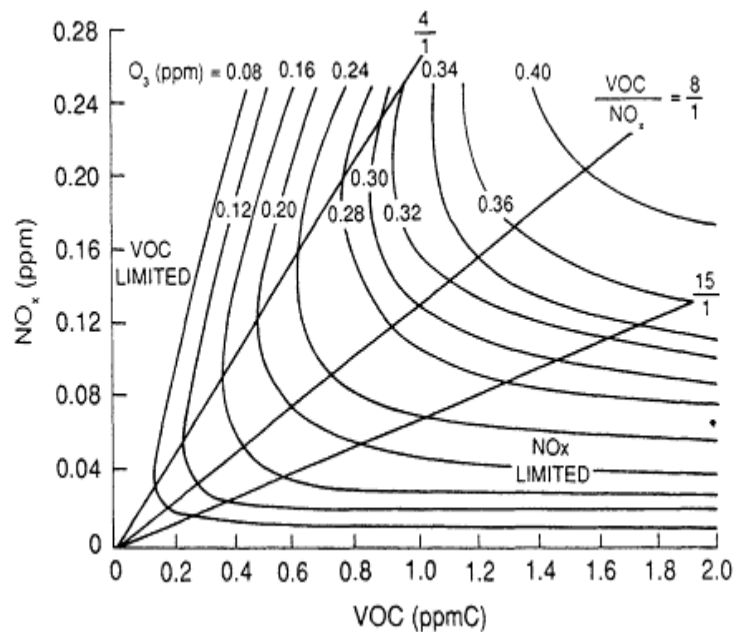
Fig. 4: Typical ozone isopleth diagram, ppmC – parts per million carbon. Adapted after National Research Council, (1992).

If in urban areas highly emitting BVOC tree species occur, conditions are shifted towards optimum ozone production with consequent high ozone episodes in city centres and formation of SOA and smog. Therefore, it is critical to choose tree composition wisely, putting emphasis on low-emitting tree species. Such specific conditions are becoming common in Mediterranean areas during heat waves with low air turbulence or in Asia, where many fast-growing tree plantations are located in the megacities (Ghirardo et al., 2016). Traits and benefits are reviewed by Grote et al. (2016).

Ozone formation potential for urban trees and shrubs was established by Benjamin and Winer (1998); taking into account different emission capacities and reactivity factors of isoprene- and MT-emitting species. The reactivity factor for isoprene-emitting species is approximately three-times higher than for MT-emitting ones. However, it should be noted, that isoprene is emitted days and nights also from storage pools, whereas monoterpenes only at daytime in temperate zones (Laffineur et al., 2011). Moreover, emissions are changing with ontogeny of leaves/plants and actual stress conditions (Brilli et al., 2007; Guenther et al., 2012).

2.5.4 Effect of ozone on environmental variables

Ozone enters inner tissue through plant stomata (Paoletti et al., 2010). After, ozone changes stomata membrane properties by inhibiting guard-cell K^+ channels (Torsethaugen et al., 1999) and causes phytotoxicity of internal tissue by generation of reactive oxygen species consisting of peroxides and free radicals (Hippeli and Elstner, 1996). Inevitable plant response after a longer period of such dreadful conditions is cell death. First plant response is to sluggish stomatal movements with CO_2 concentration, vapour pressure deficit and slower response to diverse light intensities (Paoletti, 2005). Stomatal conductance change is species specific. For example, response of *Ilex aquifolium, Ranunculus acris* and *Dactylis glomerata* is to increase stomatal conductance when ozone induced stress occurs (Wagg et al., 2013). Due to the importance of controlling stomatal ozone flux, several studies were published (Paoletti et al., 2010; Hoshika et al., 2012a). Other variables are affected by ozone uptake: maximum rate of electron transport (Paoletti, 2010; Hoshika et al., 2013), light-saturated photosynthesis (Hoshika et al., 2012a, 2013; Zhang et al., 2014), light saturation and net carbon assimilation rate (Zhang et al., 2014), water use efficiency (Hoshika et al., 2012b), photochemical efficiency of PSII in the saturated light (Paoletti et al., 2010; Zhang et al., 2014), leaf gas exchange (Hoshika et al., 2012a) and finally light- and CO_2-saturated rates of CO_2 assimilation (Handley and Grulke, 2008). Such affected stomatal properties may subsequently lower the plant's ability to control water loss and survive stress events.

Apart from aboveground plant parts, belowground parts are experiencing ozone induced damage as well. Usually, growth of roots usually depends on the products of photosynthesis (Van Den Driessche, 1991). A limited carbon pool in roots is affecting root growth (De Quijano et al., 2012), their architecture (Hoshika et al., 2013), monosaccharide and starch concentration (Thomas et al., 2005). Most studies report an altering of the root/shoot ratio with a decrease in both root and shoot carbon storage, which might finally lead to an inability to support aboveground plant parts (Franzaring et al., 2000).

Since pre-industrial time, background atmospheric concentrations in northern midlatitudes have increased. It is estimated that stomatal ozone fluxes will not decrease to non-critical levels in the near future (Klingberg et al., 2014). Moreover, modelling studies

have shown that the tropospheric ozone burden in the 1850s was 30% lower than in the present time (Young et al., 2013). Atmospheric ozone can be removed by deposition to soil and plant surfaces, by stomatal uptake or by various within-canopy reactions dominated by nitrogen oxides aging and biogenic volatile organic compounds removal. Damage of photosynthetic apparatus of plants leads to a reduced NEP, i.e. a reduced capacity of terrestrial ecosystems to capture atmospheric CO_2. As terrestrial NEP is represented by >50% of forest ecosystems, the global impact is serious.

Globally reduced carbon assimilation by forest ecosystems through ozone effects has been proven as a substantial contribution to the indirect radiative forcing of climate change (Sitch et al., 2007). It is likely that this threat to terrestrial ecosystems will remain at least throughout the current century. Increase of ozone concentration will substantially reduce the terrestrial carbon sink in the Northern Hemisphere, which will diminish or could be lost in the future (Wittig et al., 2009). Additionally, it is estimated that global NEP will decrease by 8–12% in average with largest decrease up to 20% in middle latitudes (Lombardozzi et al., 2015).

Ozone can react with a broad range of compounds depending on many micrometeorological parameters; thus estimating different ozone sinks for each locality type could help secure human welfare and health. Worldwide, a number of experiments have been conducted in open-top chambers or growth chambers under standard conditions. However, the particular conditions in chambers differ (high air turbulence, enhanced air temperature) as compared to field conditions and could change the plant response (Nussbaum and Fuhrer, 2000). Thus up-scaling of leaf-level observations to a complex ecosystem-level is needed. Such real-world measurements with consequent mathematical modelling approaches are greatly appreciated for both model validations and improvements, which are tightly linked to a better understanding of the biosphere-chemosphere continuum of a particular location.

Taking into account the NEP reduction caused by ozone, the global carbon models might be overestimated. Until now, only a few reports have incorporated the NEP loss induced by ozone into these models (Lombardozzi et al., 2015). In a wider perspective, the

world wood-stock supplies might be reduced and this ought to be discussed by local policy makers to sustain the wood stock productivity by accepting ozone risk-assessment as by Sicard et al. (2016).

3 AIMS

The main aims of the thesis are:

- to describe the role of BVOCs in plants exposed to extreme environmental conditions such as high air temperature,

- to conduct measurements of BVOC emissions, particularly monoterpenes and isoprene, in two distinct ecosystems: A mountain Norway spruce ecosystem in a temperate zone and A peri-urban Holm oak forest ecosystem in a Mediterranean zone by utilizing PTR-(TOF)-MS analysers coupled with the eddy covariance technique,

- to model diurnal and seasonal BVOC fluxes using an Inverse Lagrangian Transport Model (ILTM) and Model of Emissions of Gases and Aerosols from Nature (MEGAN),

- to identify key environmental drivers of BVOC fluxes and to quantify these fluxes in comparison with carbon fluxes in a mountain Norway spruce forest at the Bílý Kříž experimental site,

- to quantify ozone exposure on a mountain Norway spruce forest at the Bílý Kříž experimental site by measurement of ozone concentration and flux calculation.

4 MATERIAL AND METHODS

4.1 Sites descriptions: Bílý Kříž and Castelporziano

The Bílý Kříž experimental station in the Beskydy Mountains (49° 33´N, 18° 32´E, NE of the Czech Republic, 908 m a.s.l.) is one of the peculiar European "super sites", where long-term CO_2 fluxes and meteorological and environmental parameters are being measured according to standardized protocols. The experimental station is operated under the Global Change Research Institute, Czech Academy of Sciences. The site is a part of ESFRI (European Strategy Forum on Research Infrastructures) infrastructures ICOS (Integrated Carbon Observation System) and AnaEE (Infrastructure for Analysis and Experimentation on Ecosystems) and forms a part of Czech Carbon Observation System (CzeCOS).

This area has characteristics that epitomize moderately cool (annual mean air temperature 6.6°C) and humid (annual mean relative air humidity 84.7%) climate with high annual precipitation (mean for years 2009–2014 is 1152 mm). Although the prevailing winds are SE, it is likely that air pollutants are being transported from the Ostrava region and south Poland, where heavy industries are situated. Thus low NOx concentrations (maximum 10 ppbv) and high ozone concentrations reaching up to 90 ppbv during the whole growing season are typical seasonal characteristics (Zapletal et al., 2012; Zapletal et al., 2015). The experimental forest comprises of a monoculture of Norway spruce trees (99%) and *Abies alba* (1%) within the age of 39 years (2016) on a slope (11–16°) with SSW orientation. Hemispherical projected leaf area index evinces the seasonal maximum of 7.52 m^2 m^{-2} (2012). Tree density is 1 268 trees ha^{-1}, median tree height 15.5 m, median diameter in breast height 17.9 cm. For more detail see Havránková et al. (2015).

Castelporziano experimental station is located inside the Presidential Estate of Castelporziano (41° 43'N, 12° 24'E, 25 km SW of Rome, Italy, 4 m a.s.l.). Plant cover is typical for the Mediterranean region, within the area of 6 000 ha. The experimental station is operated under the CRA-RPS (Centro di Ricerca per lo Studio delle relazioni fra pianta e

suolo) with their headquarters in Rome. The area has characteristics that are described by prolonged stress aridity during summer and moderate cold stress during winter. The average annual precipitation is 805 ± 256 mm (2007–2011). It is part of the Italian network of Long-term Ecological Research Sites. Wind circulation is determined by the local sea-land regime with moderately strong S-SW winds during the morning and light N-NE winds during the afternoon. Early drought is caused by the sandy structure of the soil, which is not capable of keeping water for a long period of time. Since 1951 this area has been intact and preserved with limited access. The Large biodiversity value and vicinity to the polluted city of Rome make Castelporziano an excellent experimental place for studying biosphere-atmosphere interactions. The experimental forest located in the tower footprint comprises a Holm oak forest stand, which was planted in 1976: in 1985 the stand was converted from coppice to high forest. The tree density is 1500 trees ha^{-1}, mean height (2013) 12.5 m, mean diameter in breast height 16 cm. Variation of LAI is between 3.2–3.8 m^2 m^{-2}. For more details see Tirone et al. (2003) and Fares et al. (2009).

4.2 Methods

4.2.1 Proton transfer reaction-mass spectrometers

The development of the PTR-MS technique owes a lot to its precursors, the FA (flowing afterglow) and SIFT (selected ion flow tube) techniques. Instead of measuring rate coefficients for each specific reaction, they are presumed from earlier studies or completely omitted in the case of gas calibration. The application of the Selected Ion Flow Drift Tube technique (SIFDT), developed by Werner Lindinger and co-workers in 1994 was a key step towards the PTR-MS development. This employed a specific mass-selective reagent, H_3O^+, for subsequent reaction with trace gas. To many organic molecules proton donation is exothermic, allowing a very fast reaction. Common air constituents, such as O_2, CO_2, and N_2 have lower proton affinities than H_2O and thus proton transfer from H_3O^+ is almost selective for organic compounds presented in air.

Another benefit of using H_3O^+ as a primary ion is its soft ionization process, which tends to produce no or few fragments. Taking into account possible fragmentation is crucial for precise organic molecule identification and possible interference from fragment ions.

Abundant water molecules do react with humid analyte gas, which results in the formation of hydrated hydronium clusters H_3O^+ $(H_2O)n$. In flow drift tube, the clusters are dissociated in energetic collisions where He and H_3O^+ are regenerated. The process is balanced to avoid energy causing significant fragmentation of protonated organic ions and to ensure that the predominant reagent in flow drift tube is H_3O^+. The best solution was found to be 0.15-0.25 eV. Comparing PTR-MS to SIFT technique, the long flow tube was replaced with a short drift tube and the mass-selected H_3O^+ source was replaced with a hollow cathode discharge, which allows to deliver almost pure (> 99.5%) source of H_3O^+. A schematic design of PTR-MS instrument is shown in Fig. 5.
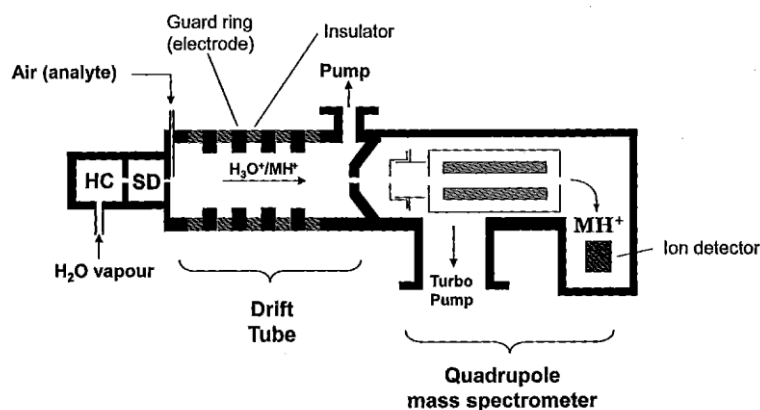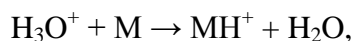

Fig. 5: Scheme of proton transfer reaction (PTR) instrument with a quadrupole mass spectrometer (MS). HC - hollow cathode discharge ion source, SD - source drift region, MH^+ - protonated mass. Adapted after Ellis and Mayhew (2014).

Principal source of organic ions in PTR-MS is proton transfer from H_3O+ as follows:

$$H_3O^+ + M \rightarrow MH^+ + H_2O,$$

where M – an investigated organic molecule. The formation of hydronium ions is minimal and considered negligible. After that, it is possible to capture mass spectrum as a plot of measured ion abundance (y-axis) and m/z (m – mass of the ion, z – charge of the ion) values of the product ions (x-axis).

Mass spectra are different in PTR-MS and PTR-TOF-MS analysers. The PTR-MS instrument is equipped with a quadrupole, four rods with changing electrical field, which allows us to select the ion we are interested in. The time-of-flight mass analyser is equipped with the flight tube. Ions are generated within the ion acceleration region in TOF, whereas in classical MS with quadrupole ions are generated externally in the drift tube. The arrival of the ions by measuring the time-of-flight provides a spectrum in the time domain. Consequently, the mass resolution in TOF is much higher. Moreover, TOF allows resolving isobaric compounds, when coupled with GC-MS. Basic comparison between PTR-MS with quadrupole (PTR-QMS) and PTR-TOF-MS is shown in Fig. 6 (Ionicon, 2015). Thus quadrupoles are robust, cheaper and enough to monitor the selected compounds, whereas TOF acquire full mass spectra in a spilt-second, allows separation of isobars thanks to high mass resolution and consequently provides more scientific insight.
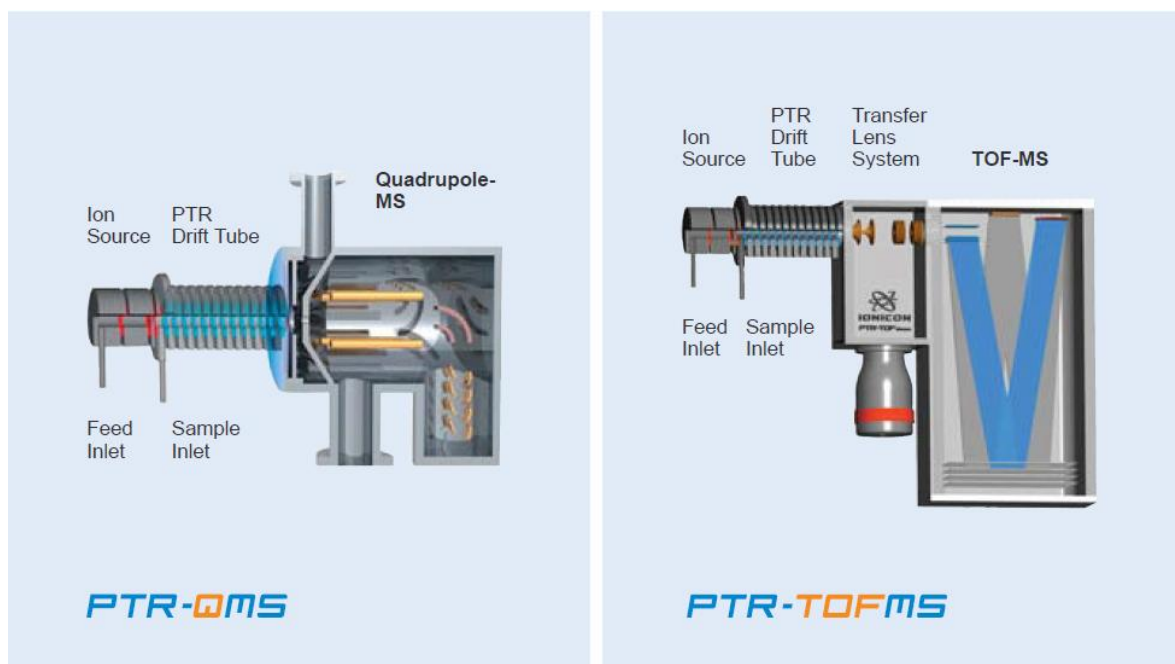
Fig. 6: Scheme of both types of PTR-MS. Quadrupole mass filter connected with secondary electron multiplier (PTR-QMS) provides mass separation and detection of the ions. Time-of-flight separates ions according to their m/z ratio. Adapted after Ionicon (2015).

4.2.2 PTR-TOF-MS experimental setup and measurement at Bílý Kříž

Measurements of BVOCs were performed at the Bílý Kříž experimental station using a proton transfer reaction mass-spectrometer with "time-of-flight" detector PTR-TOF 8000 (Ionicon, Innsbruck, Austria) in the period 15.–20.7. 2014, when high drought events were expected. For scheme of sampling schedule see Fig. 7.
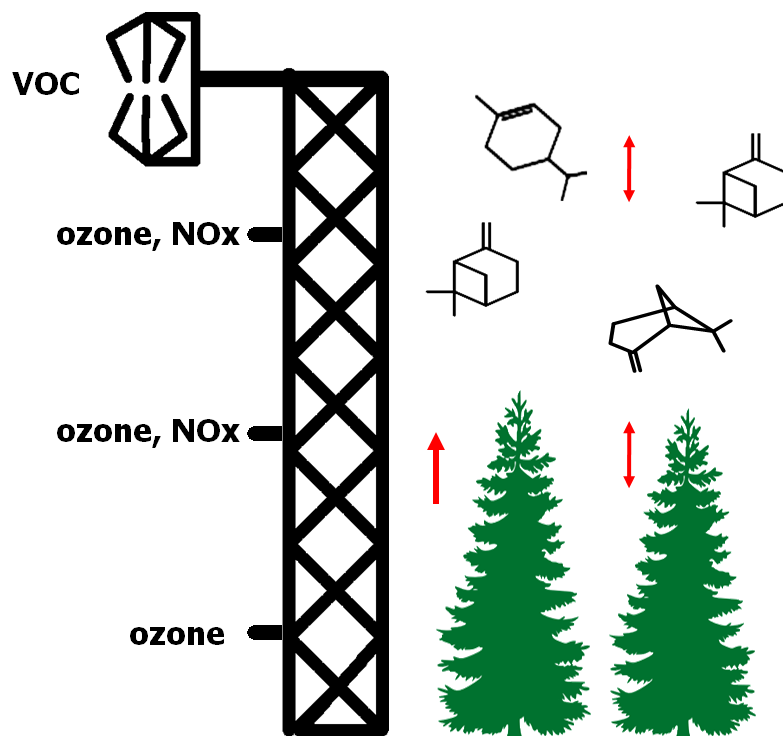

Fig. 7: Scheme of VOC sampling schedule. Experimental mast is placed within the area of mean tree height. VOCs are measured by PTR-TOF-MS coupled with eddy covariance technique. Ozone and NOx are measured as within-canopy concentration gradient. By the time of PTR-TOF-MS campaign due to technical issues ozone and NOx were not operating.

All determinations were performed by setting the drift tube pressure at 2.22 mbar, voltage at 600 V and temperature at 60 °C. The resulting ionization energy (E/N) was ~1.36 10^{-15} cm^2 V^{-1} s^{-1}. All protonated ions that were extracted from the drift tube every 30 μs, were separated in the region accordingly and detected on a multi-channel-plate (MCP,

Burle Industries, Lancaster, PA, USA). Raw data were acquired by the TofDaq software (Tofwerk AG, Switzerland) at a frequency of 10 Hz, merged in 6 minutes files and then processed according with the procedure described by Müller et al. (2013) for the ion counting correction, accurate mass scale calibration, peak identification and peak area quantification. In the low mass range, the accuracy of the scale was checked using three ions always present in the spectra background: m/z 21.022, 29.998 and 39.033 generated respectively by the $H_3O_{18}^+$, NO^+ and $H_2OH_3O_{18}^+$ ions. The high mass range was calibrated using the $(M+1)^+$ ion with m/z 330.848 generated by 1,3-diiodo-benzene, and by its most intense fragment with m/z 203.944, diffused continuously into the instrument. Calibration is shown in Fig. 9. The quantification of compounds was performed by using a calibrated gas cylinder containing known levels of different isoprenoids (Apel Riemer Environmental, Broomfield, CO, USA) diluted into VOC-free air. In here the VOC presented in the cylinder slightly differed from those used for PTR-MS calibration. The reason is in covering the different shape of transmission curve of full spectra. Clean air for background measurements and calibration dilution was produced by a home-made zero air generator (ZAG) consisting of a inox steel tube filled with a Pt-Pd catalyser held at temperatures of approximately 350 °C, releasing VOC-free air at the same humidity grade of the ambient air sampled. An example of raw spectra and mass separation is shown in Fig. 8 and Fig. 10.

In our setup, the ambient air was drawn through a PTFE tube (length from inlet to PTR-TOF-MS: 20 m; internal diameter: 6.35 mm) with a N811KT.18 pump (KNF Neuberger, Freibourg, Germany) at the constant flow rate of ~10 l min^{-1}. The inlet was provided with a 1 μm diameter filter to protect the system from dust and particles and the entire line was heated at 40 °C to prevent water condensation inside the tube. The last 20 cm of the sampling line was converted to 1/16'' to match the PEEK capillary inlet (internal diameter: 1 mm) of the PTR-TOF-MS system that was maintained to 50 °C. Other details such as detection limits, accuracy etc. are described by Graus et al. (2010).

PTR measurements were synchronized with an eddy covariance measurement of CO_2 and H_2O fluxes. The eddy covariance system consisted of a Gill HS-50 ultrasonic anemometer (Gill Instruments, Limington, UK) and a LI-7200 enclosed-path infrared gas analyser (LI-COR, Lincoln, NE, USA) installed on a micrometeorological tower, 3 m

above the canopy. Measurement was conducted continuously for 24 hours per day with short calibration gaps.
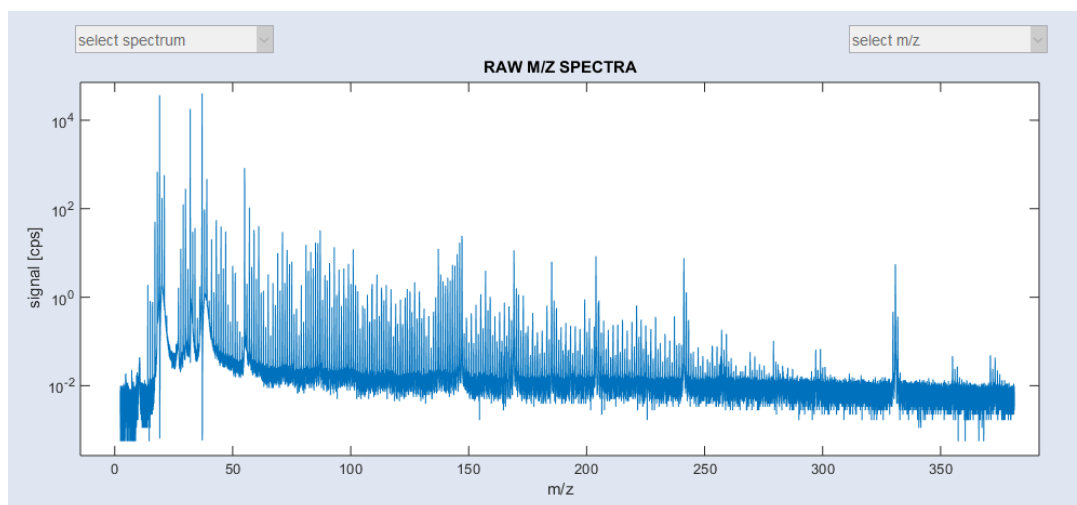

Fig. 8: Full raw m/z spectra in PTR-TOF Analyzer 4.47 software connected to PTR-TOF-MS.
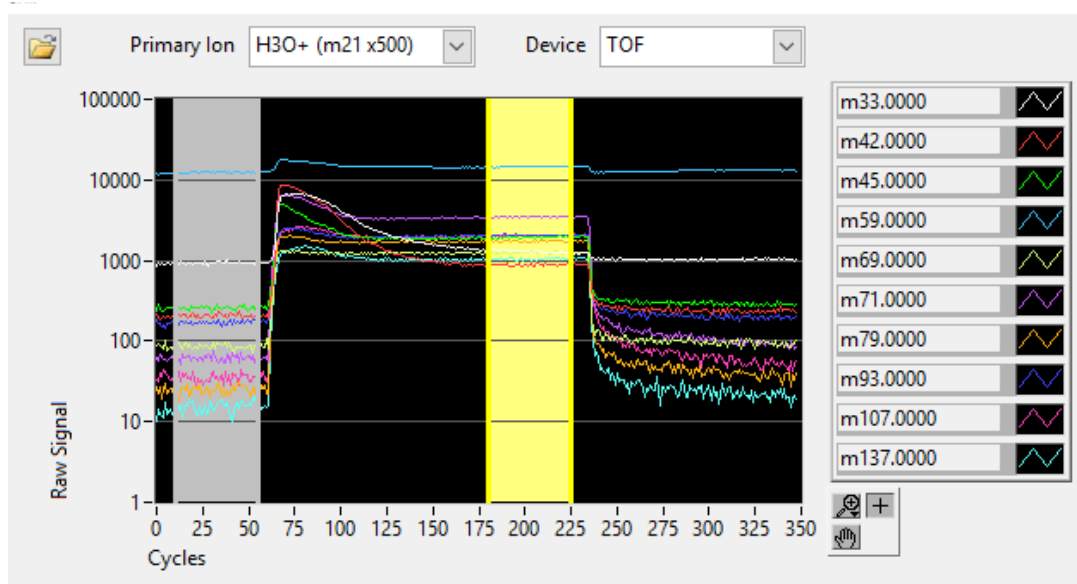

Fig. 9: Calibration from certified calibration cylinder in PTR-Viewer 3.2.2 software. Different curve colours represent different m/z.
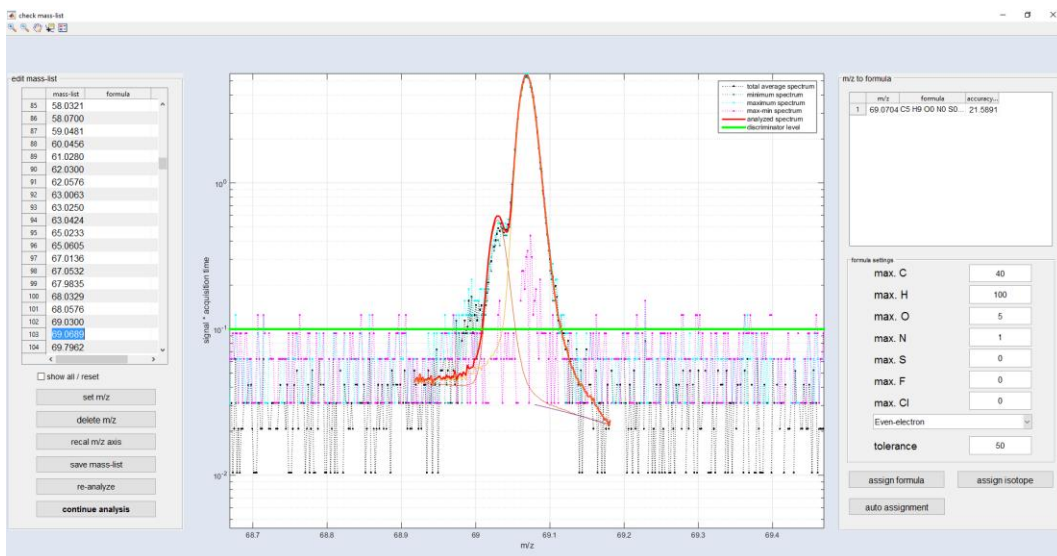
Fig. 10: Example of precise separation of isoprene (m/z 69.069) and furane (m/z 69.030) in PTR-TOF Analyzer 4.47 software.

4.2.3 Measurement of BVOC concentrations and flux calculation

Measured BVOCs for which gas standards were available were calibrated to obtain concentrations, while m/z values were derived from transmission curves where standards were not available (Taipale et al., 2008). Three wind components and BVOCs concentration data recorded by different data loggers at high frequency (10 Hz) were merged by a Matlab routine (Mathworks, USA) and grouped into half-hour values. Wind data were rotated to force mean vertical wind speed to zero according to the planar fit method (Wilczak et al., 2001).

Time shift between vertical wind velocity and BVOCs concentration was derived for each half-hour by calculating the cross-covariance function of vertical wind speed and BVOCs concentration as a function of the lag time within a range of ±50 s. Lag time was identified in correspondence with the maximum covariance. Covariance function was verified, and if a clear covariance peak was not observed the half-hour value was discarded.

BVOC vertical fluxes were calculated from high frequency BVOCs' concentration and vertical wind velocity after subtracting the time lag while following the rules of the eddy covariance technique (Baldocchi et al., 1988; Aubinet et al., 2012):

$$F = \overline{w'c'} = \frac{1}{n}\sum_{i=1}^{n}[(c_i - \bar{c}) \times (w_i - \overline{w})] \tag{Eq. 1}$$

where F is the BVOC vertical flux, c is the gas concentration (nmol mol^{-1}), and w is the vertical wind speed (m s^{-1}). Overbars denote time averaging and primes ($'$) denote fluctuations from the half-hour means.

Fluctuations of the covariance function diverted from the main lag were utilized to calculate the random flux error, estimated as the root-mean-square deviation of the covariance function from zero. We used the ranges -90 s to -30 s and 30 s to 90 s, assuming that in these ranges vertical wind velocity and BVOCs' concentration are no longer correlated (Langford et al., 2015).

Lastly, a filtering procedure was applied and fluxes were discarded if at least one of the following conditions occurred: low turbulence ($u^* < 0.13$, m s^{-1}), stationarity test (Foken and Wichura, 1996) above 50%, or flux below the random error value of the corresponding half-hour period.

4.2.4 Cylindrical wet effluent diffusion denuder sampling

MTs are assumed to be the most abundant BVOCs emitted by Norway spruce ecosystems. In order to identify particular MT species, the Cylindrical Wet Effluent Diffusion Denuder (CWEDD) technique was used to absorb the air samples (n-heptane as absorption liquid) at 5.1 m, 14.3 m and 25.3 m above the soil surface. Air samples were collected on July 21, 2010; July 29, 2011 and August 2, 2012; respectively. Those days are representatives of summer with different environmental factors including heavy rainfall (2010), post-raining period (2011) and severe drought episode (2012). The samples were collected in 5 min intervals between 11:30 and 14:00 for 2010 and 2011 and 7:00 and 20:00 of local time (GMT + 2 h) for 2012. The CWEDD was heated at 20 °C to keep the same conditions for sampling (Sklenská et al., 2002). Monoterpenes were quantified by a gas chromatography – mass spectrometry (GC-MS, Agilent, 7890A, 5975C, USA). The 2 µl samples were analysed by GC-MS (HP5-MS, 30 m, 1 µm film thickness, 0.32 mm i.d.) in splitless mode at a temperature of 260 °C. Flow of He carrier gas was 4 ml min^{-1}. Program started at 50 °C for 2 min, a gradient of 5 °C min^{-1} was applied up to 160 °C and then a next gradient of 20 °C min^{-1} was used up to 240 °C. The GC-MS was run in electron impact ionization type with energy of 70 eV and in selective ion monitoring mode. The temperatures of the ion source and transfer line were 230 °C and 280 °C, respectively.

Identification of monoterpenes was based on comparison with retention times and mass spectra of analytical standards. After each analysis, the mass concentration of components was calculated from the calibration curve of each analytical standard. Concentration in nmol mol^{-1} was calculated. Data were provided by the Institute of Analytical Chemistry CAS. For details see Křůmal et al. (2016).

4.2.5 Monoterpene flux calculation from concentration gradient at Bílý Kříž

Both temperature and global radiation were averaged over 30 min intervals derived from previous 30 min dataset. Friction velocity was calculated by EddyPro software from the covariance. Mean values of friction velocity for all three years suggesting well-developed turbulence. Air molar densities for each concentration level were calculated on the base of temperature gradient corresponding to sampling profiles and current air pressure.

As many studies have shown, within-canopy transport cannot be sufficiently described only by diffusion (Steffen and Denmead, 1988). Thus, an Inverse Lagrangian Transport Model (ILTM) was used to derive fluxes from concentration gradients (Raupach, 1989; Nemitz et al., 2000; Karl et al., 2004; Karl et al., 2008; Alves et al., 2016). Monoterpenes were considered as highly reactive within a lifetime of 60 s. Thus, within-canopy oxidant reactivity was incorporated in the model, reflecting the fast reactivity of MTs with OH radical and ozone, which occurs during its high midday concentrations.

The standard deviation of vertical wind velocity (σ_w, m s^{-1}) for canopy height was averaged from high-frequency data. For near-soil level σ_w was computed as described in Leahey et al. (1988).

$$\sigma_w = B \cdot V \tag{Eq. 2}$$

where B = parameter of static stability (dimensionless), V = scalar mean speed of horizontal wind (m s^{-1})

Factor B, stable within the canopy, was calculated by the same equation from measured data at canopy height for 30 min intervals. Values were in an agreement with Weber (1998), who reported a B value as 0.22. I computed B daily mean and standard deviations

(dimensionless) as follows 2010: 0.2 ± 0.02, 2011: 0.56 ± 0.04, 2012: 0.21 ± 0.04. Height for computed σ_w above the soil was for 2010: 7 m, 2011 and 2012 7.69 m.

Concentration scalars of three heights correlated to denuder measurements were interpolated to reach 10 levels as an input for modelling. Air molar density was calculated for all three sampling heights. Turbulence profiles and estimated Lagrangian Timescale with canopy height, height above ground, displacement height (considered as 2/3 of canopy height) were used as an input for modelling. Dispersion matrices were calculated by Lagrangian dispersion theory as described by Nemitz et al. (2000). Source-sink distribution was calculated according to

$$C - \mathbf{C_{Ref}} = \mathbf{D} \cdot S \qquad\qquad (\text{Eq. 3})$$

with C concentration vector ($\mu g\ m^{-3}$), $\mathbf{C_{Ref}}$ concentration at reference height ($\mu g\ m^{-3}$), $\mathbf{D}$ dispersion matrix (m) and S source-sink vector ($mg\ m^{-2}\ h^{-1}\ m^{-1}$).

4.2.6 Environmental parameters, ozone, NOx concentrations and CO_2 flux measurement

At the experimental forest at Bílý Kříž, those parameters we used were measured: relative air humidity (EMS33 Rotro, EMS Brno, CR), air temperature (EMS33 Rotro, EMS Brno, CR), air pressure after 2013 (PTB110 Barometer, Vaisala, Finland) and before (SPA 511 B5UB, CRESSTO, CR), precipitation (386C, MetOne, USA), incoming, transmitted and reflected photosynthetically active radiation after 2011 (EMS12, EMS Brno, CR) and before (BPW 21, Siemens CR), wind velocity by a gradient of 2-axis sonic anemometers and one 3-axis sonic anemometer (50.5 Sonic sensor, Met One, USA). Flux of CO_2 was measured by Li-7000 and Li-7200 (LI-COR, Lincoln, NE, USA) in 2010 – 2011 and 2012, respectively. Post-processing was done by EcoFlux/EdiRe and Li-7200soft/EddyPro. For all years, the flux was measured at 18 m above the soil surface. Air temperature was measured (model RHA1; Delta T, UK) at the current canopy height. Global radiation was recorded at the height of 4.8 m above the tree canopies using a pyranometer Kipp Zonen CM6B (Kipp&Zonen, Netherlands). The leaf area index was measured indirectly using the LAI2000 (LI-COR, USA).

Ozone and NOx is measured by APOA 370 and APNA 370 analysers, respectively (Horiba, Kyoto, Japan). Both are measured as within-canopy concentration gradient at 10, 15 and 20 m in case of ozone. Measurements are conducted in 15 and 20 m in case of NOx for years 2013–2014.

The post-processing of high frequency data (20 Hz) was performed by EddyPro software (LI-COR, USA) according to recent recommendations (Aubinet et al., 2012) and produced half-hourly estimates. This procedure included spike removal and quality check of the raw signals, rotation of wind velocity components into the planar fit coordinate system (Wilczak et al., 2001), and spectral corrections of computed fluxes (Moncrieff et al., 2005). The missing and excluded data, based on quality checking scheme adequate to Mauder et al. (2013), were gap-filled by marginal distribution sampling method according to Reichstein et al. (2005). Data were provided by Global Change Research Institute CAS, Department of Matters and Energy Fluxes.

4.2.7 Boundary layer calculation

Approximate height of boundary layer was calculated in MatLab (MathWorks, MA, USA) according to lifting condensation level which should fit the lowest level of *cumulus humilis* cloud deck. In case of clear sky conditions it should be close to the boundary layer height. The MatLab script was adapted after Univ. Prof., D.I., Dr. Thomas Karl´s home page, available at http://homepage.uibk.ac.at/~c7071028. For more details and comparisons between measured and modelled boundary layer height see Craven et al. (2002).

4.2.8 MEGAN model parametrisation

Emissions of VOCs (E, nmol m^{-2} s^{-1}) were calculated according to equation (4) as described in Guenther et al. (2012) with a model algorithm parameterized with an intensity of PAR and air temperature (T):

$$E = BEF \cdot \gamma \cdot \Delta \cdot LAI \cdot CE$$

$\qquad$ (Eq. 4)

where basal emission factor (BEF) was estimated separately for sun and shade shoots of representative spruce trees at fixed standard conditions of PAR (1 000 µmol m^{-2} s^{-1}) and T (30 °C) (Guenther et al., 1995). Emitted BVOCs were sampled on desorption tubes,

coupled with gas-exchange measurements of CO_2 assimilation rate and stomatal conductance, and then detected by gas chromatography coupled with mass spectrometry (HP5890; Hewlett-Packard, Palo Alto, CA, USA). Only current-year shoots were measured. See Esposito et al. (2016) for details. Sun shoots from the upper part of the canopy were considered to emit 2.72 nmol m^{-2} s^{-1}, whereas the emission rate for shade shoots from the lower part of the canopy was set at 0.55 nmol m^{-2} s^{-1} (Esposito et al., 2016). LAI is the leaf area index estimated using a LI-2200 plant canopy analyser (LI-COR, USA), CE (= 0.57) is a constant that sets the emission activity to unity at standard conditions for the MEGAN model, and γ is an emission activity factor that accounts for emission changes due to the variations of light intensity and temperature from standard conditions. For details see Fares et al. (2013c).

4.2.9 Flux calculation at Castelporziano

Fluxes of BVOCs were calculated similarly as at Bílý Kříž with some differences regarding to Inverse Lagrangian Transport Model variables input. All the BVOCs measured as within-canopy concentration gradient were considered as highly reactive within a lifetime of 120 s. Standard deviations of vertical wind velocity (σ_w) for both canopy and soil level heights were averaged from high-frequency data measured.

4.2.10 PTR-MS experimental setup and measurement at Castelporziano

Measurements of BVOCs with PTR-MS, a quadrupole version, was conducted at the Castelporziano experimental station in the periods of 8.–16.1. 2014 and 22.7.–7.8. 2014. The PTR-MS was operated at a drift pressure of 2.18 mbar. During a winter campaign, gradient measurement of BVOC concentrations was established at five heights (1, 7, 12, 15, and 19 m above the soil). The air sampling was switched to the next level every 6 minutes. Unheated Teflon sampling lines were the same length for all gradients. Reaction time was 100 μs and H_3O^+ ions were used as the primary ion source. A complete cycle was repeated every 30 minutes. Data were logged into the computer using PTR-MS controller programme developed by Ionicon (Austria). Calibration was performed six times during the campaign (Apel Riemer Environmental., Broomfield, CO, USA). Calibration cylinder contained 11 VOC species: methanol, acetaldehyde, acetone, isoprene, methyl-vinyl-ketone, benzene, toluene, xylene, α-pinene, trans-2-hexenal and cis-3-hexenol, each of

almost 1 ppm concentration (Table 3). The VOC species were diluted with pure air to reach realistic ppbv levels. After the calibration, zero air was led to pass to PTR-MS in order to subtract the instrument noise. Normalized sensitivities were calculated as described in Taipale et al. (2008) to eliminate the effect of humidity.

Table 3: Content of calibration cylinder

Compound	m/z	concentration [ppbv]
Methanol	33	941
Acetaldehyde	45	993
Acetone	59	961
Isoprene	69	892
Methyl vinyl ketone	71	862
Benzene	79	969
Toluene	93	951
Xylene	107	268
α-pinene	137	980
trans-2-hexenal	99	940
cis-3-hexenol	101	988

For the summer campaign the first half hour gradient levels at the same heights as in winter were measured. Moreover, for the second half hour, the eddy covariance technique was deployed. It is assumed, that one cycle of consequent canopy profile and eddy covariance measurements were was recorded simultaneously.

For determination of instrumental noise, zero air from cylinder was passed to the PTR-MS and the zero point was determined. For determination of other compounds than those presented in the calibration cylinder, a transmission curve was built and the zero point was determined and subtracted from the spectra. The equation derived out of the transmission curve was used to calculate the concentration of compounds not presented in the calibration cylinder. As an example, the transmission curve for 4.8.2014 calibration with the subtracted zero point is shown (Fig. 11).
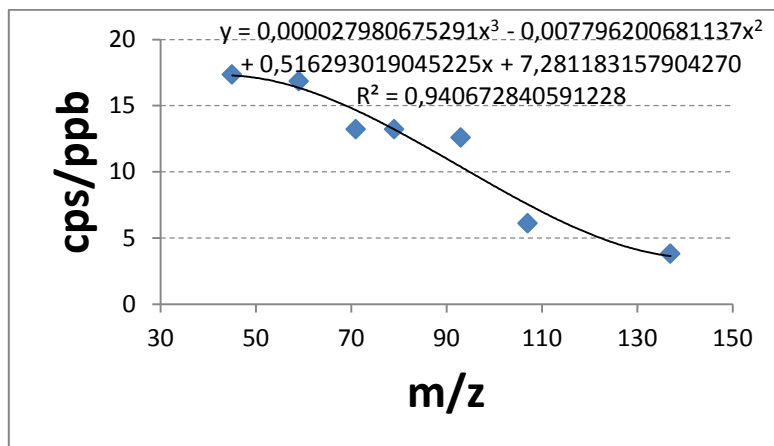
Fig. 11 Transmission curve with equation for other BVOC species calculation. cps –
counts per second.

In case of spikes, data 10 times higher than the standard deviation were deleted for 2
hours lag windows. Uncertain data during the first two minutes after the switching of the
valves were removed to correct for the memory effect. It is assumed again, that one cycle of
consequent canopy profile measurement was recorded simultaneously. Final values are in
30 min resolution.

4.2.11 Environmental parameters measurement at Castelporziano

Meteorological sensors were installed at canopy level (14 m) onto a 19 m high tower.
Relative air humidity, air temperature, global radiation, precipitation were measured every
minute and averaged at 30-min intervals with a Davis vantage pro meteorological station
(Davis Instruments, Hayward, CA, USA). A sonic anemometer Gill HS-50 (Gill,
Instruments, Lymington, UK) was used to instantaneously measure wind speed and
direction.

Ozone concentrations were measured using a UV photometric ozone analyser 49i
(Thermo Scientific, Waltham, MA, USA), with a precision of 0.5 ppbv. Measurement
heights were 19.7 m (above canopy), 14.9 m (canopy level) and 2.4 m (soil level). Air was
sampled using separate sampling lines (20 m long Teflon tubes, with 4 mm inner diameter)
through which air flowed continuously to avoid any memory or surface effects. To avoid
contamination and flow problems, Teflon filters (PFA holder, PTFE membrane, 2 μm pore

size) were installed at the sampling inlets and replaced every two weeks. A custom-made valve system sampled ozone sequentially for 6 min at each measuring height. Data collection and sampling system control were performed using a data logger CR3000 (Campbell Scientific, Shepshed, UK).

5 RESULTS

5.1 Bílý Kříž

5.1.1 Eddy covariance measurement

Diurnal courses of environmental variables and VOC fluxes estimated using the eddy covariance technique coupled with PTR-TOF-MS detection are summarized in Figs. 12 and 13. Air temperature daily maxima reached about 26 °C during the campaign. However, on the last day of the campaign the temperature dropped suddenly due to rainy conditions. Vertical wind velocity was enough to allow eddy covariance measurement, especially during the day. Methyl ethyl ketone (MEK; m/z 73.065), MTs (m/z 137.134) and short-chain oxygenated compounds showed significant diurnal fluxes characterized by significant daytime emissions and mild night time depositions. In contrast, benzene (m/z 79.053) and toluene (m/z 93.071) showed different flux patterns. Formaldehyde (m/z 31.003) evinced emissions during the central hours of the day. Methanol (m/z 33.033) emissions peaked during daylight hours, while substantial depositions were observed during the night. Acetaldehyde (m/z 45.033) and formic acid (m/z 47.026) emissions decreased around noon hours with mild depositions during the night.

Deposition of acetic acid (m/z 60.047) was observed during the night time and a peak above the detection limit before noon. On the contrary, in the afternoon fluxes ranged around the detection limit. As much as 0.28 nmol m^{-2} s^{-1} was the maximum flux throughout the whole campaign. Isoprene and MBO (both at m/z 69.067) maximum emission of 1.6 nmol m^{-2} s^{-1} was registered with daily average emission of 0.77 nmol m^{-2} s^{-1}. Small deposition during the early morning hours was observed. Oxidation products of isoprene - methyl vinyl ketone (MVK) and methacrolein (MAC) both at m/z 71.049 showed significant emissions only at noon hours. MEK and butanal (both at m/z 73.065) were in deposition during the night and emitted during the daytime and evening hours. The sum of MTs (m/z 137.134) showed maximum fluxes around noon with daily mean maximum of 1.29 nmol m^{-2} s^{-1} and a maximum for the overall campaign of 2.03 nmol m^{-2} s^{-1}. Deposition of total MTs was not observed throughout the whole campaign.

Daytime emission and night time deposition of acetone and propanal (m/z 59.049) was observed. Significant flux of benzene (m/z 79.053) was not observed. Conversely, toluene (m/z 93.071) had significant emissions during the daytime, peaking at 09:00 with a consequent flux decrease up to 18:00. A small peak in the decreasing flux was observed around 15:00.
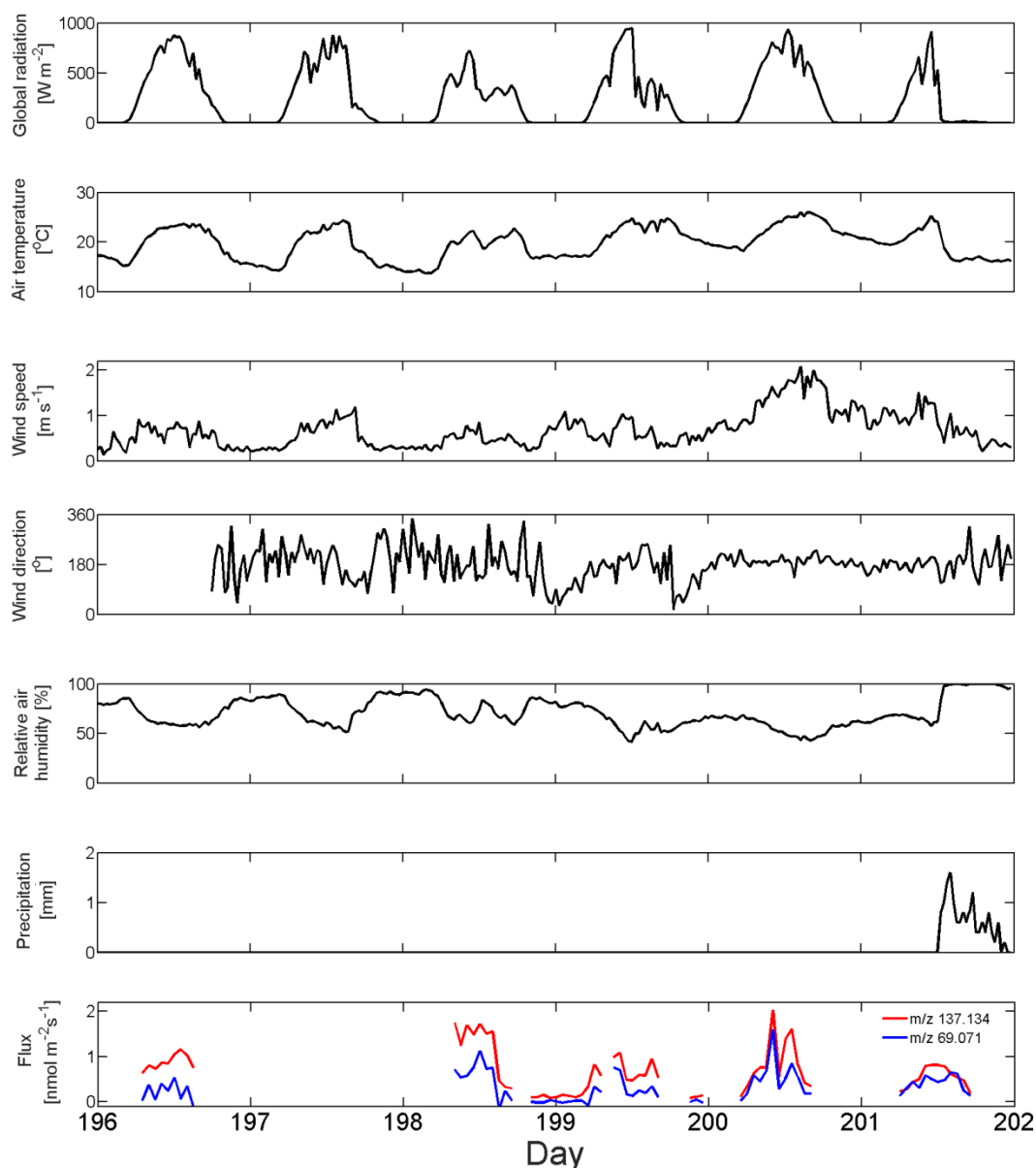

Fig. 12: Environmental variables at the time of the eddy covariance campaign on July 15–20, 2014 together with monoterpenes (m/z 137.134), and isoprene plus 2-methyl-3-buten-2-ol (m/z 69.071).
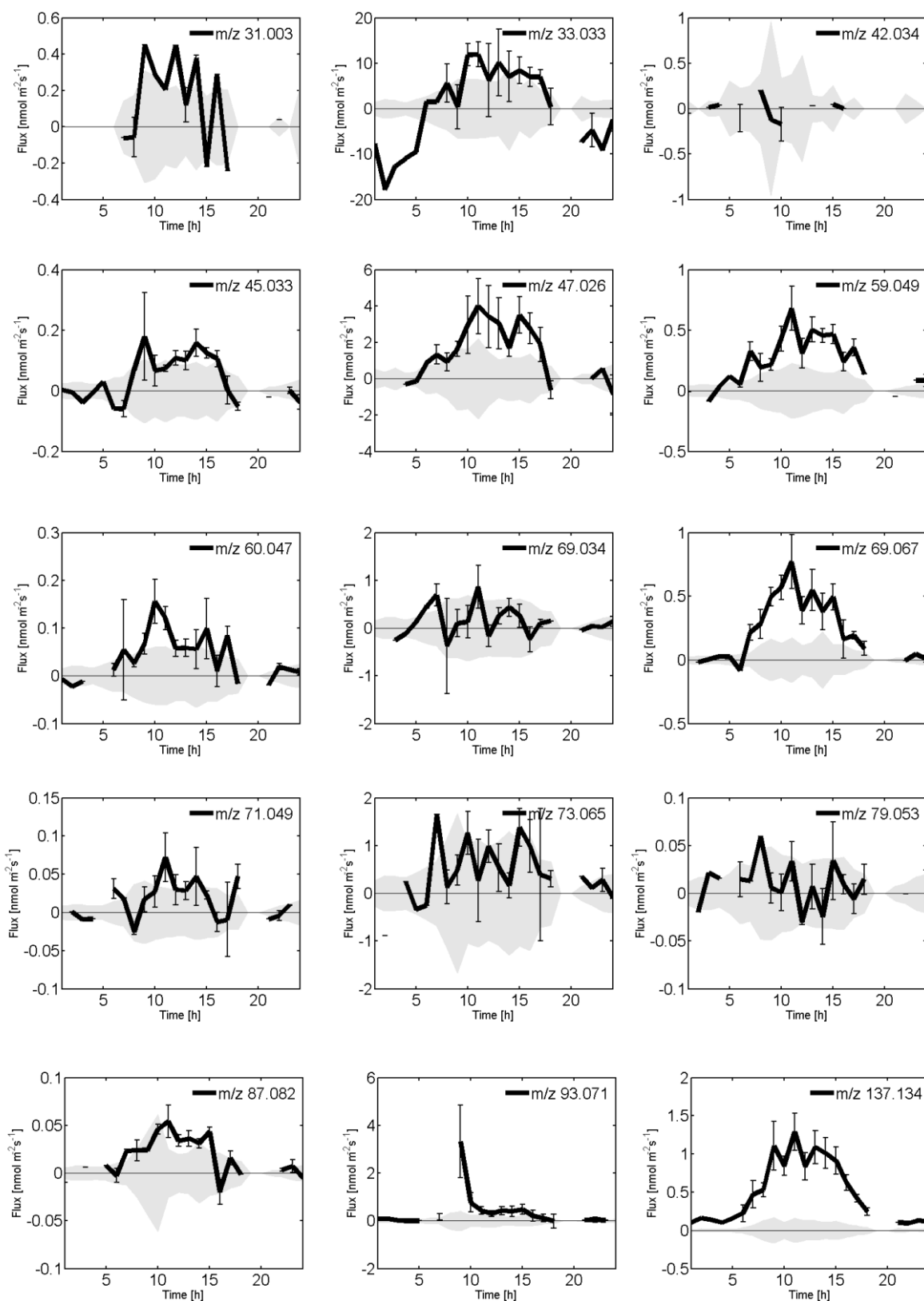
Fig. 13: Diel fluxes of volatile organic compounds at Bílý Kříž experimental forest covered by Norway spruce trees. Measured by the eddy covariance technique coupled with PTR-TOF-MS detection. Mean values originate from previous hour dataset. Means and standard deviations (vertical error bars) were estimated for the period July 15–20, 2014 (n = 6). The grey area represents the random error. Mass-to-charge ratio $(m/z + 1)^+$ notation is: 31.003 = formaldehyde, 33.033 = methanol, 42.034 = acetonitrile, 45.033 = acetaldehyde, 47.026 = formic acid, 59.049 = acetone and propanal, 60.047 = acetic acid, 69.034 = furan, 69.067 = isoprene and 2-methyl-3-buten-2-ol, 71.049 = methyl vinyl ketone and methacrolein, 73.065 = methyl ethyl ketone and butanal, 79.053 = benzene, 87.082 = 2-methyl-3-buten-2-ol, 93.071 = toluene, 137.134 = monoterpenes. Presumable interferences with other compounds are discussed in the discussion section.

In the whole spectra other compounds peeking above the detection limit were identified: m/z 41.039 – C_3H_5 compounds, m/z 43.018 - protonated ketene, m/z 57.034 – methyl ketene, m/z 57.046 – C_3H_5O compounds, m/z 57.070 – butane, m/z 75.045 – acetic acid methyl ester and formic acid ethyl ester and m/z 87.044 – $C_4H_7O_2$ compounds (data not shown). Molecular formulas are related to specific compounds as shown in supplement by Müller et al. (2016).
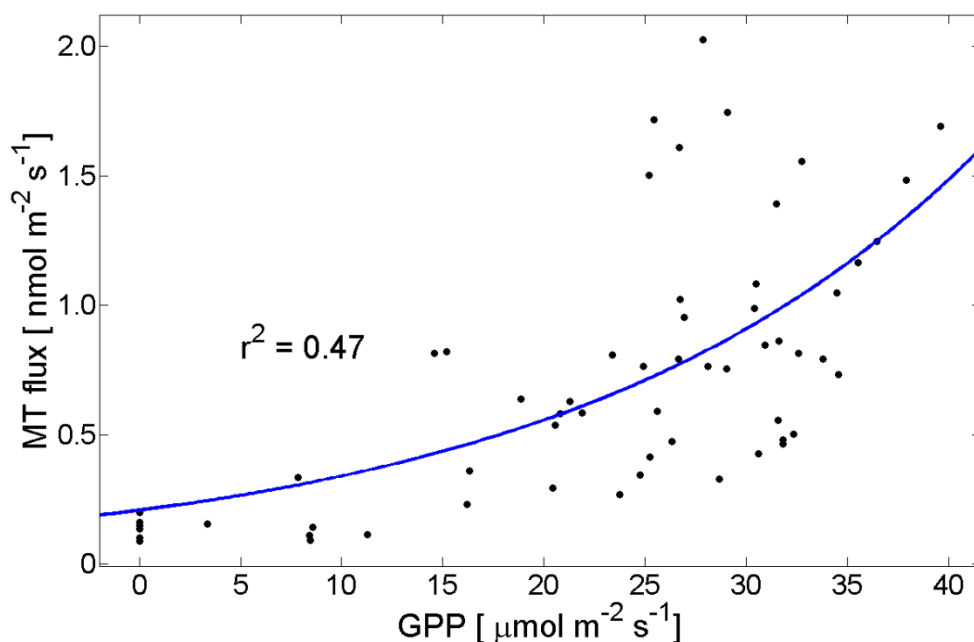
Fig. 14: Relationship between ecosystem gross primary production (photosynthetic CO_2 uptake; GPP) and a flux of total monoterpenes (MT flux) during the time of the eddy covariance campaign (15–20 July 2014). The exponential function fitted to flux data is $y = 0.2135 \cdot e^{0.04831 \cdot x}$ ($r^2 = 0.47$; $p < 0.01$).

A close exponential relationship ($p < 0.01$; $r^2 = 0.47$) was found between photosynthetic CO_2 uptake, represented by ecosystem GPP (gross primary production), and MT emission rate (Fig. 14). The carbon fraction from GPP released back to the atmosphere (carbon loss) in the form of BVOCs is shown in Fig. 15. The mean fraction of daytime (06:00–17:00) carbon loss was approximately 0.3% of GPP with maxima peaking at 1.5% of GPP. Among all BVOCs, MTs and methanol were contributing most (by 51% and 25%, respectively) to the loss of assimilated carbon. In contrast to MEK (8.6%), acetone (6%), and isoprene+MBO (7.4%), the contributions of MVK and acetaldehyde among other BVOCs were below 1%.
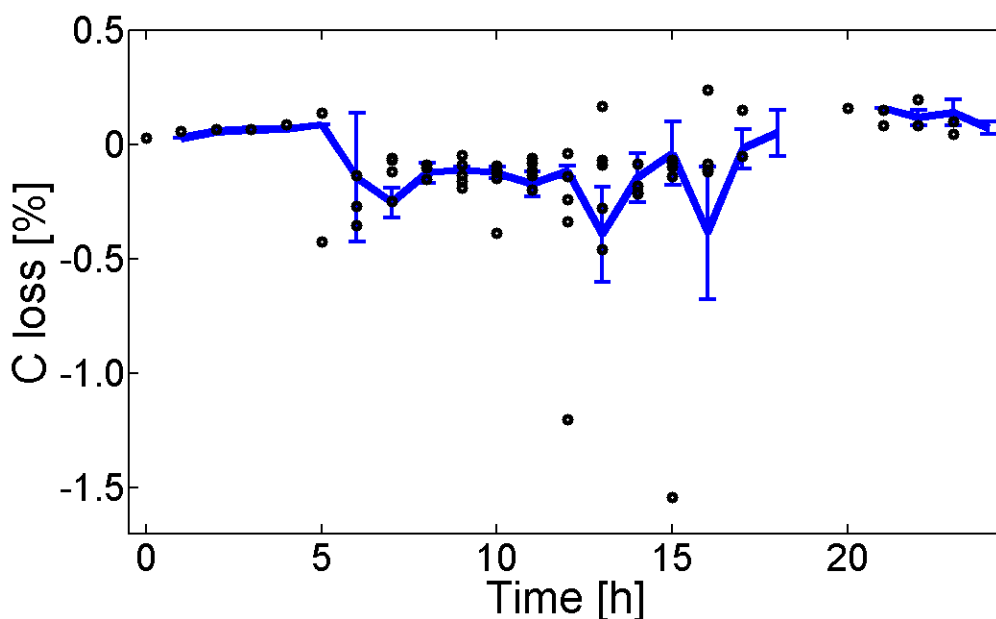
Fig. 15: Diurnal pattern of assimilated carbon loss (C loss) from gross primary production due to BVOC emissions. Blue line represents the mean value, error bars are standard deviations. Highest portion to the loss of assimilated carbon belong to monoterpenes (51%) and methanol (25%) followed by methyl ethyl ketone (8.6%), acetone (6%), and isoprene + 2-methyl-3-buten-2-ol (7.4%), the contribution of methyl vinyl ketone and acetaldehyde were below 1% among other BVOCs.

5.1.2 MT fluxes modelled by ILTM and MEGAN

Estimated fluxes show bell-shaped hourly behaviour of flux dynamics (Fig. 16), which is consistent among all monoterpenes measured and is consistent with a diurnal course of global radiation intensity and air temperature. The highest emissions were observed for α-pinene, followed by β-pinene in all years studied. On the contrary, fluxes of limonene, Δ-3-carene and camphene were substantially lower. Tricyclene fluxes are not shown, since its concentration was close to the detection limit of GC–MS system. The highest emissions were observed at around noon hours, while small deposition of MTs occurred early in the morning, suggesting that the canopy or soil may act as a sink for certain MTs such as α-pinene and limonene. Boundary layer dynamics are shown in Fig. 18.
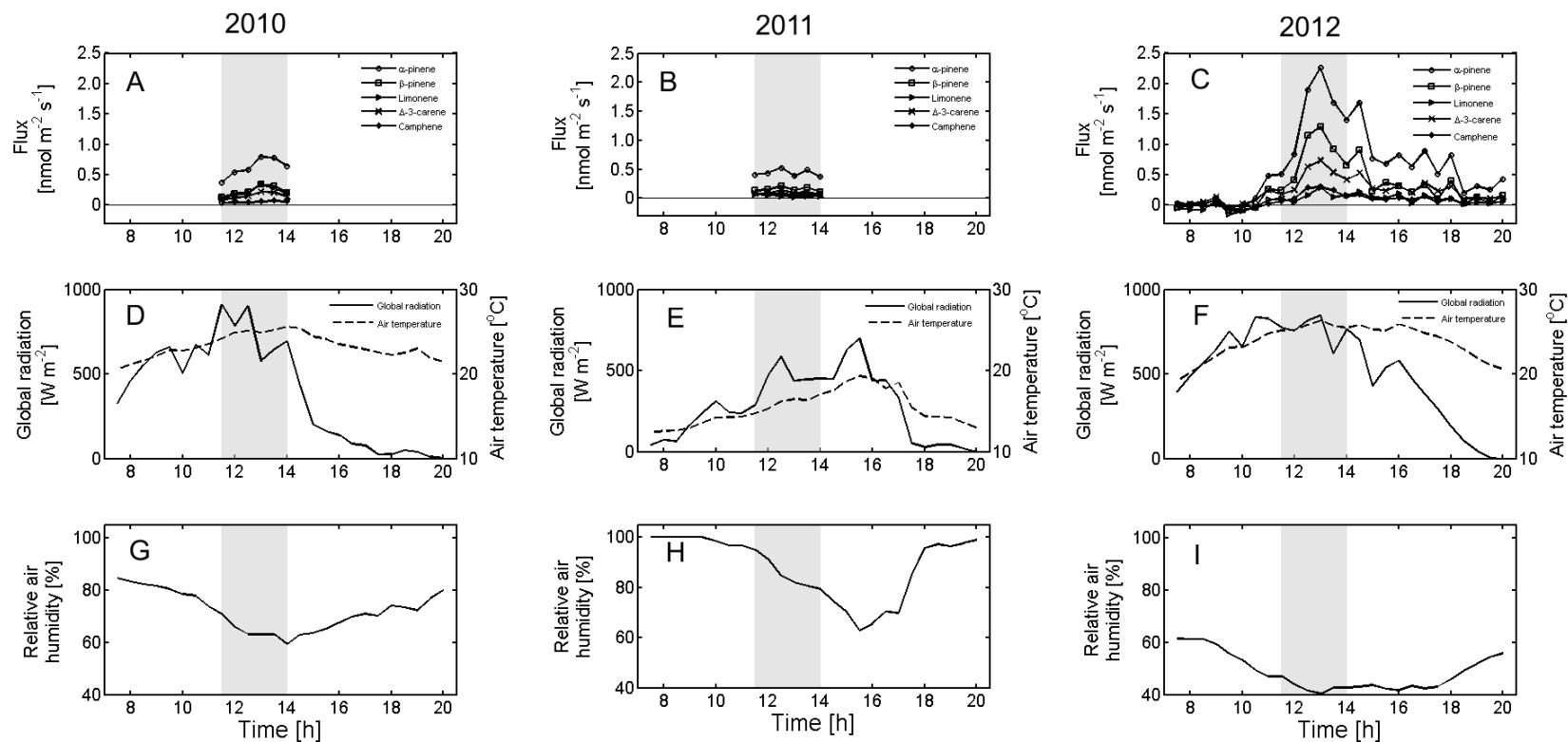
Fig. 16: Diurnal fluxes of different monoterpenes in mountain Norway spruce forest (A–C) and environmental variables (D–I) during measuring campaigns in 2010–2012. Monoterpene fluxes were modelled by Inverse Lagrangian Transport Model on the base of monoterpene within canopy concentrations profiles.

Comparison of MT fluxes in three consecutive years revealed high variability (Fig. 16). Surface plot of α-pinene showing concentration along the vertical profile throughout the day is shown in Fig. 17. Highest concentration was observed at central hours of a day and at the evening. Evening concentration burst is attributed to the boundary layer shrinking (Fig. 18).
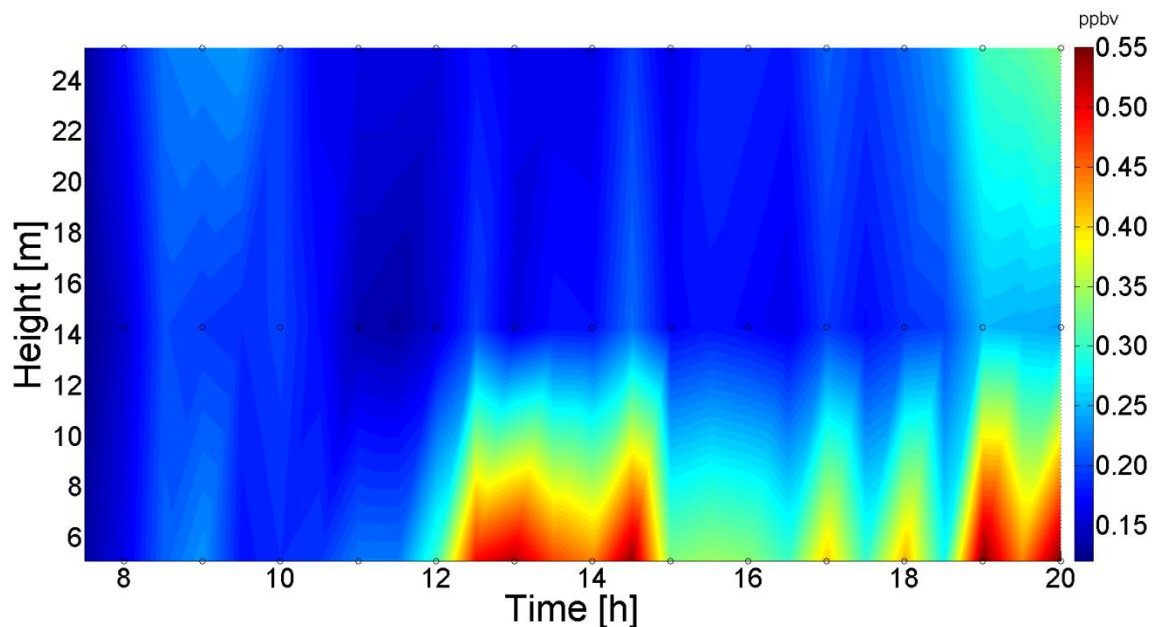

Fig. 17: Concentration of α-pinene throughout the day of August 2, 2012.

To investigate how individual environmental drivers control MT emissions, principal component analysis (PCA) of a whole dataset was processed (Fig. 21). Monoterpenes as α- and β-pinene, limonene and camphene seem to be influenced more by radiation conditions rather than by temperature which on the other hand affected considerably the emission of Δ-3-carene. The effect of net ecosystem exchange of CO_2 (CO_2 flux) on MT emissions was found as relatively minor.
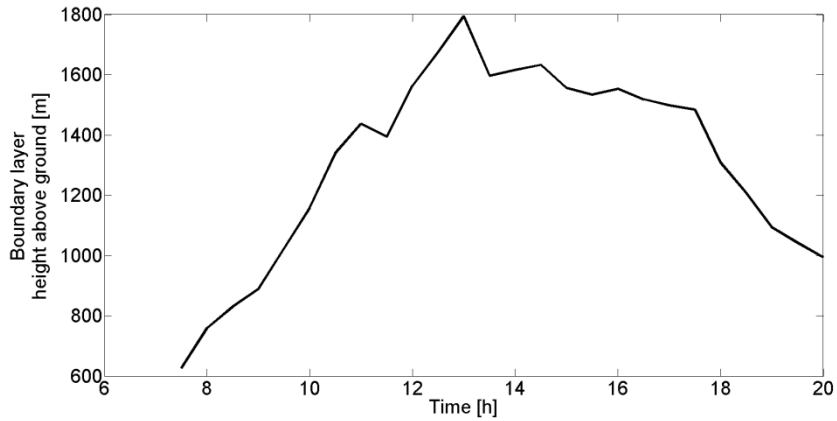
Fig: 18: Boundary layer height calculated for August 2, 2012, corresponding thus with Fig. 16C and Fig. 17.

This variability is explained by the differences in meteorological conditions among the years. Average temperatures in 2010, 2011, and 2012 were 5.68 °C, 6.79 °C, and 6.48 °C, respectively (Table 4). High variability is also shown by MEGAN prediction (Fig. 20A), which reports high underestimation or overestimation of fluxes depending whether a single BEF value was used as opposed to different BEF values for sunlit and shade leaves. Large variability is also explained by interannual dynamics of fluxes (Fig. 16), strictly depending on meteorological conditions (Table 4).
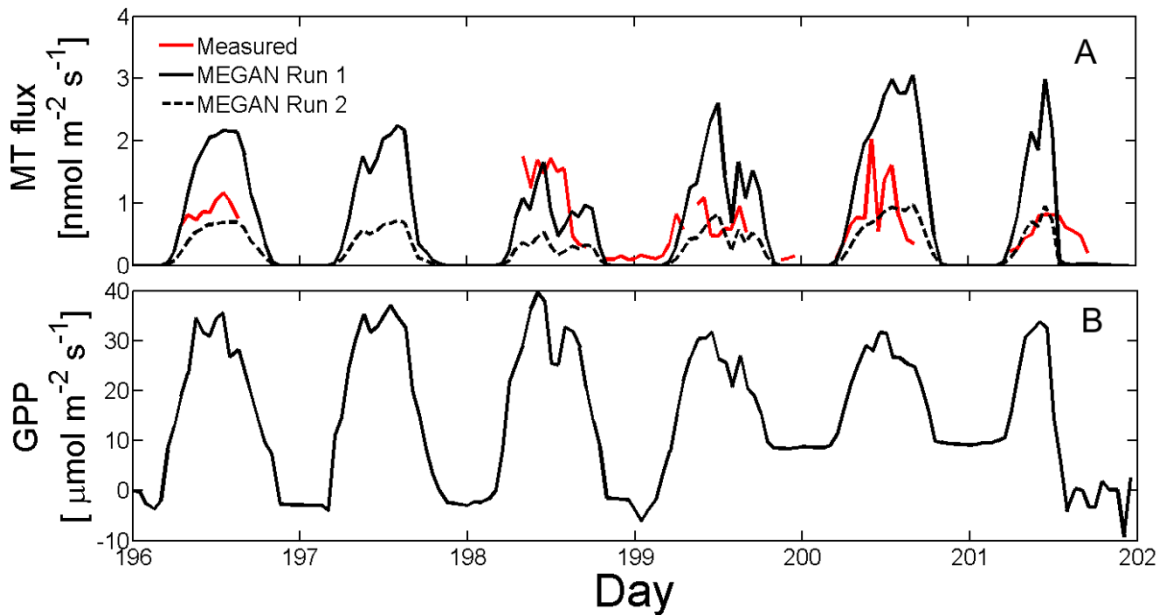
Fig. 19A: Diurnal fluxes of monoterpenes (MT) as measured by the eddy covariance technique (red line) during 15–20 July 2014 and modelled by MEGAN for the same period. The same basal emission factors for both sun and shade needles (2.72 nmol m^{-2} s^{-1}) were considered in MEGAN Run 1 (thin solid line), whereas these were 2.72 nmol m^{-2} s^{-1} and 0.55 nmol m^{-2} s^{-1} for sun and shade needles, respectively, in MEGAN Run 2 (thin dashed line). r^2 with excluded outliers (Run 1 and measured, linear) = 0.42, r^2 (Run 2 and measured, linear) = 0.43. Regression slope (Run 1) = 1.42 and (Run 2) = 0.46, without exclusion of outliers.

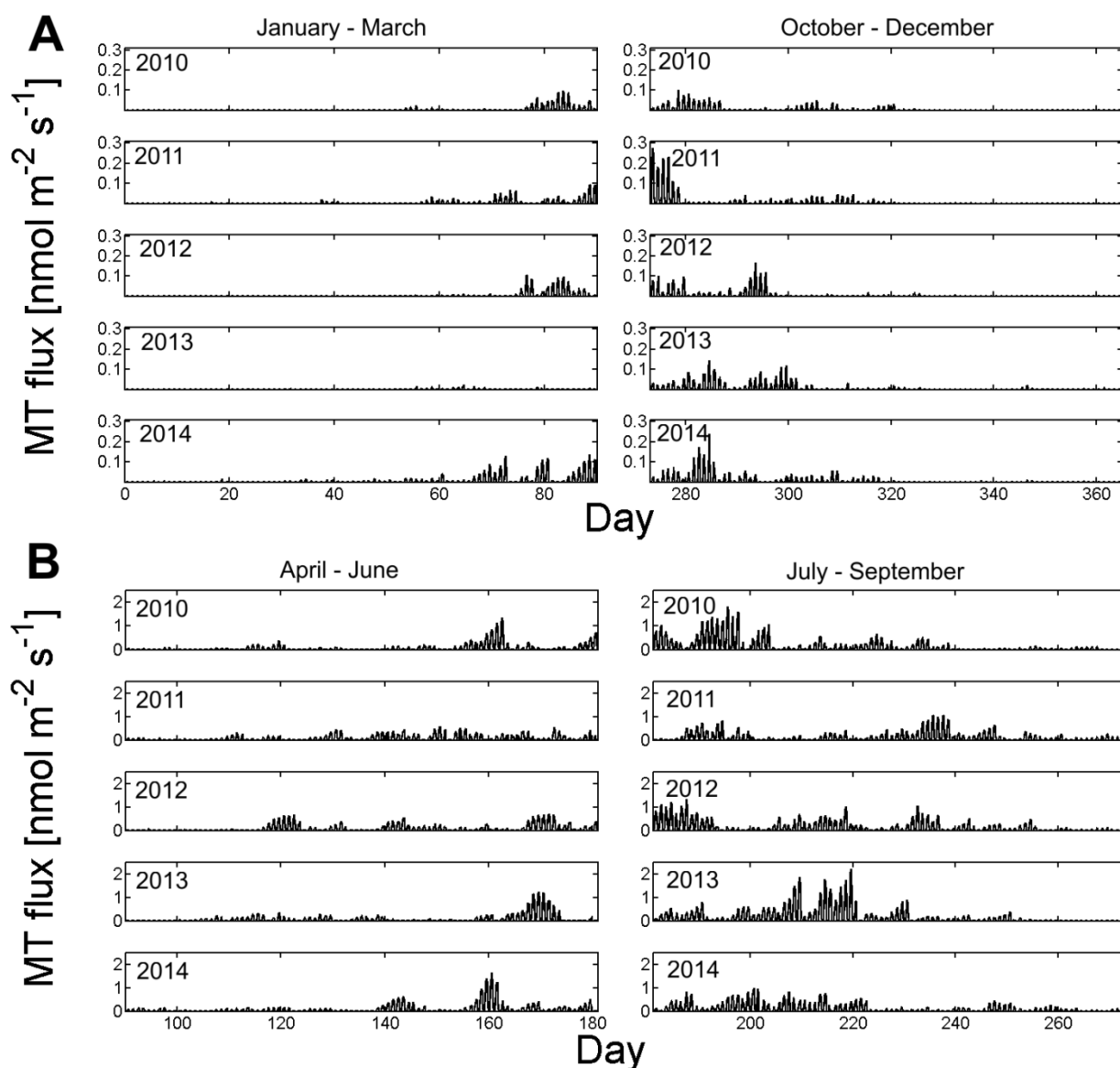Fig. 19B: Corresponding GPP for the same time period.

Fig. 20A: Out of season (January–March and October–December) monoterpene (MT) fluxes as modelled by MEGAN with basal emission factors 2.72 nmol m^{-2} s^{-1} and 0.55 nmol m^{-2} s^{-1} for sun and shade needles, respectively (Run 2). Each point is 1 h flux derived from previous hour's data set. Highest emissions are in October 2011 reaching up to 0.28 nmol m^{-2} s^{-1}.

Fig. 20B: Seasonal spring (April–June) and summer (July–September) MT fluxes as modelled by MEGAN. MEGAN shows the seasonal variation, with highest emissions slightly exceeding 2 nmol m^{-2} s^{-1}.

Table 4: Annual and summer (July–September) sums of monoterpene (MT) emissions estimated per unit of ground area by MEGAN model with the same basal emission factors for sun and shade needles (2.72 nmol m^{-2} s^{-1}; Run 1) and with basal emission factors 2.72 nmol m^{-2} s^{-1} and 0.55 nmol m^{-2} s^{-1} for sun and shade needles, respectively (Run 2). In addition, annual and summer mean air temperature (*T*air) and annual and summer sums of precipitation are presented.

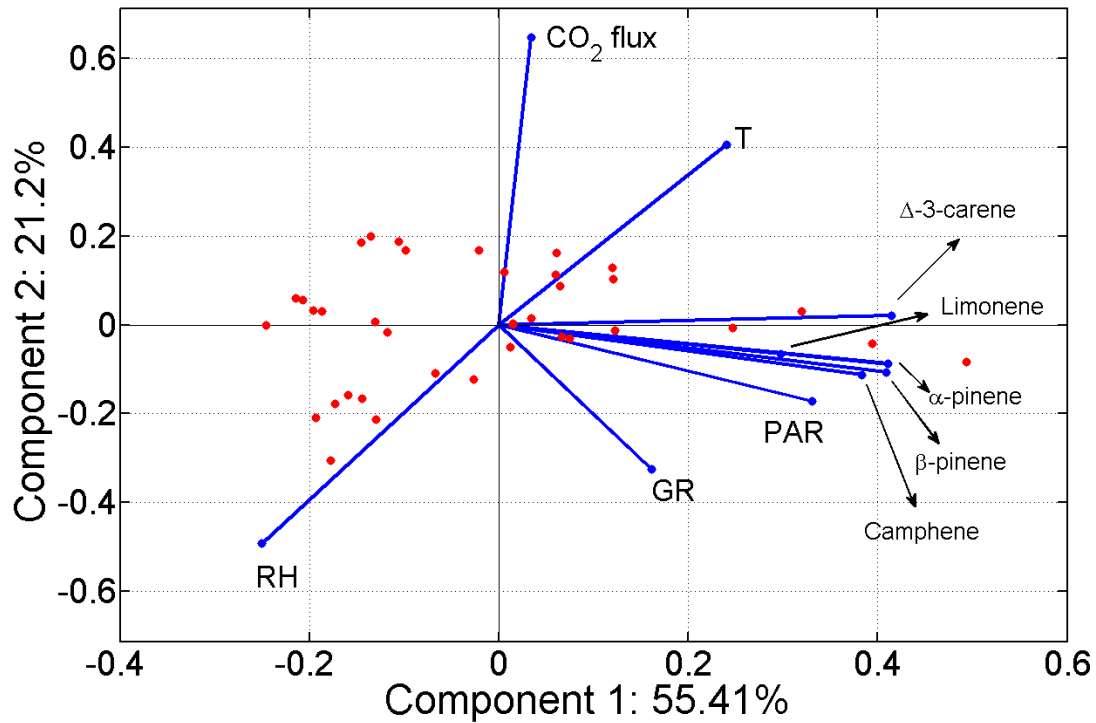| Year	Annual MT emission [mg m^{-2}]		Summer MT emission [mg m^{-2}]		Mean *T*air [^{o}C]		Precipitation [mm]	
	Run 1	Run 2	Run 1	Run 2	Annual	Summer	Year	Summer
2010	507.82	170.65	332.44	111.37	5.68	14.49	1519	584
2011	464.37	158.98	267.78	90.98	6.79	14.81	1011	397
2012	460.02	181.60	282.80	110.36	6.48	15.51	1065	247
2013	550.26	199.21	364.28	132.11	6.28	14.60	1043	291
2014	518.41	168.42	268.80	88.02	7.66	14.54	1199	395

Fig. 21: Principal component analysis based on the modelled data by ILTM (Fig. 16) with other environmental factors, in half-hour resolution. MT fluxes are loaded into the analysis as nmol m^{-2} s^{-1} units, other variables are as follows: CO_2 flux – CO_2 flux measured by eddy covariance [μmol m^{-2} s^{-1}], GR – Global radiation intensity above a canopy [W m^{-2}], PAR – sum of photosynthetically active radiation penetrating to the soil surface [J m^{-2}], RH – relative air humidity [%], T –air temperature [°C]. Limonene and α-pinene share part of the line.

5.1.3 Ozone and NOx

Diurnal concentration data of chosen months are shown in Fig. 22. Highest concentrations were measured during summer months (July), see Fig. 23, and lowest were during winter (January).
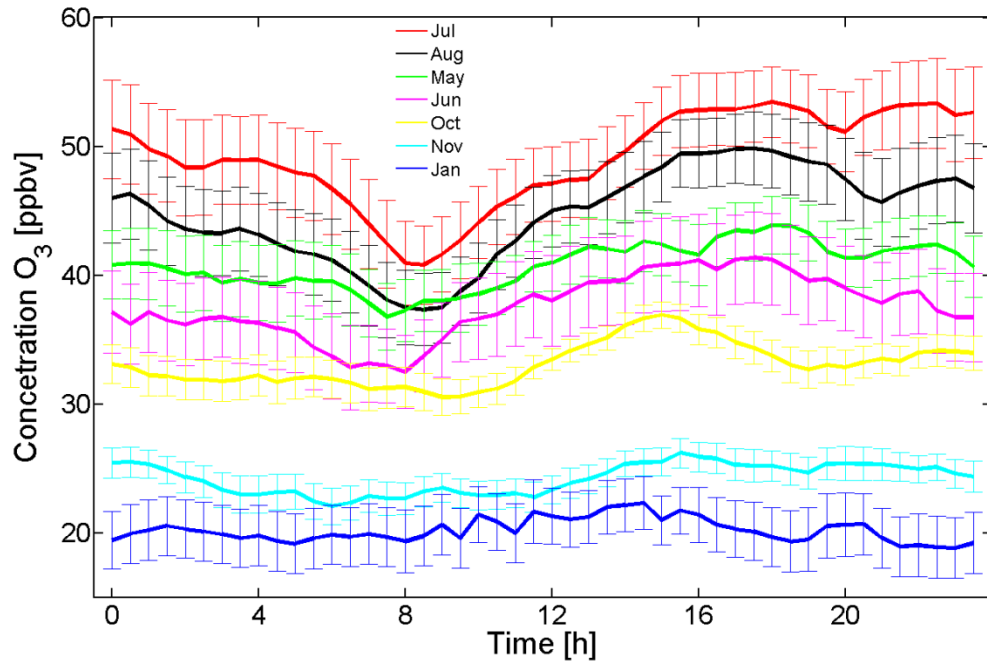

Fig. 22: Ozone concentration at chosen months measured at 15 m above the ground in 2013. Only months with sufficiently long datasets are shown. Data are averaged from half-hours measures. Overbars represents standard deviations.
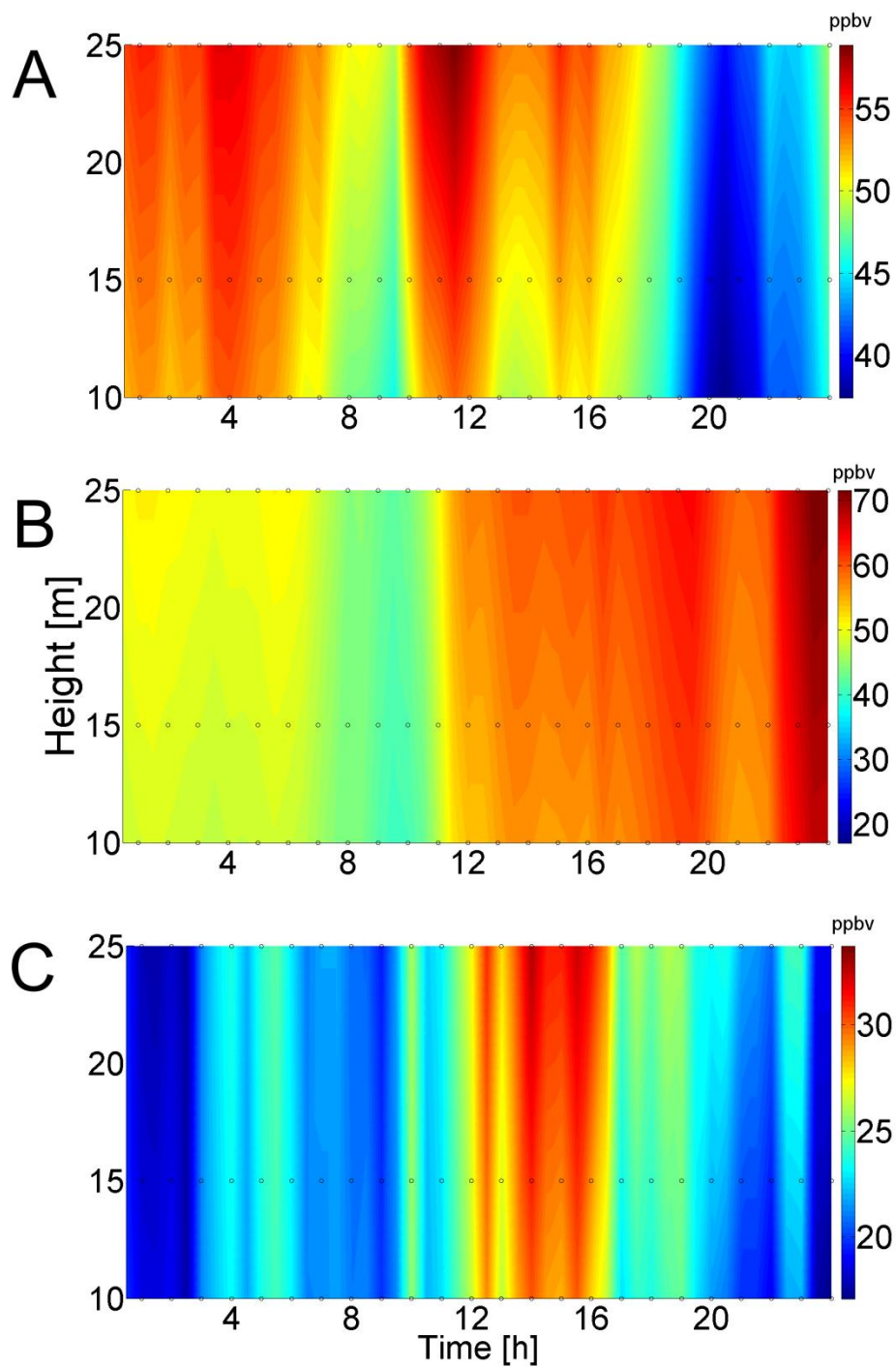
Fig. 23: Typical summer ozone concentration profile throughout the day of July 8, 2014 (A) and July 4, 2014 (B), which are representative days of clear sky conditions with no precipitation. On the contrary the day of July 10, 2014 (C) was cloudy day of lower air temperature than the two previous ones.

June and July 2013 concentration profile were modelled by applying principles of the ILTM approach. Results are shown in Fig. 24. The highest flux towards the forest, here expressed as negative, was during the noon. In the night at July the flux was reaching zero. Contrary to that, June night time flux was still negative.
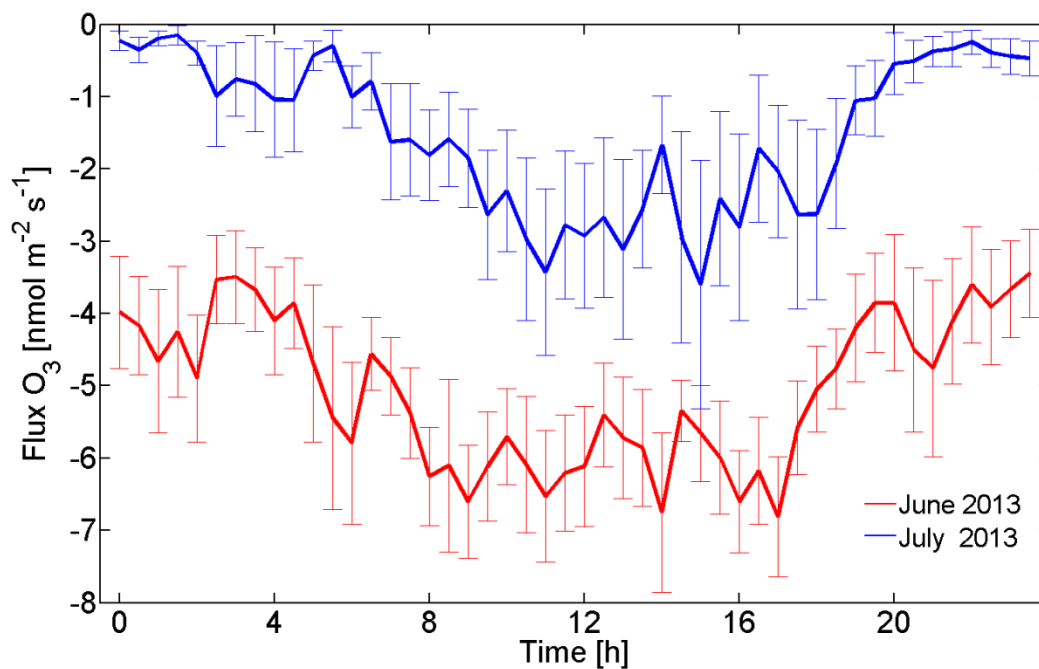
Fig: 24: Total ozone flux as modelled by ILTM in June and July 2013. Data are averaged from half-hours modelled values.
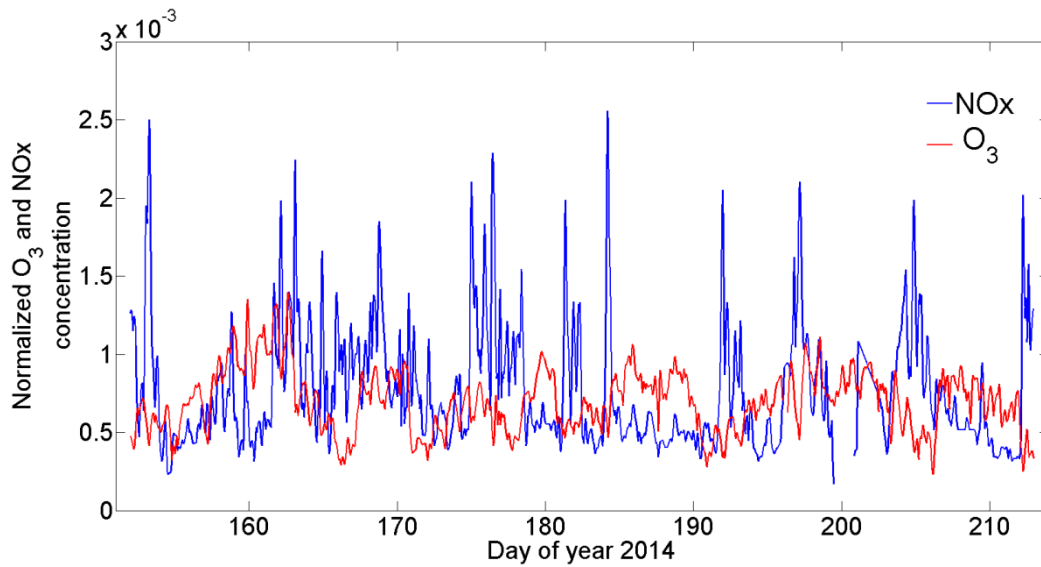
Fig: 25: Normalized concentration of ozone (O_3) and NOx ($NO+NO_2$), dimensionless. Sum of each data points, ozone and NOx concentration values are one.

Normalized summer 2014 (June–August) concentration data of ozone and NOx are shown in Fig. 25. Periods of relative high NOx concentration lead to low ozone concentration. Contrary to that high ozone concentration lead mostly to low NOx concentration (Fig. 26).
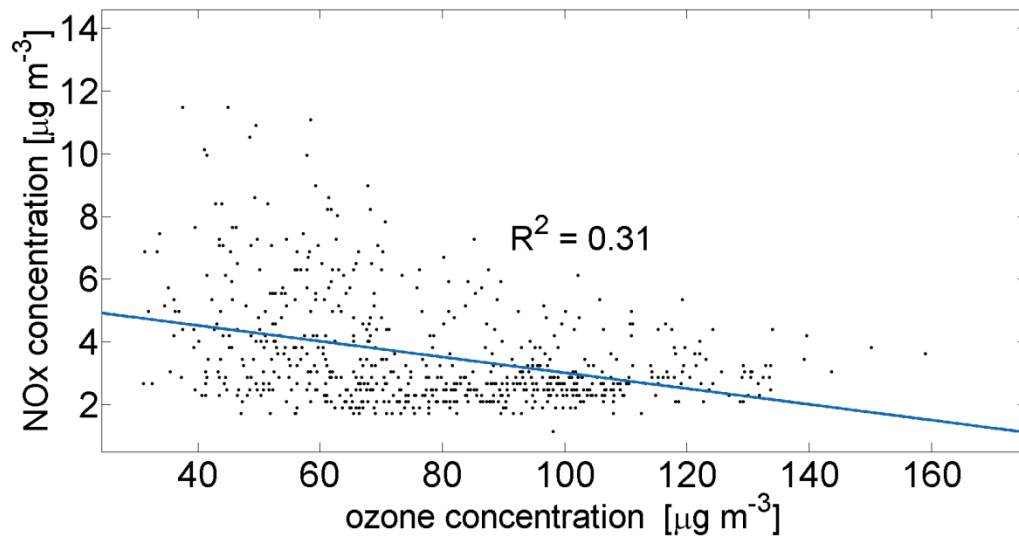
Fig. 26: Scatter plot of chosen periods from Fig. 25 with high or low NOx and ozone concentration.

5.2 Castelporziano, Italy

The main compounds emitted by the ecosystem were monoterpenes and isoprene in winter (Fig. 27). During the night a positive flux of isoprene and monoterpenes were observed, suggesting to be driven by air temperature in the case of monoterpenes. In case of isoprene flux there is no relevant explanation, since isoprene is strongly driven by photosynthesis and light.
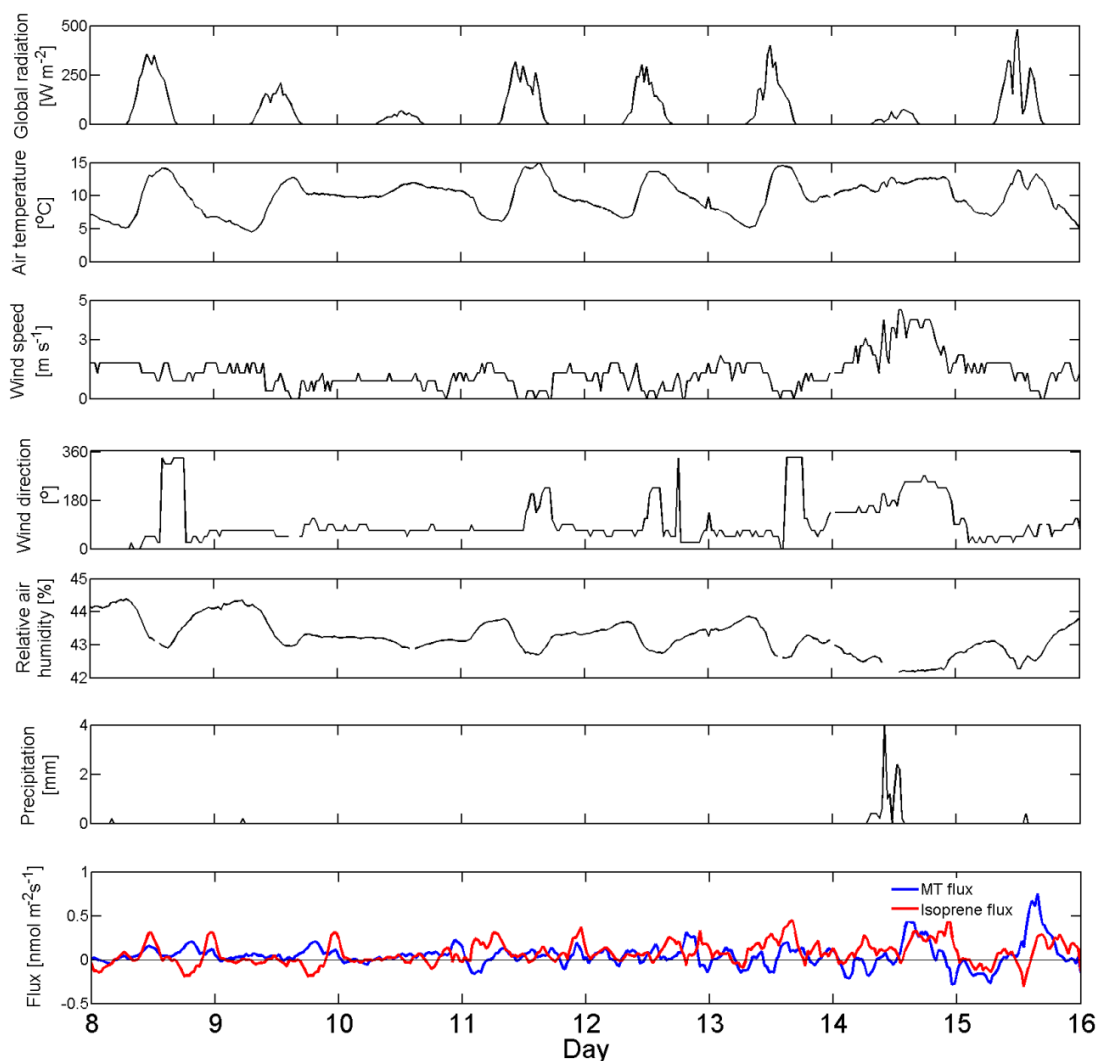
Fig. 27: Daily courses of environmental variables, monoterpene (MT), and isoprene fluxes during the time of winter PTR-MS campaign at January 8–16, 2014. Isoprene and monoterpene fluxes were modelled by Inverse Lagrangian Transport Model (ILTM).
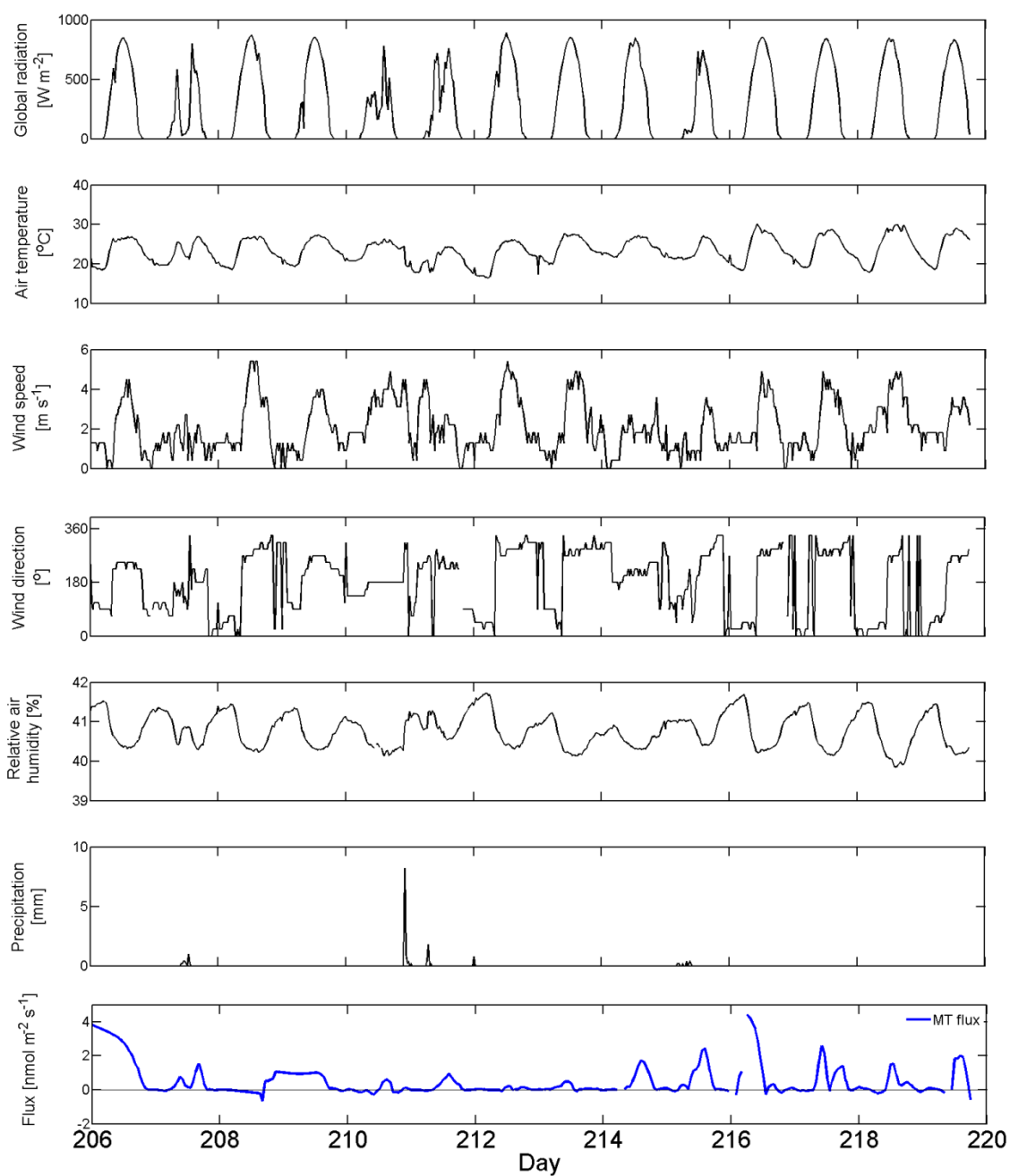
Fig. 28: Daily courses of environmental variables, smoothed monoterpene (MT) fluxes measured by eddy covariance during the time of summer PTR-MS campaign at 25.7–8.8, 2014.

Summer MT fluxes follow a typical bell-shaped curve with maxima peeking around noon (Fig. 28). Maximum fluxes during the whole summer campaign peeked around 4.56 nmol m^{-2} s^{-1} with mean value of 0.62 nmol m^{-2} s^{-1}. Maximal daily averaged fluxes peeked around 15:00 with 1.13 nmol m^{-2} s^{-1}. The relationship between the air temperature and MT flux was found (Fig. 29) for the summer field campaign. Moreover, the comparison between measured and calculated fluxes is shown in Fig. 30.
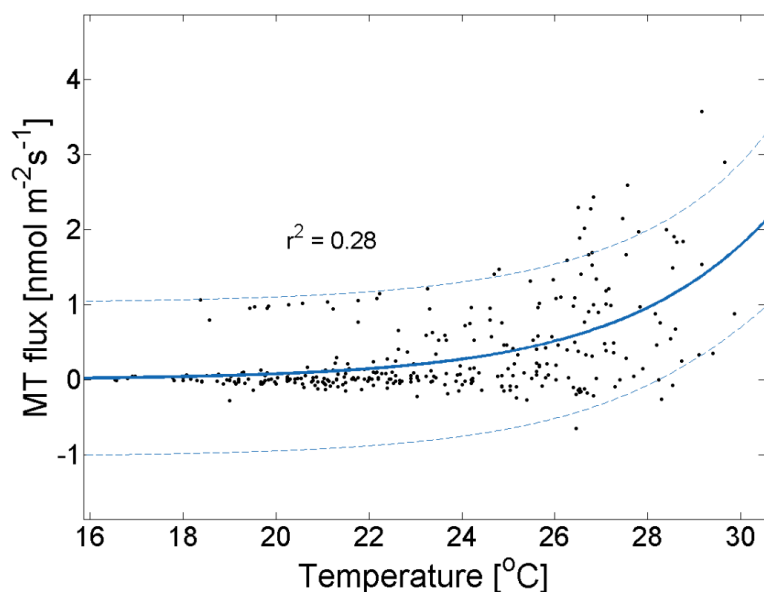
Fig. 29: Relationship between air temperature and MT flux with excluded outliers and 95% confidence bounds (dashed blue line) for summer campaign. The exponential function fitted to flux data is y = 0.000151·e$^{\,0.3127 \cdot x}$ (r^2 = 0.28; p <0.05).
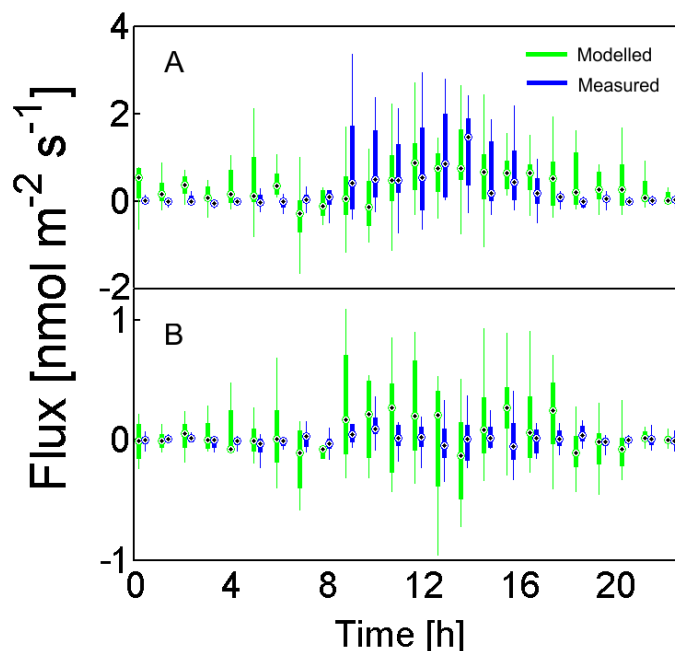
Fig. 30: Fluxes of monoterpenes (A) and isoprene (B) measured by eddy covariance technique (blue) and modelled by ILTM (green) in summer 2014 with standard deviations as thin coloured lines. Data are shown as mean values for the time of the PTR-MS campaign. Dots represent median values, boxes standard deviations, and lines out of box are minimum and maximum values.

Concentrations of aromatic AVOCs, toluene and benzene are shown in rose plot in Fig. 32. Location of Castelporziano experimental mast is within the red point in Fig. 31. Maximum values were 1.07 ppbv and 1.13 ppbv for benzene and toluene, respectively. Mean of toluene to benzene ratio is 0.7 with maximum value of 7.2. Thus, 92% of benzene and toluene emissions are attributed to exhaust emissions, whereas the remaining 8% are refuelling emissions. For separation between those two sources, a benzene to toluene ratio of 1.7 was applied, as suggested by Halliday et al. (2016).
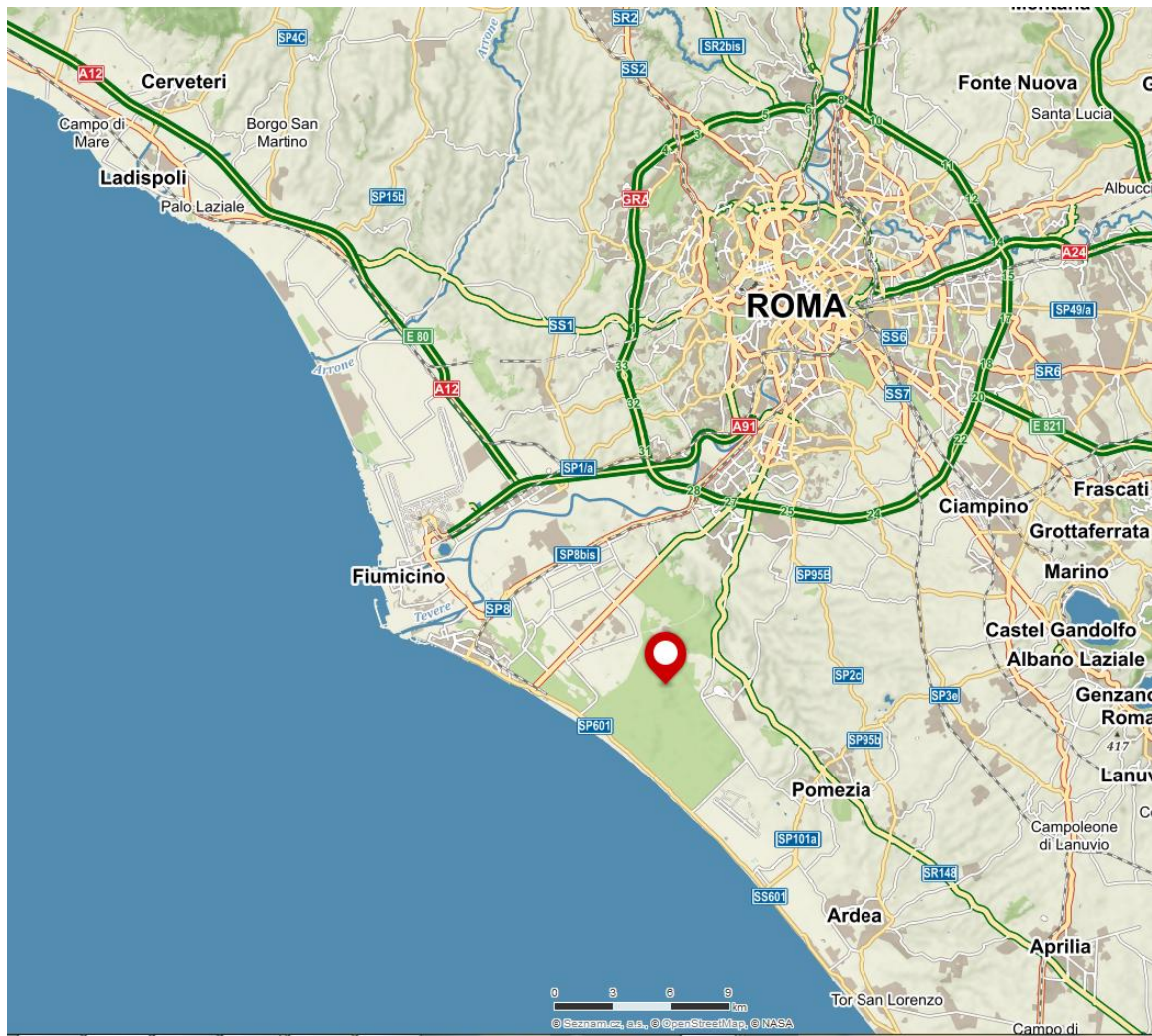
Fig. 31: Map of location of Castelporziano experimental mast, shown as red point. Source: Mapy.cz
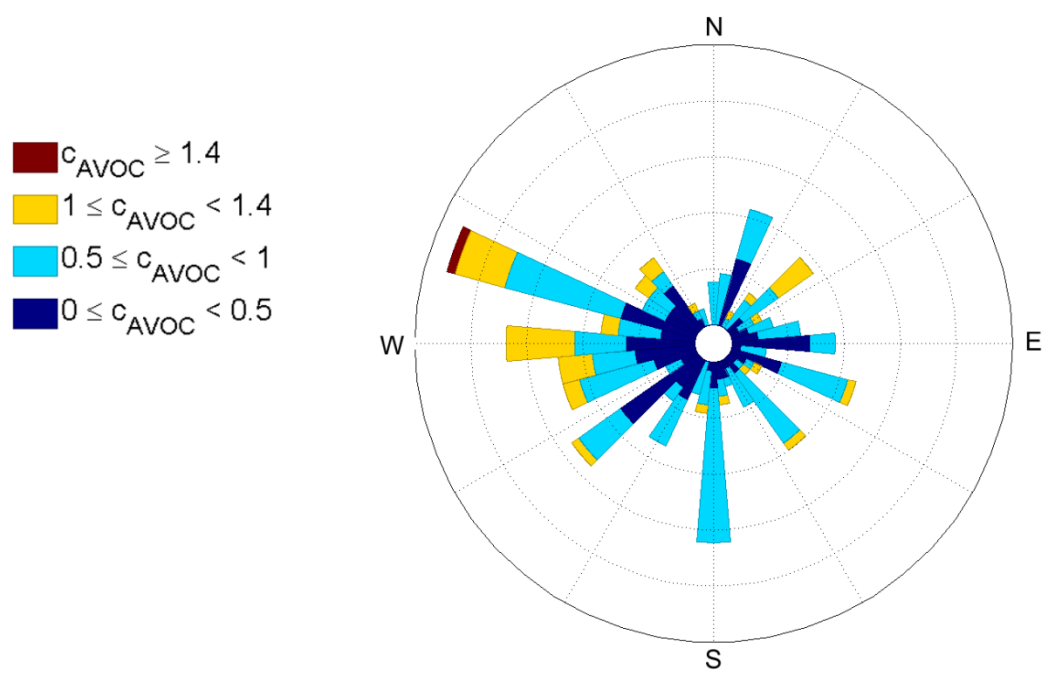
Fig. 32: Sector concentration of toluene and benzene together (m/z 93 and 79) shown as c_{AVOC} in ppbv coupled with wind direction for summer PTR-MS campaign. Both concentration and wind direction dataset originates from hourly dataset. Mean values are 0.22 ppbv and 0.43 ppbv for benzene and toluene, respectively.

6 DISCUSSION

6.1 Bílý Kříž

6.1.1 MT emission and its relevance to GPP

Monoterpene fluxes measured using PTR-TOF-MS, showed a typical diurnal course peaking with maximum emission rate of 2.03 nmol m^{-2} s^{-1} at around noon. M/z 137.134 is considered to indicate pure MTs, and an interference with other compounds such as linalool is unlikely because fluxes of its fragments (m/z 155.147 and 95.088) were not detected. Deposition of MTs was not observed, however. Conversely, sesquiterpenes were not observed at all in this study. This likely was due to the shortness of their lifetimes, as well as the long residence time to reach the detector and heated PTFE lines, which alter the chemical reactions. A similar MT flux pattern has been observed in Bavarian spruce forests, with maximum daytime emission rates up to 2 nmol m^{-2} s^{-1} (Graus et al., 2006). MT fluxes were likely influenced by the substantial rainfall (totalling 19.2 mm) registered 2 days before the campaign. Such favourable conditions enable high stomatal conductance and intercellular CO_2 concentration leading to a high photosynthetic CO_2 uptake (Urban et al., 2012), as demonstrated by high GPP values even during the noon hours (Fig. 19A and 19B). In accordance with the hypothesis tested, a significant exponential relationship was found between MT emission and GPP (Fig. 14). The coefficient of determination indicates that 47% of the variance in MT emissions is predictable from the GPP. Moreover, PCA revealed close relationships of camphene, limonene, as well as α- and β-pinene with solar radiation intensity (Fig. 21), which is of course a variable closely related to plant photosynthesis (Baldocchi et al., 1988). On the contrary, Δ-3-carene flux is induced by both radiation and air temperature. Ghirardo et al. (2010) had reported that newly synthetized, and thus light-dependent MTs, accounted for 34% of total MT emissions from bark and needles, with emissions of α- and β-pinene dominating. Inasmuch as the storage pools could be in needles, woody tissues under bark, and roots, we hypothesize that emissions from storage pools are driven by temperature under low light intensities or in darkness. In daytime conditions, emission drivers will be changing rapidly depending on the shading

and light availability within the canopy. This makes the light versus temperature dependency among MTs difficult to sort out.

The mean carbon fraction from GPP released back to the atmosphere in the form of BVOCs was approximately 0.3% while maxima were near 1.5% during daytime within the period investigated (Fig. 15). The loss of assimilated carbon was particularly associated with MT emissions (52% among other BVOCs). This accords with the findings of Seco et al. (2015), who reported the fraction of carbon lost to be 2% of GPP in broadleaved temperate forest within the central USA. In contrast to our study, isoprene was contributing the most to the loss of assimilated carbon (approximately 98% among other BVOCs measured), while MTs peaks were up to 0.8% of GPP. It also has been shown (Hakola et al., 2006; Holzke et al., 2006; Seco et al., 2015) that the carbon loss substantially increases during drought episodes to as much as 9% of GPP when vapour pressure deficit increases and CO_2 fluxes are substantially reduced.

6.1.2 Modelling of diurnal and annual MT emissions

Until now, only near-to-real time analyses for different MTs have been available, and even then with unrealistically low detection limits (Pallozzi et al., 2016). Therefore, a complete and precise separation of isobaric compounds (which the MTs are) was not possible. Here, we present real-time fluxes of individual MTs obtained on the basis of an ILTM approach. Daily mean values (± standard deviation) of static stability B (Eq. 2) were 0.20 ± 0.02 (2010), 0.56 ± 0.04 (2011), and 0.21 ± 0.04 (2012) and are in agreement with those reported by Weber (1998). A relatively high B value in 2011 evidences low horizontal wind velocity and high standard deviation of vertical wind velocity. MTs lifetime of 60 s was applied in ILTM (Warland and Thurtell, 2000), taking into account atmospheric oxidation capacity. Other authors report lifetimes for specific MTs of 80 s when only ozonolysis was taken into account or of less for very reactive VOCs (Wolfe et al., 2011). Thus, we assume that presence of other atmospheric oxidants, such as OH radicals, lead to slightly faster oxidation.

It has been shown that wet effluent diffusion denuder coupled with gas chromatography and mass spectrometry allows sampling of individual MTs within short

time intervals of 2–5 min and provides a suitable tool for determining concentrations of individual MTs (Křůmal et al., 2016).

Diurnal changes in MT concentrations reported by Yassaa et al. (2012) are in agreement with our results, with highest MT concentrations observed during the evening hours when the boundary layer starts to shrink (Fig. 18). Subsequently calculated MT emission rates (Fig. 16) are consistent with those determined for Norway spruce forest in Denmark by Christensen et al. (2000), with daytime average of about 1 nmol m^{-2} s^{-1}, maximum of 2 nmol m^{-2} s^{-1}, and domination by α- and β-pinene. Yassaa et al. (2012) reported the highest emissions for limonene, then α-pinene, β-phellandrene, β-pinene, 1,8-cineole, and Δ-3-carene. Relatively high daytime MT emission rates were observed by Noe et al. (2011) in hemiboreal mixed forest. These reached as high as 33 nmol m^{-2} s^{-1}, and the most abundant MTs were Δ-3-carene, α-pinene, and α-phellandrene. These emissions were measured, however, using enclosed branch cuvettes with an artificial air circulation.

In accordance with Bourtsoukidis et al. (2014b), we observed weak negative correlation between relative air humidity and MTs flux (Fig. 21). All in all, ILTM seems to be an interesting tool for deriving fluxes from concentration gradient for isomeric compounds. We cannot explain the slight overestimation of fluxes derived by ILTM, which is widely used (Karl et al., 2008; Alves et al., 2016), due to the lack of parallel measurement and modelling.

MEGAN was parameterized using the same BEFs for upper sun and lower shade needles (2.72 nmol m^{-2} s^{-1}) in Run 1, and then these parameters were set to 2.72 nmol m^{-2} s^{-1} for sun and 0.55 nmol m^{-2} s^{-1} for shade needles for Run 2 to investigate whether predictions of MT emissions are improved comparing to eddy covariance measurement. Both BEF values had been measured using enclosure cuvettes a week after the eddy covariance campaign (Esposito et al., 2016). BEFs had been estimated according to Wang et al. (2007) in shoots of representative trees of the footprint area exposed to an ambient CO_2 concentration of 400 μmol mol^{-1}, PAR intensity of 1,000 μmol m^{-2} s^{-1}, air temperature of 30 °C, and relative humidity of 50%. Generally, a huge variation of BEFs for Norway spruce in the range of 0.2–7.8 μg g$^{-1}_{dw}$ h^{-1} is reported across the literature (Hewitt and Street, 1992; Simpson et al., 1995; Wiedinmyer et al., 2004; Tarvainen et al., 2007; Bourtsoukidis et al., 2014a). In addition, BEFs exhibit significant seasonal

variability, as shown for ponderosa pine (Holzinger et al., 2006) or Norway spruce (Esposito et al., 2016), which is caused by ontogenetic/physiological stage, tree and leaf age, impact of different stressors, as well as incident variations in abiotic factors, and particularly temperature (reviewed in Niinemets et al., 2010).

MEGAN Run 1 overestimated MT emissions (Fig. 19A), especially during episodes characterized by high intensity of global radiation and air temperatures (i.e. days 196 and 199–201). Meanwhile, predicted and measured MT emissions were consistent during a cloudy day with reduced intensity of global radiation (day 198). Application of BEFs for sun and shade leaves (MEGAN Run 2) thus substantially improves the prediction of MT emissions under clear sky conditions. Both scenarios were unable to track rapid changes in MT emissions observed at day 200, however.

Seasonal variability (Fig. 20A, Fig. 20B) of modelled MT emissions is attributed to climate and temperature change and drought events. Strong seasonal variation has been well described by numerous authors (e.g. Hakola et al., 2006; Holzke et al., 2006), who have linked emission changes to synthase activity. Due to scarce summer rainfall, summer emissions during 2013 contributed most (greater than 66%) to the full-year flux budget in both MEGAN scenarios. In contrast, the highest summer precipitation in 2010 – which year had a very different rainfall distribution – also led to a high summer emission budget that contributed 65% to the yearly budget. The highest yearly average temperature was recorded in 2014, but the highest average summer temperature was not. Therefore, we found summer emissions to be 52% of the full-year emission budget (Table 4). This suggests that warmer periods outside of summer have a limited impact on annual emissions, whereas high temperatures in summer play a major role in determining MT emissions due to the exponential relationship between MTs and temperature. This view is in agreement with Huang et al. (2015). Looking to the future, it can be assumed that prolonged extreme drought events coupled with scarce precipitation could lead to larger annual emission budgets. I want to clarify, however, that the empirical formulation of MEGAN in this study did not include possible drought stress effects on emissions.

6.1.3 Abundance of other volatile organic compounds

We observed a significant flux of MBO at m/z 87.082 peaking during noontime hours. Similarly to Fall et al. (2001), who showed that there could be interference at m/z 69.067 due to the fragmentation of MBO with a possible abundance at 13–25% of total signal, we found the r^2 between m/z 87.082 and m/z 69.067 to be 0.62. This suggests that fragmentation of MBO could contribute to m/z 69.067 at our site. It is well known that isoprene and MBO are not accurately separable when using H_3O^+ as primary ions. Thus, a part of the flux found at m/z 69.067 is attributed to MBO (Fig. 13). In our experiments, the ratio of m/z 87.082 to m/z 69.067 flux is 0.055 when calculated using half-hour mean values for the entire data set. Nevertheless, as proposed by Karl et al. (2012), who did laboratory measurement with MBO standard, MBO fragments by 25% into m/z 87.082, thus it could be assumed that by multiplying m/z 87.082 by a factor of 4 we can roughly determine the maximum daily average value of MBO flux of 0.22 nmol m^{-2} s^{-1}. Thus, MBO flux could reach up to 29% of m/z 69.067 flux. To distinguish more precisely between MBO and isoprene flux, however, NO^+ primary ions would need to be used (Karl et al., 2012, 2014). For this reason, we show m/z 69.067 as the sum of MBO and isoprene, which should in theory be conserved (Karl et al., 2012). MBO emissions had been observed for the first time by Goldan et al. (1993) in a North American pine forest, and these emissions can be further enhanced by *Ips typographus* infestation. Harley et al. (1999) quantified MBO emissions from many spruce species (but not Norway spruce) and stated that MBO is emitted in huge amounts with a diurnal course similar to that of isoprene (Schade et al., 2000). Similarly to pine forests, MBO emissions in Norway spruce forests can be substantially increased by *I. typographus* infestation (Wiedinmyer et al., 2004), which is reported to be prevalent, too, in central European forests (FAO, 2009) and also was present during the field campaign (Krascsenitsová et al., 2013). Park et al. (2013) reported a significant flux of MBO (referred to there as m/z 87.077) in citrus orchard, where MBO m/z 87.077 mean daily flux occupied 26% of flux related to the sum of isoprene and MBO. In contrast to our finding, daytime deposition and night-time emissions were observed in the citrus orchard.

MBO has important implications for the atmospheric chemistry. In daytime, MBO reacts with OH radicals, ozone, and nitrate radical to produce acetone, aldehydes, formic

acid, as well as organic, carbonyl and peroxy nitrates (summarized in Finlayson-Pitts and Pitts, 2000). This affects atmospheric oxidative capacity, as discussed by Lamanna and Goldstein (1999) in relation to a ponderosa pine forest, as well as local photochemistry and atmospheric ozone formation, as shown in Scots pine dominated forests (Tarvainen et al., 2005). Quantification of MBO fluxes in other forest types and tree species is lacking, however, and therefore future research is essential.

Although Norway spruce generally is not considered to be an isoprene producer, and this view has been supported by chamber measurements on sun and shade shoots on the same spruce trees (Esposito et al., 2016), relatively high isoprene fluxes with maxima at about 1–1.5 nmol m^{-2} s^{-1} were, by contrast, measured by Graus et al. (2006). These contradictory results may suggest the existence of different Norway spruce chemotypes, as reported for other coniferous tree species (Yassaa et al., 2012). Moreover, Kännaste et al. (2013) introduced limonene- and bornyl acetate-chemotypes for Norway spruce seedlings. Moreover, forest species heterogeneity and forest understorey, particularly when covered by *Vaccinium myrtillus* and *Calamagrostis* species, have a potential to enhance isoprene fluxes. Among others, Bryan et al. (2015) have shown that convection or advection transports of BVOCs could increase these fluxes by as much as 34%.

The isoprene oxidation products methyl vinyl ketone (MVK) and methacrolein (MAC) found at m/z 71.049 as isomers cannot be separated by means of the instrument configuration utilized in our study. Additionally, 2-hydroxy-2-methylpropanal (HMPR) is reported to be a major MBO OH oxidation product (Alvarado et al., 1999) and its ion fragment interferes with MVK and MAC. A study by Kaser et al. (2013) showed that fragmentation coming from HMPR can contribute up to 15% when measured by calibration in the laboratory. Flux at m/z 71.049 peaked at noontime at 0.16 nmol m^{-2} s^{-1}. Regression of our flux data points between the m/z 69.067 and 71.049 is very poor ($r^2 = 0.24$), suggesting that MVK and MAC are not the only oxidation products of isoprene and that MBO emissions oxidize to different products, mainly acetone (Ferronato et al., 1998; Alvarado et al., 1999).

High methanol (m/z 33.003) fluxes were observed, with substantial deposition during the night and emission in daytime. Bourtsoukidis et al. (2014b) found methanol fluxes in

Norway spruce forest to be highest during August, suggesting that seasonality plays a major role.

Using dry and VOC-free air generated by ZAG, we minimized the possible interference between formaldehyde and water (Hansel et al., 1998). This measuring protocol allowed us to observe significant emissions of formaldehyde (m/z 31.003) during noon hours. However, our measurements revealed rapid changes between emission and deposition in early morning and late afternoon hours. Therefore, we attribute formaldehyde formation to be a result of rapid daytime BVOC oxidation. Similar findings were reported for ponderosa pine forest (DiGangi et al., 2011) and for Norway spruce forest in Bavaria (Klemm et al., 2006). Formaldehyde deposition to the soil is often observed in subalpine coniferous forests (Gray et al., 2014).

Acetone found at m/z 59.049 cannot be separated from its isomer propanal. However, the contribution of propanal to m/z 59.049 flux has previously been estimated to be less than 5% (Kaser et al., 2013).

High daytime toluene fluxes (m/z 93.071; Fig. 13) were observed at wind directions of 150–200°, when polluted air from the Ostrava region (40 km away in a direct line) is transported during the night. Along with an adjacent part of southern Poland, the Ostrava region is among the most polluted areas in Europe. It has an annual mean benzene concentration of 5 µg m^{-3} (EEA Report No 5/2014). Moreover, the HYSPLIT model (Stein et al., 2015) was applied to calculate backward trajectories for night-time data. At the highest morning toluene flux (4.9 nmol m^{-2} s^{-1}), the air masses originated in the Ostrava (Czech Republic) and Katowice (Poland) regions (Fig. S1A); at the lowest fluxes (up to 0.125 nmol m^{-2} s^{-1}), the origin was identified from a forested western part of Slovakia (Fig. S1B). Therefore, it is likely that toluene and benzene are being accumulated under the shallow boundary layer and resuspended at daytime with a high peak after the turbulence starts and slight decrease until turbulence drops to a minimum during the evening hours. Toluene fluxes are linked to high variability in the early morning around 10:00, followed thereafter by a general decrease in the flux, albeit with a small flux increase at 15:00 which might suggest emission by vegetation (Misztal et al., 2015). Inasmuch as the lifetime of toluene, with respect to its reaction with OH radical, is only one-fifth that of benzene

(Atkinson, 2000), we assume the source of toluene must be closer to the experimental station than is the benzene source.

6.1.4 Tropospheric ozone

The lowest ozone concentration was observed from November to January months (Fig. 22) with a small concentration peek around 16:00. On the contrary, during other months, the concentration drop was observed around 8:00 with a peak around 18:00, suggesting ozone removal during the night and ozone production dominating in the afternoon. Relationship with BVOCs is suggested, as those are oxidized during the night predominantly by ozone and during the day by OH radical, explaining thus the ozone concentration drop before the sunrise (Atkinson 2000). Canopy concentration gradients throughout the day are presented in Fig. 23A and Fig. 23B, showing a concentration drop in lower canopy structures due to stomatal removal during the central hours of a day, followed by a concentration drop at all heights during the night. During the day lower canopy structures evince lower ozone concentration than above canopy. Fig 23C is typical for periods of lower air temperature with the sky covered by clouds, which in terms of ozone concentration is represented by a smaller vertical concentration gradient due to less stomatal removal and suppressed ozone production by very low amount of UV radiation.

By applying the ILTM approach, examples of ozone flux were calculated for June and July 2013, as shown in Fig. 24. Interestingly, June ozone flux into the forest is much higher than in July. Moreover, in June, night time flux remains still negative, suggesting non-stomatal removal, as stomata are closed. This might be attributed to BVOCs removal or dilution in the liquid phase in case of rainy events. This is in agreement with Fares et al. (2012), who found a non-stomatal sink in a citrus orchard to be dominating the path of ozone removal. Similarly, Zapletal et al. (2012) reports 47.5% of ozone uptake being accepted by stomata at the same forest at Bílý Kříž, thus more than 50% must represent non-stomatal deposition. Ozone accepted by stomata affects NEE, as calculated for this forest stand by Zapletal et al. (2011). A recent study conducted by Subramanian et al. (2015) at a Norway spruce forest of Sweden has shown, that up to 4.3–15.5% (differing by the geographical zone) biomass production is reduced, as compared to the ambient ozone concentration to that of preindustrial time.

During the day, ozone is used for oxidation of NO towards NOx, which is shown in Fig. 25 for June–August, 2014. Data are normalized to see lines of ozone and NOx close to each other. Periods of low ozone concentrations with high NOx concentrations and oppositely were chosen for Fig. 26, which shows scatter plot of higher NOx concentrations under the presence of lower ozone concentrations. That is in accordance with NO being oxidized by ozone into NOx with ozone removal. As Bílý Kříž is NOx limited area with very low NO concentration (Zapletal et al., 2015), such conditions are occurring only to a limited extent.

6.2 Castelporziano

6.2.1 Winter and summer fluxes of monoterpenes and isoprene

Holm oak forests emit both isoprene and monoterpenes, being thus specific among other trees, since most of them emit isoprene or monoterpenes exclusively (Fares et al., 2013c). Winter night time fluxes of isoprene were observed (Fig. 27). Those are likely to be attributed to PTR-MS failure or low wind velocity together with boundary layer shrinking, which is enhancing mixing ratios. Strong boundary layer effect has been observed by Aromolo et al. (2015). Nonetheless holm oak forest has been proven as substantial source of BVOCs also during the winter time.

Contrary to winter, monoterpenes summer fluxes (Fig. 28) were one order of magnitude higher, which is in agreement with observations conducted by Seco et al. (2011) at the same type of ecosystem. Exponential relationship between air temperature and MT flux was observed (Fig. 29), which is in agreement with Guenther at al. (1993), Fares et al. (2013c) and other references across the literature.

Inverse Lagrangian Transport model seems to be interesting tool for calculation of fluxes from its concentration gradients. As shown in Fig. 30A, MT fluxes are slightly overestimated during the night, whereas during the daylight hours exhibit opposite behaviour. Contradicting results are reported for isoprene (Fig. 30B), where modelled fluxes are overestimated for the whole day averaged. Such disagreement in night time fluxes could be caused both by slow vertical mixing, which is not suitable for use of eddy covariance technique. Another possibility is fast change of isoprene oxidation throughout

the day, which is leading to different lifetime. In ILTM a fixed value of lifetime 120 s was applied. Since isoprene fluxes are bidirectional with faster changes than fluxes of MTs, the change of isoprene oxidation during the day might be significant. Nonetheless, ILTM approach is widely used and its possible error is still within the reasonable boundaries.

Quantification of biogenic emissions at this peculiar site is important for further model parametrizations, since opposite to world emission budgets, this ecosystem is not dominated by biogenic isoprene emissions, but monoterpenes with consequences to atmospheric chemistry. Domination of MTs was observed also in previous seasons by Fares and Loreto (2014). Maximum MT fluxes measured peeked around 4.56 nmol m^{-2} s^{-1} with mean value of 0.62 nmol m^{-2} s^{-1}. Davison et al. (2009) reported highest MT fluxes from dune vegetation of Castelporziano around 1.75 nmol m^{-2} s^{-1}, however those were measured at the end of spring and at different ecosystem. It is clear, that in summer time during the heat waves MT fluxes are higher.

6.2.2 Summer benzene and toluene pollution

Thanks to the vicinity of Rome, Castelporziano is perfect place to study influence of anthropogenic pollutants on peri-urban forest ecosystems. Wind rose graph (Fig. 32) shows sector concentration of aromatics – toluene and benzene together captured at experimental mast located as shown in Fig. 31. The highest concentrations originate from direction towards Leonardo da Vinci airport, demonstrating thus pollution arriving from aircraft. A small concentration peek was found from direction originating in Rome from vehicle exhaust. Interestingly, part of the pollution originates from the sea, which is probably attributed to the aircraft, since they are before and after landing making changes of flight direction above the sea. Similarly, PM 2.5 and PM 10 pollution was investigated at Castelporziano together with HYSPLIT model. Main pollution sources were identified to originate in Rome with consequent movement throughout the experimental mast toward the sea. Part of the pollution was absorbed by the vegetation cover (Fares et al., 2016). Halliday et al. (2016) found 0.53 ppbv of benzene concentration with its maximum of 29.3 ppbv close to the oil and gas production field in Denver, USA. Thus, aircrafts seems to be twice lower (0.22 ppbv mean value for benzene) pollution source than oil wells. However, it is clear, that much higher concentration should be at the airport directly, suggesting thus, that

those two world-leading pollution sources might be equal with regards to benzene pollution. Mean toluene to benzene ratio of 0.7 suggest refuelling emissions originating at the airport, whereas maximum value 7.2 is attributed to the vehicle exhaust. Similar findings were published by Schürmann et al. (2007), who conducted a study of benzene to toluene ratio at Zurich airport.

Benzene and toluene as long-lived AVOCs could be transported by air masses for long distance, as in the case of SMEAR II station, Finland, where polluted air masses were observed from various sources including Northern Poland, Kaliningrad and Western Russia (Patokoski et al., 2015). Thus, it can be concluded that benzene and toluene pollutions originating at the airport have much broader influence and huge tropospheric ozone forming potential (Edwards et al., 2014). Polluted air masses from city of Rome with regards to tropospheric ozone pollution were described by Fares et al. (2014), who separated its sinks to soil, stomata and cuticles.

7 CONCLUSIONS

Volatile organic compounds were measured and identified by various approaches in ozone polluted forest ecosystems at Bílý Kříž, Czech Republic and Castelporziano, Italy, dominated by Norway spruce and Holm oak forests, respectively. In the first and broader part of investigation, I focused on the Bílý Kříž experimental forest. PTR-TOF-MS coupled with the eddy covariance technique was deployed. Fluxes of VOCs were captured, from which the highest were monoterpenes and isoprene together with MBO. Fluxes of MBO were observed for the first time in the Norway spruce ecosystem, therefore suggesting the presence of different Norway spruce chemotypes. Fluxes of oxygenated VOCs were observed to a large extent and exhibit bi-directional behaviour. Surprisingly, toluene and benzene were largely present; toluene being accumulated below the shrinking boundary layer and resuspended back after the sunrise. Source of toluene was identified at Ostrava region with adjacent part of Poland around Katowice, where heavy metallurgical industry is located. Nonetheless, a small peek of toluene flux in the afternoon was observed, which might be attributed to the flux from vegetation cover, therefore making wide-spread Norway spruce trees partly responsible for toluene pollution.

The portion of carbon loss in terms of the fraction of BVOCs to GPP was calculated. Maximum values were around 1.5% of carbon fixed by photosynthesis, dominated by monoterpenes and methanol. Up to 47% of MT fluxes can be predicted from actual GPP. The ILTM approach was used to derive fluxes using the within-canopy concentration gradient. Consequent PCA analysis revealed dependencies of MT fluxes to other driving environmental parameters. Most of the MT flux was attributed to radiation at the ground level, except Δ-3-carene, which exhibited the opposite behaviour. This suggests strong influence of the flux by decaying litter.

The MEGAN model was parametrized with measured basal emission factors in order to test the hypothesis, whether basal emission factors of sun-exposed and shaded leaves separately used or only sun-exposed will fit the measured fluxes better. A comparison revealed that distinguishing sun and shaded leaves is a better way for estimating the ecosystem MT flux. Moreover, five consequent years of MEGAN calculated MT fluxes

were compared. High inter-annual variation was observed. It is assumed, that prolonged drought and high temperature events have a higher impact on MT emissions than higher temperature out of the summer period. The reason is exponential temperature dependence of MT fluxes, which was observed as well. Results are published and discussed in more detail in Juráň et al. (2017). Tropospheric ozone canopy concentration profiles for different weather conditions, modelled ozone fluxes by ILTM and NOx concentration dependence on ozone concentration was measured and calculated. Ozone concentrations were found to be the highest during summer months and the lowest in winter. Night time ozone fluxes suggested both stomatal and non-stomatal depositions.

In the second and shorter part of investigation, two field campaigns covering different climatic periods were conducted in Castelporziano, Italy in Holm oak dominated forest. PTR-MS technique with and without eddy covariance was deployed in summer and winter, respectively. The forest showed itself to be predominantly a monoterpene emitter, whereas isoprene was emitted in smaller quantities. Winter emissions were substantially smaller compared to summer emissions. The ILTM approach was tested to fit measured data regarding MT and isoprene fluxes with relatively good precision for monoterpene flux calculation. In the case of isoprene, the correlation was rather scarce, probably due to instrumentation failure or the different capacity of isoprene to be oxidised throughout the day. Due to the vicinity of the polluted city of Rome and Leonardo da Vinci airport, high benzene and toluene concentrations were observed from those two sectors. By calculating the toluene to benzene concentration ratio, it is concluded, that most of the emission is due to combustion processes, only a small portion is attributed to refuelling emissions at the airport.

The use of different cutting-edge instrumentation together with consequent modelling approaches have been proven as a useful way to identify, quantify and calculate fluxes of volatile organic compounds of both biogenic and anthropogenic origin and moreover to identify their sources. To my knowledge, the use of PTR-MS technique for above mentioned purposes was done for the first time in Central Europe. Thus, the first step to understand biosphere-atmosphere interactions under present climate change, with the influence of anthropogenic pollution sources has been done at Bílý Kříž and partly at Castelporziano experimental forests.

8 REFERENCES

Adam K. P., Zapp J. (1998) Biosynthesis of the isoprene units of chamomile sesquiterpenes. Phytochemistry 48, 953–959.

Alvarado, A., Tuazon, E.C., Aschmann, S.M., Arey, J., Atkinson, R. (1999) Products and mechanisms of the gas-phase reactions of OH radicals and O3 with 2-methyl-3-buten-2-ol, Atmos. Environ. 33, 2893–2905.

Alves, E.G., Jardine, K., Tota, J. et al. (2016) Seasonality of isoprenoid emissions from a primary rainforest in central Amazonia. Atmos. Chem. Phys. 16, 3903–3925.

Andreae, M. O., Crutzen, P. J. (1997) Atmospheric aerosols: Biogeochemical sources and role in atmospheric chemistry. Science, 276, 1052–1058.

Arneth, A., Niinemets U. (2010) Induced BVOCs: how to bug our models? Trends in Plant Sci. 15 (3): 118–125.

Aromolo, R., Savi, F., Salvati, L., Ilardi, F., Moretti, V., Fares, S. (2015) Particulate matter and meteorological conditions in Castelporziano forest: a brief commentary. Rend. Lincei, 26, 269–273.

Atkinson, R. (2000) Atmospheric chemistry of VOCs and NOx. Atmos. Environ. 34, 2063–2101.

Atkinson R., Aschmann S.M. (1993) Atmospheric chemistry of the monoterpene reaction products nopinone, camphenilone, and 4-acetyl-1-methylcyclohexene. J. Atmos. Chem. 16 (4), 337–348.

Aubinet, M., Vesala, T., Papale, D., 2012. Eddy Covariance. Springer Dordrecht Heidelberg London New York.

Baldocchi, D.D., Hicks, B.B., Meyers, T.P. (1988) Measuring biosphere-atmosphere exchanges of biologically related gases with micrometeorological methods. Ecology 69, 1331–1340.

Barsanti, K.C., Pankow, J.F. (2004) Thermodynamics of the formation of atmospheric organic particulate matter by accretion reactions - Part 1: Aldehydes and ketones. Atmos. Environ. 38 (26), 4371–4382.

Barton, D. H. R., Ozbalik, N., Schmitt, M. (1989) Radical chemistry based on (+)-cis-pinonic acid. Tetrahedron Lett. 30 (25), 3263–3266.

Bao, H., Kondo, A., Kaga, A. et al. (2008) Biogenic volatile organic compound emission potential of forests and paddy fields in the Kinki region of Japan. Environ. Res. 106, 156–169.

Benjamin, M.T., Winer, A.M. (1998) Estimating the ozone-forming potential of urban trees and shrubs. Atmos. Environ. 32, 53–68.

Bianchi, F., Tröstl, J., Junninen, H. et al. (2016) New particle formation in the free troposphere: A question of chemistry and timing. Science, 352 (6289), 1109–1112.

Biesenthal, T.A., Shepson, P.B. (1997) Observations of anthropogenic inputs of the isoprene oxidation products methyl vinyl ketone and methacrolein to the atmosphere. Geophysi. Res. Lett. 24 (11), 1375–1378.

Biesenthal, T.A., Wu Q., Shepson P.B., Wiebe H.A., Anlauf K.G., Mackay G.I. (1997) A study of relationships between isoprene, its oxidation products, and ozone, in the Lower Fraser Valley, BC. Atmos. Environ. 31(14), 2049–2058.

Bourtsoukidis, E., Bonn, B., Noe, S.M. (2014a) On-line field measurements of BVOC emissions from Norway spruce (Picea abies) at the hemiboreal SMEAR-Estonia site under autumn conditions. Boreal Environ. Res. 19, 153–167.

Bourtsoukidis, E., Williams, J., Kesselmeier, J., Jacobi, S., Bonn, B. (2014b) From emissions to ambient mixing ratios: Online seasonal field measurements of volatile organic

compounds over a Norway spruce-dominated forest in central Germany. Atmos. Chem. Phys. 14, 6495–6510.

Bouvier-Brown, N.C., Schade, G.W., Misson, L., Lee, A., McKay, M., Goldstein, A.H. (2012) Contributions of biogenic volatile organic compounds to net ecosystem carbon flux in a ponderosa pine plantation. Atmos. Environ. 60, 527–533.

Braun S., Schindler C., Rihm B. (2014) Growth losses in Swiss forests caused by ozone: Epidemiological data analysis of stem increment of Fagus sylvatica L. and Picea abies Karst. Environ. Pollut. 192, 129–138.

Brégonzio-Rozier, L., Siekmann, F., Giorio, C. et al. (2015) Gaseous products and secondary organic aerosol formation during long term oxidation of isoprene and methacrolein. Atmos. Chem. Phys. 15, 2953–2968.

Brilli F., Barta C., Fortunati A., Lerdau M., Loreto F., Centritto M. (2007) Response of isoprene emission and carbon metabolism to drought in white poplar (Populus alba) saplings. New Phytol. 175: 244–254.

Brilli F., Gioli B., Zona D. et al. (2014) Simultaneous leaf- and ecosystem-level fluxes of volatile organic compounds from a poplar-based SRC plantation. Agricult. Forest Meterol. 187, 22–35.

Brilli, F., Hortnagl L., Bamberger I. et al. (2012) Qualitative and quantitative characterization of volatile organic compound emissions from cut grass. Environ. Sci. Technol. 46 (7): 3859–3865.

Brown, S.S., Degouw, J.A., Warneke, C. et al. (2009) Nocturnal isoprene oxidation over the Northeast United States in summer and its impact on reactive nitrogen partitioning and secondary organic aerosol. Atmos. Chem. Phys. 9 (9), 3027–3042.

Bryan, A. M., Cheng, S. J., Ashworth, K. et al. (2015) Forest-atmosphere BVOC exchange in diverse and structurally complex canopies: 1-D modeling of a mid-successional forest in northern Michigan. Atmos. Environ. 120, 217–226.

Calogirou A., Jensen N.R., Nielsen C.J., Kotzias D., Hjorth J. (1999) Gas-Phase Reactions of Nopinone, 3-Isopropenyl-6-oxo-heptanal, and 5-Methyl-5-vinyltetrahydrofuran-2-ol with OH, NO3, and Ozone. Environ. Sci. Technol. 33 (3), 453–460.

Chameides, W., Lindsay, R., Richardson, J., Kiang, C. (1988) The role of biogenic hydrocarbons in urban photochemical smog: Atlanta as a case study. Science 241, 1473–1475.

Cantrell, C. A., Lind, J. A., Shetter, R. E. et al. (1992) Peroxy radicals in the ROSE experiment: Measurement and theory. J. Geophys. Res. 97 (D18), 20671–20686.

Chan, A. W. H., Chan, M. N., Surratt, J. D. et al. (2010) Role of aldehyde chemistry and NOx concentrations on secondary organic aerosol formation. Atmos. Chem. Phys. 10, 7169–7188.

Cheung K., Guo H., Ou J.M. et al. (2014) Diurnal profiles of isoprene, methacrolein and methyl vinyl ketone at an urban site in Hong Kong. Atmos. Environ. 84, 323–331.

Christensen, C.S., Hummelshøj, P., Jensen, N.O. et al. (2000) Determination of the terpene flux from orange species and Norway spruce by relaxed eddy accumulation. Atmos. Environ. 34, 3057–3067.

Ciccioli, P., Brancaleoni, E., Frattoni, M. et al. (1999) Emission of reactive terpene compounds from orange orchards and their removal by within-canopy processes. J Geophys Res-Atmos, 104 (D7), 1998JD100026, 8077–8094.

CLRTAP, 2015: Manual on Methodologies and Criteria for Modelling and Mapping Critical Loads & Levels and Air Pollution Effects, Risks and Trends. UNECE Convention on Long-range Transboundary Air Pollution, UNECE Convention on Long-range Transboundary Air Pollution [vid 2015_10_20]. Available at www.icpmapping.org

Craven, J.P., Jewell, R.E., Brooks, H.E. (2002) Comparison between observed convective cloud-base heights and lifting condensation level for two different lifted parcels. Weather Forecas. 17 (4), 885–890.

Crounse J.D., Nielsen L.B., Jørgensen S., Kjaergaard H.G., Wennberg P.O. (2013) Autoxidation of Organic Compounds in the Atmosphere. J. Phys. Chem. Lett. 4 (20), 3513–3520.

Dani K.G.S., Jamie I.M., Prentice I.C., Atwell B.J. (2014) Evolution of isoprene emission capacity in plants. Trends. Plant. Sci. 19: 439–446.

Davison, B., Taipale, R., Langford, B. et al. (2009) Concentrations and fluxes of biogenic volatile organic compounds above a Mediterranean Macchia ecosystem in western Italy. Biogeosciences, 6 (8), 1655–1670.

De Quijano, M.D., Schaub, M., Bassin, S., Volk, M., Penuelas, J. (2012) Ozone visible symptoms and reduced root biomass in the subalpine species Pinus uncinata after two years of free-air ozone fumigation. Environ. Pollut. 169, 250–257.

DiGangi, J. P., Boyle, E. S., Karl, T. et al. (2011) First direct measurements of formaldehyde flux via eddy covariance: implications for missing in-canopy formaldehyde sources. Atmos. Chem. Phys. 11, 10565–10578.

Dodge M. C. (1990) A Comparison of Three Photochemical Reaction Mechanisms. J. Geophys. Res. 94, 5121–5136.

Edwards, P.M., Brown, S.S., Roberts, J.M. et al. (2014) High winter ozone pollution from carbonyl photolysis in an oil and gas basin. Nature, 514 (7522), 351–354.

EEA, 2014. Air Quality in Europe – 2014 Report. European Environment Agency, Luxembourg: Publications Office of the European Union.

Ehn, M., Thornton, J.A., Kleist, E. et al. (2014) A large source of low-volatility secondary organic aerosol. Nature, 506 (7489), 476–479.

Eisenreich W, Rohdich F, Bacher A. (2001) Deoxyxylulose phosphate pathway to terpenoids. Trends. Plant. Sci. 6 78–84.

Ellis A.M., Mayhew C.A., 2014, Proton-Transfer Reaction Mass Spectrometry Principles and Applications, Chichester, UK, Wiley, 350 p, ISBN 978-1-4051-7668-2

Emberson, L.D., Wieser, G., Ashmore, M.R. (2000) Modelling of stomatal conductance and ozone flux of Norway spruce: Comparison with field data. Environ. Pollut. 109 (3), 393–402.

Esposito, R., Lusini, I., Večeřová, K. et al. (2016) Shoot-level terpenoids emission in Norway spruce (Picea abies) under natural field and manipulated laboratory conditions. Plant Physiol. Biochem. 108, 530–538.

Fall, R., Karl, T., Jordon, A., Lindinger, W. (2001) Biogenic C5VOCs: release from leaves after freeze-thaw wounding and occurrence in air at a high mountain observatory. Atmos. Environ. 35, 3905–3916.

FAO, 2009. Global review of forest pests and diseases 2009. FAO forestry paper 156, ISBN 978-92-5-106208-1.

Fares, S., Loreto, F. (2014) Isoprenoid emissions by the Mediterranean vegetation in Castelporziano. Rend. Lincei, 26, 493–498.

Fares S., Loreto F., Kleist E., Wildt J. (2008) Stomatal uptake and stomatal deposition of ozone in isoprene and monoterpene emitting plants. Plant. Biol. (Stuttg), 10 (1): 44–54.

Fares S., Matteucci G., Scarascia Mugnozza G. et al. (2013a) Testing of models of stomatal ozone fluxes with field measurements in a mixed Mediterranean forest. Atmos. Environ. 67: 242–251.

Fares, S., Mereu, S., Scarascia Mugnozza, G. et al. (2009) The ACCENT-VOCBAS field campaign on biosphere-atmosphere interactions in a Mediterranean ecosystem of Castelporziano (Rome): site characteristics, climatic and meteorological conditions, and eco-physiology of vegetation. Biogeosciences, 6, 1043–1058.

Fares, S., Savi, F., Fusaro, L. et al. (2016) Particle deposition in a peri-urban Mediterranean forest. Environ. Pollut. 218, 1278–1286.

Fares, S., Savi, F., Muller, J., Matteucci, G., Paoletti, E. (2014) Simultaneous measurements of above and below canopy ozone fluxes help partitioning ozone deposition

between its various sinks in a Mediterranean Oak Forest. Agricult. Forest Meterol. 198, 181–191.

Fares, S., Schnitzhofer, R., Jiang, X., Guenther, A., Hansel, A., Loreto, F. (2013c) Observations of diurnal to weekly variations of monoterpene-dominated fluxes of volatile organic compounds from mediterranean forests: Implications for regional modelling. Environ. Sci. Technol. 47 (19), 11073–11082.

Fares, S., Vargas, R., Detto, M. et al. (2013b) Tropospheric ozone reduces carbon assimilation in trees: Estimates from analysis of continuous flux measurements. Glob. Change Biol. 19 (8), 2427–2443.

Fares S., Weber R., Park J.H., Gentner D., Karlik J., Goldstein A.H. (2012) Ozone deposition to an orange orchard: Partitioning between stomatal and non-stomatal sinks. Environ. Pollut. 169: 258–266.

Felzer, B., Kicklighter, D., Melillo, J., Wang, C., Zhuang, Q., Prinn, R. (2004) Effects of ozone on net primary production and carbon sequestration in the conterminous United States using a biogeochemistry model. Tellus B, 56, 230–248.

Ferronato, C., Orlando, J.J., Tyndall, G.S. (1998) Rate and mechanism of the reactions of OH and Cl with 2-methyl-3-buten-2-ol. J. Geophys. Res. 103, 25579–25586.

Finlayson, B.J., Pitts J.N. (1999) Chemistry of the Lower and Upper Atmosphere, Theory Experiments and Applications. Academic Press, San Diego, USA.

Finlayson-Pitts, B.J., Pitts Jr., J.N., 2000. Chemistry of the upper and lower atmosphere. Academic Press, San Diego, California.

Foken, T., Wichura, B. (1996) Tools for quality assessment of surface-based flux measurements. Agric. For. Meteorol. 78, 83–105.

Franzaring, J., Tonneijck, A.E.G., Kooijman, A.W.N., Dueck, T.A. (2000) Growth responses to ozone in plant species from wetlands. Environ. Exp. Bot. 44, 39–48.

Glasius, M.; Calogirou, A.; Jensen, N. R.; Hjorth, J.; Nielsen, C. (1997) Kinetic study of gas-phase reactions of pinonaldehyde and structurally related compounds. J. Int. J. Chem. Kinet. 29, 527–533.

Galloway, M. M., Huisman, A. J., Yee, L. D. et al. (2011) Yields of oxidized volatile organic compounds during the OH radical initiated oxidation of isoprene, methyl vinyl ketone, and methacrolein under high-NOx conditions. Atmos. Chem. Phys. 11, 10779–10790.

Genard-Zielinski, A.-C., Boissard, C., Fernandez, C. et al. (2015) Variability of BVOC emissions from a Mediterranean mixed forest in southern France with a focus on Quercus pubescens. Atmos. Chem. Phys. 15 (1): 431–446.

Ghirardo, A., Koch, K., Taipale, R., Zimmer, I., Schnitzler, J. P., Rinne, J. (2010) Determination of *de novo* and pool emissions of terpenes from four common boreal/alpine trees by 13CO2 labelling and PTR-MS analysis. Plant Cell Environ. 33, 781–792.

Ghirardo, A., Xie, J., Zheng, X. et al. (2016) Urban stress-induced biogenic VOC emissions and SOA-forming potentials in Beijing. Atmos. Chem. Phys. 16 (5), 2901–2920.

Goldan, P.D., Kuster, W.C., Fehsenfeld, F.C. (1993) The observation of a C5 alcohol emission in a North American pine forest. Geophys. Res. Lett. 20, 1039–1042.

Graus, M., Hansel, A., Wisthaler, A. et al. (2006) A relaxed-eddy-accumulation method for the measurement of isoprenoid canopy-fluxes using an online gas-chromatographic technique and PTR-MS simultaneously. Atmos. Environ. 40, 43–54.

Graus M., Müller M., Hansel A. (2010) High Resolution PTR-TOF: Quantification and Formula Confirmation of VOC in Real Time. J. Am. Soc. Mass. Spectr. 21 (6), 1037–1044.

Gray, C.M., Monson, R.K., Fierer, N. (2014) Biotic and abiotic controls on biogenic volatile organic compound fluxes from a subalpine forest floor. J. Geophys. Res. 119, 547–556.

Grote, R., Samson, R., Alonso, R. et al. (2016) Functional traits of urban trees: Air pollution mitigation potential. Front. Ecol. Environ. 14 (10), 543–550.

Guenther, A., Hewitt, C.N., Erickson, D. et al. (1995) A global model of natural volatile organic compound emissions. J. Geophys. Res. 100, 8873–8892.

Guenther, A. B., Jiang, X., Heald, C. L. et al. (2012) The model of emissions of gases and aerosols from nature version 2.1 (MEGAN2.1): An extended and updated framework for modelling biogenic emissions. Geosci. Model Dev. 5, 1471−1492.

Guenther, A.B., Zimmerman, P.R., Harley, P.C., Monson, R.K., Fall, R. (1993) Isoprene and monoterpene emission rate variability: model evaluations and sensitivity analyses. J. Geophys. Res. 98, 12609–12617.

Hakola, H., Tarvainen, V., Bäck, J. et al. (2006) Seasonal variation of mono- and sesquiterpene emission rates of Scots pine. Biogeosciences 3, 93–101.

Halliday, H.S., Thompson, A.M., Wisthaler, A. et al. (2016) Atmospheric benzene observations from oil and gas production in the Denver-Julesburg Basin in July and August 2014. J. Geophys. Res-Atmos. 121 (18), 11 055–11 074.

Hallquist M., Wängberg I., Ljungström E., Barnes I., Becker KH. (1999) Aerosol and product yields from NO3 radical-initiated oxidation of selected monoterpenes. Environ. Sci. Technol. 33 (4): 553–559.

Handley, T., and Grulke, N.E. (2008) Interactive effects of O3 exposure on California black oak (Quercus kelloggii Newb.) seedlings with and without N amendment. Environ. Pollut. 156, 53–60.

Hansel, A., Wisthaler, A., Schwarzmann, M., Lindinger, W. (1998) Energy dependencies of the proton transfer reactions H3O+ + CH2O <−> CH2OH+ + H2O. Int. J. Mass Spectrom. 167−168, 697–703.

Hanson D.T., Swanson S., Graham L.E., Sharkey T.D. (1999) Evolutionary significance of isoprene emission from mosses. Am. J. Bot. 86:634–639.

Harley P.C., Monson R.K., Lerdau M.T. (1999) Ecological and evolutionary aspects of isoprene emission from plants. Oecologia, 118: 109–123.

Harrison, R. M. Yin, J. (2000) Particulate matter in the atmosphere: which particle properties are important for its effects on health? Sci. Total Environ. 249, 85–101.

Havránková K., Šigut L., Macálková L., Dušek J., Sedlák P., Pavelka M. (2015) Ecosystem stations - a tool for global change observations. In Urban O., Klem K. (Eds), Global change & ecosystems (pp. 58–67). Brno: Global Change Research Centre, Academy of Sciences of the Czech Republic, v. v. i, ISBN 978-80-87902-14-1.

Helmig, D., L. F. Klinger, Guenther, A, Vierling, L, Geron, C, Zimmerman, P. (1999) Biogenic volatile organic compound emissions (BVOCs) II. Landscape flux potentials from three continental sites in the US. Chemosphere 38(9): 2189–2204.

Hewitt, C.N. et al. 2016: Database on volatile organic compound emissions from plants. Lancaster University [vid. 2016_12_20]. Available at http://www.es.lancs.ac.uk/cnhgroup/iso-emissions.pdf.

Hewitt, C.N., Street, R.A. (1992) A qualitative assessment of the emission of non-methane hydrocarbon compounds from the biosphere to the atmosphere in the U.K.: present knowledge and uncertainties. Atmos. Environ. 26, 3069–3077.

Hippeli, S., Elstner, E.F. (1996) Mechanisms of oxygen activation during plant stress: biochemical effects of air pollutants. J. Plant. Physiol. 148, 249–257.

Holzinger, R., Lee, A., McKay, M., Goldstein, A.H. (2006) Seasonal variability of monoterpene emission factors for a Ponderosa pine plantation in California. Atmos. Chem. Phys. 6 (5), 1267–1274.

Holzke, C., Hoffmann, T., Jaeger, L., Koppmann, R., Zimmer, W. (2006) Diurnal and seasonal variation of monoterpene and sesquiterpene emissions from Scots pine (Pinus sylvestris L.). Atmos. Environ. 40, 3174–3185.

Hoshika, Y., Omasa, K., Paoletti, E. (2012a) Whole-tree water use efficiency is decreased by ambient ozone and not affected by O3-induced stomatal sluggishness. PLoS ONE. 7–6, e39270.

Hoshika, Y., Tatsuda, S., Watanabe, M. et al. (2013) Effect of ambient ozone at the somma of Lake Mashu on growth and leaf gas exchange in Betula ermanii and Betula platyphylla var. japonica. Environ. Exp. Bot. 90, 12–16.

Hoshika, Y., Watanabe, M., Inada, N., Koike, T. (2012b) Ozone-induced stomatal sluggishness develops progressively in Siebold's beech (Fagus crenata). Environ. Pollut. 166, 152–156.

Hoshika Y., Watanabe M., Kitao M. et al. (2015) Ozone induces stomatal narrowing in European and Siebold's beeches: a comparison between two experiments of free-air ozone exposure. Environ. Pollut. 196, 527–533.

Huang, L., McGaughey, G., McDonald-Buller, E., Kimura, Y., Allen, D.T. (2015) Quantifying regional, seasonal and interannual contributions of environmental factors on isoprene and monoterpene emissions estimates over eastern Texas. Atmos. Environ. 106, 120–128.

Ionicon, 2015: Technologies overview: Proton Transfer Reaction – Mass Spectrometry [online]. Ionicon GmbH [vid. 2015_30_11]. Available from http://www.ionicon.com/sites/default/files/uploads/downloads/flyer_2013_IONICON_PTR -MS_technology_overview.pdf

Jeffries H.E., Sexton K.G., Arnold J.R., Kale T.L. Validation Testing of New Mechanisms with Outdoor Chamber Data Analysis of VOC Data for the CB4 and CAL Photochemical Mechanisms, vol. 2 (1989) Final Report, EPA-600/3-89-010b.

Juráň, S., Pallozzi, E., Guidolotti, G. et al. (2017) Fluxes of biogenic volatile organic compounds above temperate Norway spruce forest of the Czech Republic. Agric. For. Meteorol. 232, 500–513.

Karl, M., Dorn, H. P., Holland, F. et al. (2006) Product study of the reaction of OH radicals with isoprene in the atmosphere simulation chamber SAPHIR. J. Atmos. Chem. 55, 167–187.

Karl, T., Guenther, A., Turnipseed, A., Patton, E.G., Jardine K. (2008) Chemical sensing of plant stress at the ecosystem scale. Biogeosciences, 5, 1287–1294.

Karl, T., Guenther, A., Yokelson, R.J. et al. (2007) The tropical forest and fire emissions experiment: emission, chemistry, and transport of biogenic volatile organic compounds in the lower atmosphere over Amazonia. J. Geophys. Res. Atmos. 112 (D18).

Karl, T., Hansel, A., Cappellin, L., Kaser, L., Herdlinger-Blatt, I., Jud, W. (2012) Selective measurements of isoprene and 2-methyl-3-buten-2-ol based on NO+ ionization mass spectrometry. Atmos. Chem. Phys. 12, 11877–11884.

Karl, T., Kaser, L., Turnipseed, A. (2014) Eddy covariance measurements of isoprene and 232-MBO based on NO+ time-of-flight mass spectrometry. Int. J. Mass Spectrom. 365–366, 15–19.

Karl, T., Potosnak, M., Guenther, A. et al. (2004) Exchange processes of volatile organic compounds above a tropical rain forest: Implications for modeling tropospheric chemistry above dense vegetation. J. Geophys. Res. 109, D18306.

Kännaste, A., Zhao, T., Lindström, A., Stattin, E., Långström, B., Borg-Karlson, A.-K. (2013) Odors of Norway spruce (Picea abies L.) seedlings: Differences due to age and chemotype. Trees-Struct. Funct. 27, 149–159.

Kaser, L., Karl, T., Schnitzhofer, R. et al. (2013) Comparison of different real time VOC measurement techniques in a ponderosa pine forest. Atmos. Chem. Phys. 13, 2893–2906.

Kirkby, J., Duplissy, J., Sengupta, K. et al. (2016) Ion-induced nucleation of pure biogenic particles. Nature, 533 (7604), 521–526.

Klemm, O., Held, A., Forkel, R. et al. (2006) Experiments on forest/atmosphere exchange: Climatology and fluxes during two summer campaigns in NE Bavaria. Atmos. Environ. 40, 3–20.

Klingberg, J., Engardt, M., Karlsson, P. E., Langner, J., Pleijel, H. (2014) Declining ozone exposure of european vegetation under climate change and reduced precursor emissions. Biogeosciences, 11 (19), 5269–5283.

Knudsen JT, Gershenzon J. (2006) The chemistry diversity of floral scent. In: Dudareva N, Pichersky E, editors. Biology of floral scent. Boca Raton, Florida: CRC Press; 27–52.

Kolb, T.E., Matyssek, R. (2001) Limitations and perspectives about scaling ozone impact in trees. Environ. Pollut. 115, 373–393.

Krascsenitsová, E., Kozánek, M., Ferenčík, J., Roller, L., Stauffer, C., Bertheau, C. (2013) Impact of the Carpathians on the genetic structure of the spruce bark beetle Ips typographus. J. Pest Sci. 86, 669–676.

Křůmal, K., Mikuška, P., Večeřová, K., Urban, O., Pallozzi, E., Večeřa, Z. (2016) Wet effluent diffusion denuder: The tool for determination of monoterpenes in forest. Talanta, 153, 260–267.

Kulmala, M., Suni, T., Lehtinen, K.E.J. et al. (2004) A new feedback mechanism linking forests, aerosols, and climate. Atmos. Chem. Phys. 4 (2), 557–562.

Laffineur, Q., Aubinet, M., Schoon, N. et al. (2011) Isoprene and monoterpene emissions from a mixed temperate forest. Atmos. Environ. 45 (18), 3157–3168.

Lamanna, M.S., Goldstein, A.H. (1999) In situ measurements of C2-C10 volatile organic compounds above a Sierra Nevada ponderosa pine plantation. J. Geophys. Res. 104, No. D17, 21247–21262.

Langford, B., Acton, W., Ammann, C., Valach, A., Nemitz, E. (2015) Eddy-covariance data with low signal-to-noise ratio: Time-lag determination, uncertainties and limit of detection. Atmos. Meas. Tech. 8 (10), 4197–4213.

Leahey D. M., Hansen M. C., Schroeder M. B. (1988) An Analysis of Wind Fluctuation Statistics Collected under Stable Atmospheric Conditions at Three Sites in Alberta, Canada. J. Appl. Meteor. 27, 774–777.

Lindwall, F., Faubert P., Rinnan, R. (2015) Diel Variation of Biogenic Volatile Organic Compound Emissions- A field Study in the Sub, Low and High Arctic on the Effect of Temperature and Light. PLoS One 10 (4): e0123610.

Lombardozzi, D., Levis, S., Bonan, G., Hess, P.G., Sparks, J.P. (2015) The influence of chronic ozone exposure on global carbon and water cycles. J. Climate, 28 (1), 292–305.

Loreto, F., Bagnoli, F., Calfapietra, C. et al. (2014) Isoprenoid emission in hygrophyte and xerophyte European woody flora: Ecological and evolutionary implications. Global Ecol. Biogeogr. 23(3), 334–345.

Loreto, F., Mannozzi, M., Maris, C., Nascetti, P., Ferranti, F., Pasqualini, S. (2001) Ozone quenching properties of isoprene and its antioxidant role in leaves. Plant Physiol. 126, 993–1000.

Loreto F, Schnitzler J. P. (2010) Abiotic stresses and induced BVOCs. Trends Plant Sci. 15: 154–166.

Marenco, A., Gouget, H., Nedelec, P., Pages, J.-P. (1994) Evidence of a long-term increase in tropospheric ozone from Pic du Midi data series. Consequences: Positive radiative forcing. J. Geophys. Res. 99 (D8), 16 617–16 632.

Martín-Reviejo, M., Wirtz, K. (2005) Is benzene a precursor for secondary organic aerosol? Environ. Sci. Technol. 39, 1045–1054.

Matsumoto J. (2014) Measuring Biogenic Volatile Organic Compounds (BVOCs) from Vegetation in Terms of Ozone Reactivity. Aerosol Air Qual. Res. 14: 197–206.

Matyssek, R., Baumgarten, M., Hummel, U., Häberle, K.-H., Kitao, M., Wieser, G. (2015) Canopy-level stomatal narrowing in adult Fagus sylvatica under O3 stress - Means of preventing enhanced O3 uptake under high O3 exposure? Environ. Pollut. 196, 518–526.

Matyssek, R., Bytnerowicz, A., Karlsson, P.-E. et al. (2007) Promoting the O3 flux concept for European forest trees. Environ. Pollut. 146 (3), 587–607.

Matyssek, R., Karnosky, D.F., Wieser, G. et al. (2010) Advances in understanding ozone impact on forest trees: messages from novel phytotron and free-air fumigation studies. Environ. Pollut. 158, 1990–2006.

Matyssek, R., Wieser, G., Nunn, A.J. et al. (2004) Comparison between AOT40 and ozone uptake in forest trees of different species, age and site conditions. Atmos. Environ. 38 (15), 2271–2281.

Mauder, M., Cuntz, M., Drüe, C. et al. (2013) A strategy for quality and uncertainty assessment of long-term eddy-covariance measurements. Agric. For. Meteorol. 169, 122–135.

Misztal, P.K., Hewitt, C.N., Wildt, J. et al. (2015) Atmospheric benzenoid emissions from plants rival those from fossil fuels. Sci. Rep. 5, 12064.

Miyoshi, A., Hatakeyama, S., Washida, N. (1994) OH radical-initiated photooxidation of isoprene: an estimate of global CO production. J. Geophys. Res. Atmos. 99, 18779–18787.

Mohd Zul Helmi Rozaini (2012) *The Chemistry of Dicarboxylic Acids in the Atmospheric Aerosols, Atmospheric Aerosols - Regional Characteristics - Chemistry and Physics*, Dr. Hayder Abdul-Razzak (Ed.), InTech, ISBN: 978-953-51-0728-6.

Moncrieff, J., Clement, R., Finnigan, J., Meyers, T. 2005 *Handbook of Micrometeorology*, Handbook of Micrometeorology.

Müller, M., Anderson, B.E., Beyersdorf, A.J. et al. (2016) In situ measurements and modeling of reactive trace gases in a small biomass burning plume. Atmos. Chem. Phys. 16 (6), 3813–3824.

Müller M., Mikoviny T., Jud W., D'Anna B., Wisthaler A. (2013) A new software tool for the analysis of high resolution PTR-TOF mass spectra. Chemomet. Intell. Lab. 127, 158–165.

National Research Council, 1992: *Rethinking the Ozone Problem in the Urban and Regional Air Pollution*, Washington, D.C.: National Academy Press, 524 p., ISBN: 0-309-56037-3.

Nemitz, E., Sutton, M. A., Gut, A., Jose, R. S., Husted, S., Schjoerring, J. K. (2000) Sources and sinks of ammonia within an oilseed rape canopy. Agr. Forest Meteorol. 105, 385–404.

Ng, N.L., Chhabra, P.S., Chan, A.W.H. et al. (2007) Effect of NOx level on secondary organic aerosol (SOA) formation from the photooxidation of terpenes. Atmos. Chem. Phys. 7, 5159–5174.

Niinemets, Ü., Arneth, A., Kuhn, U., Monson, R.K., Peñuelas, J., Staudt, M. (2010) The emission factor of volatile isoprenoids: stress, acclimation, and developmental responses. Biogeosciences 7, 2203–2223.

Nishimura H., Shimadera H., Kondo A., Bao H., Shrestha KH, Inoue Y. (2015) Evaluation of light dependence of monoterpene emission and its effect on surface ozone concentration. Atmos. Environ. 104, 143–153.

Noe, S.M., Kimmel, V., Hüve, K. et al. (2011) Ecosystem-scale biosphere-atmosphere interactions of a hemiboreal mixed forest stand at Järvselja, Estonia. For. Ecol. Manage. 262, 71–81.

Nowak, D.J., Civerolo, K.L., Rao, S.T., Sistla, S., Luley, C.J., Crane, D.E. (2000) A modeling study of the impact of urban trees on ozone. Atmos. Environ. 34, 1601–1613.

Nussbaum, S., Fuhrer, J. (2000) Difference in ozone uptake in grassland species between open-top chambers and ambient air. Environ. Pollut. 109, 463–471.

Oliveira R.C., Bauerfeldt G.F. (2015) Ozonolysis reactions of monoterpenes: a variational transition state investigation. J. Phys. Chem. A, 119 (12): 2802–2812.

Pallozzi, E., Guidolotti, G., Ciccioli, P., Brilli, F., Feil, S., Calfapietra, C. (2016) Does the novel fast-GC coupled with PTR-TOF-MS allow a significant advancement in detecting VOC emissions from plants? Agr. Forest Meteorol. 216, 232–240.

Paoletti, E. (2007) Ozone impacts on forests. CAB reviews: perspectives in agriculture, veterinary science. Nutr. Nat. Resour. 2 (No. 68), 13 pp.

Paoletti, E. (2005) Ozone slows stomatal response to light and leaf wounding in a Mediterranean evergreen broadleaf, Arbutus unedo. Environ. Pollut. 134, 439–445.

Paoletti, E., Bytnerowicz, A., Andersen, C. et al. (2007) Impacts of air pollution and climate change on forest ecosystems - Emerging research needs, TheScientificWorldJournal, 7 (1), 1–8.

Paoletti E., Contran N., Bernasconi P., Günthardt-Goerg MS., Vollenweider P. (2010) Structural and physiological responses to ozone in Manna ash (Fraxinus ornus L.) leaves of seedlings and mature trees under controlled and ambient conditions. Sci Total Environ. 407 (5), 1631–1643.

Park, J.-H., Goldstein, A.H., Timkovsky, J. et al. (2013) Eddy covariance emission and deposition flux measurements using proton transfer reaction - Time of flight - Mass spectrometry (PTR-TOF-MS): Comparison with PTR-MS measured vertical gradients and fluxes. Atmos. Chem. Phys. 13, 1439–1456.

Patokoski, J., Ruuskanen, T.M., Kajos, M.K. et al. (2015) Sources of long-lived atmospheric VOCs at the rural boreal forest site, SMEAR II. Atmos. Chem. Phys. 15 (23), 13413–13432.

Paulot, F., Crounse, J. D., Kjaergaard, H. G., Kroll, J. H., Seinfeld, J. H., Wennberg, P. O. (2009) Isoprene photooxidation: new insights into the production of acids and organic nitrates. Atmos. Chem. Phys. 9, 1479–1501.

Penuelas J., Staudt M. (2010) BVOCs and global change. Trends Plant. Sci. 15: 133–144.

Potosnak M.J., LeStourgeon L., Pallardy S.G. et al. (2014) Observed and modeled ecosystem isoprene fluxes from an oak-dominated temperate forest and the influence of drought stress. Atmos. Environ. 84, 314–322.

Pleijel, H., Danielsson, H., Emberson, L., Ashmore, M. R., Mills, G. (2007) Ozone risk assessment for agricultural crops in Europe: Further development of stomatal flux and flux-response relationships for European wheat and potato. Atmos. Environ. 41, 3002–3040.

Pretzsch, H., Dieler, J., Matyssek, R., Wipfler, P. (2010) Tree and stand growth of mature Norway spruce and European beech under long-term ozone fumigation. Environ. Pollut. 158, 1061–1070.

Rasmussen, R. (1972) What do the hydrocarbons from trees contribute to air pollution. J. Air Pollut. Contr. Assoc. 22, 537–543.

Raupach, M. R. (1989) A practical Lagrangian method for relating scalar concentrations to source distributions in vegetation canopies. Q. J. Roy. Meteor. Soc. 115, 609–632.

Reichstein, M., Falge, E., Baldocchi, D. et al. (2005) On the separation of net ecosystem exchange into assimilation and ecosystem respiration: review and improved algorithm. Glob. Chang. Biol. 11, 1424–1439.

Roberts, J.M., Marchewka, M., Bertman, S.B. et al. (2006) Analysis of the isoprene chemistry observed during the New England Air Quality Study (NEAQS) 2002 intensive experiment. J. Geophys. Res. Atmos. 111(D23).

Robinson, A.L., Donahue, N.M., Shrivastava, M.K. et al. (2007) Rethinking organic aerosols: semivolatile emissions and photochemical aging. Science 315, 1259–1262.

Ryan, M.G., Phillips, N., Bond, B.J. (2006) The hydraulic limitation hypothesis revisited. Plant Cell. Environ. 29, 367–381.

Sapir-Mir, M., Mett, A., Belausov, E. et al. (2008) Peroxisomal localization of Arabidopsis isopentenyl diphosphate isomerases suggests that part of the plant isoprenoid mevalonic acid pathway is compartmentalized to peroxisomes. Plant Physiol. 148, 1219–1228.

Schade, G.W., Goldstein, A.H., Gray, D.W., Lerdau, M.T. (2000) Canopy and leaf level 2-methyl-3-buten-2-ol fluxes from a ponderosa pine plantation. Atmos. Environ. 34, 3535–3544.

Schürmann, G., Schäfer, K., Jahn, C. et al. (2007) The impact of NOx, CO and VOC emissions on the air quality of Zurich airport. Atmos. Environ. 41 (1), 103–118.

Seco, R., Karl, T., Guenther, A. et al. (2015) Ecosystem-scale volatile organic compound fluxes during an extreme drought in a broadleaf temperate forest of the Missouri Ozarks (central USA). Glob. Change Biol. 21, 3657–3674.

Seco, R., Peñuelas, J., Filella, I. et al. (2011) Contrasting winter and summer VOC mixing ratios at a forest site in the Western Mediterranean Basin: The effect of local biogenic emissions. Atmos. Chem. Phys. 11 (24), 13161–13179.

Sharkey, T. D., Singsaas, E. L. (1995) Why plants emit isoprene. Nature 374 (6525), 769.

Sicard P., De Marco A., Dalstein-Richier L., Tagliaferro F., Renou C., Paoletti E. (2016) An epidemiological assessment of stomatal ozone flux-based critical levels for visible ozone injury in Southern European forests. Sci. Total Environ. 541, 729–741.

Simpson, D., Guenther, A., Hewitt, C.N., Steinbrecher, R. (1995) Biogenic emissions in Europe. 1. Estimates and uncertainties. J. Geophys. Res. 100, 22875–22890.

Sindelarova, K., Granier, C., Bouarar, I. et al. (2014) Global data set of biogenic VOC emissions calculated by the MEGAN model over the last 30 years. Atmos. Chem. Phys. 14 (17): 9317–9341.

Sitch, S., Cox, P. M., Collins, W. J, Huntingford, C. (2007) Indirect radiative forcing of climate change through ozone effects on the land-carbon sink. Nature, 448, 791–794.

Sklenská, J., Broškovičová, A., Večeřa, Z. (2002) Wet effluent diffusion denuder technique and the determination of volatile organic compounds in air: II. Monoterpenes. J. Chromatogr. A, 973 (1–2), 211–216.

Steffen, W. L., Denmead O. T. (Eds.) (1988), Flow and Transport in the Natural Environment: Advances and Applications, pp. 95–127, Springer-Verlag, New York.

Stein, A.F., Draxler, R.R, Rolph, G.D., Stunder, B.J.B., Cohen, M.D., Ngan, F. (2015) NOAA's HYSPLIT atmospheric transport and dispersion modeling system. Bull. Amer. Meteor. Soc., 96, 2059–2077.

Steinbrecher, R., Smiatek, G., Köble, R. et al. (2009) Intra- and inter-annual variability of VOC emissions from natural and semi - natural vegetation in Europe and neighbouring countries. Atmos. Environ. 43, 1380–1391.

Subramanian, N., Karlsson, P.E., Bergh, J., Nilsson, U. (2015) Impact of Ozone on sequestration of Carbon by Swedish forests under a changing climate: A modeling study. Forest Sci. 61 (3), 445–457.

Taipale, R., Ruuskanen, T. M., Rinne, J. et al. (2008) Technical Note: Quantitative long-term measurements of VOC concentrations by PTR-MS − measurement, calibration, and volume mixing ratio calculation methods. Atmos. Chem. Phys. 8, 6681–6698.

Tarvainen, V., Hakola, H., Hellén, H., Bäck, J., Hari, P., Kulmala, M. (2005) Temperature and light dependence of the VOC emissions of Scots pine. Atmos. Chem. Phys. 5, 989–998.

Tarvainen, V., Hakola, H., Rinne, J., Hellén, H., Haapanala, S. (2007) Towards a comprehensive emission inventory of terpenoids from boreal ecosystems. Tellus Ser. B-Chem. Phys. Meteorol. 59, 526–534.

Thiel R., Adam K. P. (2002) Incorporation of [1-13C]1-deoxyd-xylulose into isoprenoids of the liverwort Conocephalum conicum. Phytochemistry, 59 269–59 274.

Thomas, V.F.D., Braun, S., Fluckiger, W. (2005) Effects of simultaneous ozone exposure and nitrogen loads on carbohydrate concentrations, biomass, and growth of young spruce trees (Picea abies). Environ. Pollut. 137, 507–516.

Tingey, D.T., Evans, R.C., Bates, E.H., Gumpertz, M.L. (1987) Isoprene emissions and photosynthesis in three ferns: the influence of light and temperature. Physiol. Plantarum, 69, 609–616.

Tirone, G., Dore, S., Matteucci, G., Greco, S., Valentini, R. 2003 Evergreen mediterranean forests: carbon and water fluxes, balances, ecological and ecophysiological determinants. In: Valentini R, Ed. Fluxes of carbon, water and energy of European forest. Ecological Studies 163. Berlin: Springer. 125–150.

Torsethaugen, G., Pell, E.J., Assmann, S.M. (1999) Ozone inhibits guard cell K+ channels implicated in stomatal opening. PNAS, 96, 13577–13582.

Tuazon, E. C. Atkinson, R. (1990) A product study of the gas-phase reaction of isoprene with the OH radical in the presence of NOx. Int. J. Chem. Kinet. 22, 1221–1236.

Urban, O., Klem, K., Ac, A., Havrankova, K. et al. (2012) Impact of clear and cloudy sky conditions on the vertical distribution of photosynthetic CO2 uptake within a spruce canopy. Funct. Ecol. 26, 46–55.

Van Den Driessche, R. (1991) New root growth of Douglas-fir seedlings at low carbon dioxide concentration. Tree Physiol. 8, 289–296.

Verpoorte, R., Alfermann, A.W. (2000) .Metabolic Engineering of Plant Secondary Metabolism. Kluwer Acadamic Publisher, The Netherlands, pp. 286.

Vitale, M., Salvatori, E., Loreto, F., Fares, S., Manes, F. (2008) Physiological responses of Quercus ilex leaves to water stress and acute ozone exposure under controlled conditions. Water Air Soil Poll. 189 (1–4), 113–125.

Vlasáková-Matoušková, L., Hůnová, I. (2015) Stomatal ozone flux and visible leaf injury in native juvenile trees of Fagus sylvatica L.: a field study from the Jizerske hory Mts., the Czech Republic. Environ. Sci. Pollut. R. 22 (13), 10034–10046.

Vranová, E., Coman, D., Gruissem, W. (2012) Structure and dynamics of the isoprenoid pathway network. Mol. Plant. 5, 318–333.

Wagg, S., Mills, G., Hayes, F., Wilkinson, S., Davies, W.J. (2013) Stomata are less responsive to environmental stimuli in high background ozone in Dactylis glomerata and Ranunculus acris. Environ. Pollut. 175, 82–91.

Wang, Y.-F., Owen, S.M., Li, Q.-J., Peñuelas, J. (2007) Monoterpene emissions from rubber trees (Hevea brasiliensis) in a changing landscape and climate: chemical speciation and environmental control. Glob. Change Biol. 13, 2270–2282.

Wang, H., Zhou, W., Wang, X. et al. (2012) Ozone uptake by adult urban trees based on sap flow measurement. Environ. Pollut. 162, 275–286

Warland, J. S., Thurtell, G.W. (2000) A Lagrangian solution to the relationship between a distributed source and concentration profile. Bound.-Layer Meteor. 96, 453–471.

Watson, J., J., Probert, J., A., Piccot, S., D. Jones, J., W. (1991) Global Inventory of Volatile Organic Compound Emissions from Anthropogenic Sources. EPA-report EPA-600/8-91-002

Weber R.O. (1998) Estimators for the standard deviateons of lateral, longitudinal and vertical wind components. Atmos. Environ. 32 (21), 3639–3646.

Wei W., Shuxiao W., Jiming H., Shuiyuan C. (2011) Projection of anthropogenic volatile organic compounds (VOCs) emissions in China for the period 2010–2020, Atmos. Environ. 45 (38), 6863–6871

Went, F.W. (1960) Blue hazes in the atmosphere. Nature, 187 (4738), 641–643.

WHO, (2013) Review of Evidence on Health Aspects of Air Pollution - REVIHAAP Project. Technical Report. World Health Organization, Regional Office for Europe, Copenhagen, Denmark.

Wiedinmyer, C., Guenther, A., Harley, P., Hewitt, N., Geron, C., Artaxo, P., Steinbrecher, R., Rasmussen, R, 2004. Global organic emissions from vegetation, in: Granier, C., Artaxo, P., Reeves, C.E. (Eds.), Emissions of Atmospheric Trace Compounds (Advances in Global Change Research), Kluwer Academic Publishers, Dordrecht – Boston – London, pp. 115–170.

Wieser, G., Matyssek, R., Köstner, B., Oberhuber, W. (2003) Quantifying ozone uptake at the canopy level of spruce, pine and larch trees at the alpine timberline: An approach based on sap flow measurement. Environ. Pollut. 126 (1), 5–8.

Wilczak, J.M., Oncley, S.P., Stage, S.A. (2001) Sonic anemometer tilt correction algorithms. Bound. Layer Meteor. 99, 127–150.

Wittig, V.E., Ainsworth, E.A., Long, S.P. (2007) To what extent do current and projected increases in surface ozone affect photosynthesis and stomatal conductance of trees? A meta-analytic review of the last 3 decades of experiments. Plant. Cell. Environ. 30, 1150–1162.

Wittig, V. E., Ainsworth, E. A., Naidu, S. L., Karnosky, D. F., Long, S. P. (2009) Quantifying the impact of current and future tropospheric ozone on tree biomass, growth, physiology and biochemistry: a quantitative metaanalysis. Glob. Change Biol. 15, 396–424.

Wolfe, G.M., Thornton, J.A., McKay, M., Goldstein, A.H. (2011) Forest-atmosphere exchange of ozone: Sensitivity to very reactive biogenic VOC emissions and implications for in-canopy photochemistry. Atmos. Chem. Phys. 11, 7875–7891.

Yassaa, N., Song, W., Lelieveld, J., Vanhatalo, A., Bäck, J., Williams, J. (2012) Diel cycles of isoprenoids in the emissions of Norway spruce, four Scots pine chemotypes, and in Boreal forest ambient air during HUMPPA-COPEC-2010. Atmos. Chem. Phys. 12, 7215–7229.

Young, P. J., Archibald, A. T., Bowman, K. W. et al. (2013) Pre-industrial to end 21st century projections of tropospheric ozone from the Atmospheric Chemistry and Climate Model Intercomparison Project (ACCMIP). Atmos. Chem. Phys. 13, 2063–2090.

Zapletal, M., Cudlín, P., Chroust, P. et al. (2011) Ozone flux over a Norway spruce forest and correlation with net ecosystem production. Environ. Pollut. 159 (5), 1024–1034.

Zapletal, M., Jonášová, M. E., Juráň, S., Urban, O., Pokorný, R., Pavelka, M., Janouš, D., Cudlín, P. (2015) Effect of ozone concentration on net ecosystem production: A case study in a Norway spruce forest. In: Global Change & Ecosystems. Volume 1., Brno: Global Change Research Centre, Academy of Sciences of the Czech Republic, v. v. i. 138–149. ISBN 978-80-87902-14-1.

Zapletal, M., Pretel, J., Chroust, P. et al. (2012) The influence of climate change on stomatal ozone flux to a mountain Norway spruce forest. Environ. Pollut. 169, 267–273.

Zhang, W., Feng, Z., Wang, X., Niu, J. (2014) Elevated ozone negatively affects photosynthesis of current-year leaves but not previous-year leaves in evergreen Cyclobalanopsis glauca seedlings. Environ. Pollut. 184, 676–681.

Zhang, J., Hartz, K.E.H., Pandis, S.N., Donahue, N.M. (2006) Secondary organic aerosol formation from limonene ozonolysis: homogeneous and heterogeneous influences as a function of NOx. J. Phys. Chem. A, 110, 11 053–11 063.

9 SUPPLEMENT

LIST OF SUPPLEMENTS

1. List of abbreviations
2. List of graphs
3. HYSPLIT model

9.1 List of abbreviations

AOT40 – Accumulated exposure Over a Threshold of 40 ppbv

AVOCs – Anthropogenic Volatile Organic Compounds

BEF – Basal Emission Factor

BVOCs – Biogenic Volatile Organic Compounds

cps – Counts per second

CRA-RPS – Centro di Ricerca per lo Studio delle Relazioni fra Pianta e Suolo

CWEDD – Cylindrical Wet Effluent Diffusion Denuder

CzeCos – Czech Carbon observation system

ESFRI – European Strategy Forum on Research Infrastructures

FA – Flowing Afterglow

GPP – gross primary production

HC – Hollow Cathode discharge ion source

CH_2O – formaldehyde

ICOS – Integrated Carbon Observation System

ILTM – Inverse Lagrangian Transport Model

IPOH – 3-isopropenyl-6-oxoheptanal

ISOP – isoprene

LAI – Leaf Area Index

m/z - m – mass of the ion + 1, z – charge of the ion

MACR – methacrolein

MBO – 2-methyl-3-buten-2-ol

MEGAN – Model of Emissions of Gases and Aerosols from Nature

MEK – Methyl ethyl ketone

MEP – 2-C-methyl-D-erythritol-4-phosphate pathway

MH^+ – protonated mass

MTs – Monoterpenes

MVK – Methyl vinyl ketone

MVT – 5-vinyltetrahydrofuran-2-ol

NEE – Net Ecosystem Exchange

NEP – Net Ecosystem Production

NO_x – $NO + NO_2$

PAR – Photosynthetically Active Radiation

PCA – Principal Component Analysis

PODY – Phytotoxic Ozone Dose above a flux threshold Y

ppbv – parts per billion per volume

ppmC – parts per million carbon

pptv – parts per trillion per volume

PTR-MS – Proton-Transfer-Reaction-Mass-Spectrometer

PTR-QMS – PTR-MS with quadrupole

PTR-TOF-MS – Proton-Transfer-Reaction-Mass-Spectrometer with time of flight

SD – Source Drift region

SIFDT – Selected Ion Flow Drift Tube technique

SIFT – Selected Ion Flow Tube

SOA – Secondary Organic Aerosol

VOC – Volatile Organic Compounds

ZAG – Zero Air Generator

9.2 List of graphs

1. Isoprene oxidation by OH radicals.
2. Structure of selected monoterpenes.
3. Evolution of ozone in free troposphere over Western Europe.
4. Typical ozone isopleth diagram.
5. Scheme of proton transfer reaction instrument with a quadrupole mass spectrometer.
6. Scheme of both types of PTR-MS.
7. Scheme of VOC sampling schedule.
8. Full raw m/z spectra in PTR-TOF Analyzer 4.47 software connected to PTR-TOF-MS.
9. Calibration from certified calibration cylinder in PTR-Viewer 3.2.2 software.
10. Example of precise separation of isoprene and furane in PTR-TOF Analyzer 4.47 software.
11. Transmission curve with equation for other BVOC species calculation.
12. Environmental variables at the time of the eddy covariance campaign on July 15–20, 2014.
13. Diel fluxes of volatile organic compounds at Bílý Kříž experimental forest covered by Norway spruce trees.
14. Relationship between ecosystem gross primary production and a flux of total monoterpenes.
15. Diurnal pattern of assimilated carbon loss from gross primary production due to BVOC emissions.
16. Diurnal fluxes of different monoterpenes in mountain Norway spruce forest and environmental variables.
17. Concentration of α-pinene throughout the day of August 2, 2012.
18. Boundary layer height calculated for August 2, 2012.
19. Diurnal fluxes of monoterpenes corresponding with GPP.
20. Seasonal and out of seasonal MEGAN fluxes.
21. Principal component analysis based on the modelled data by ILTM with other environmental factors.

9.3 HYSPLIT model
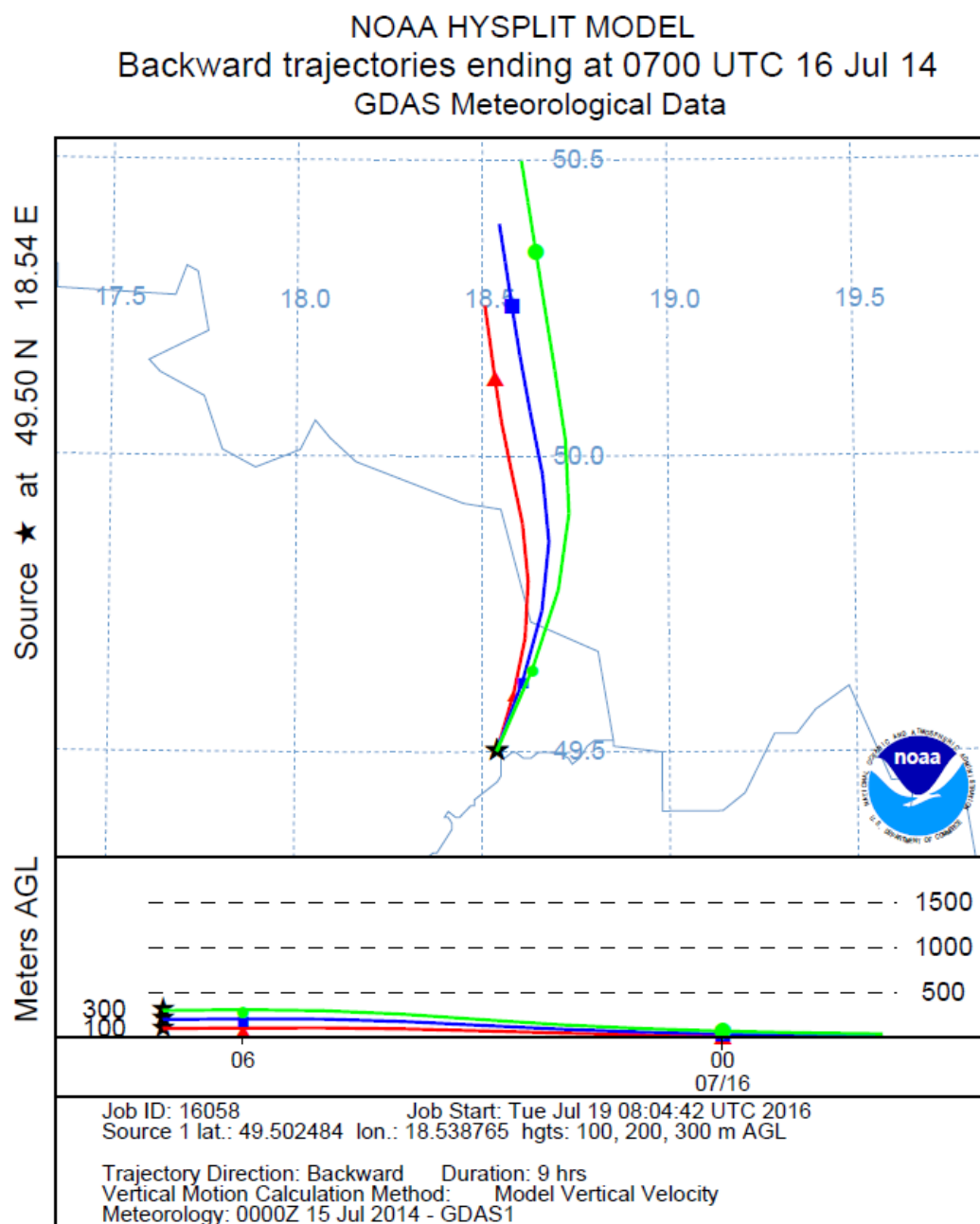

Fig. S1A: Backward trajectories from HYSPLIT model for the Bílý Kříž for the night before highest toluene flux.
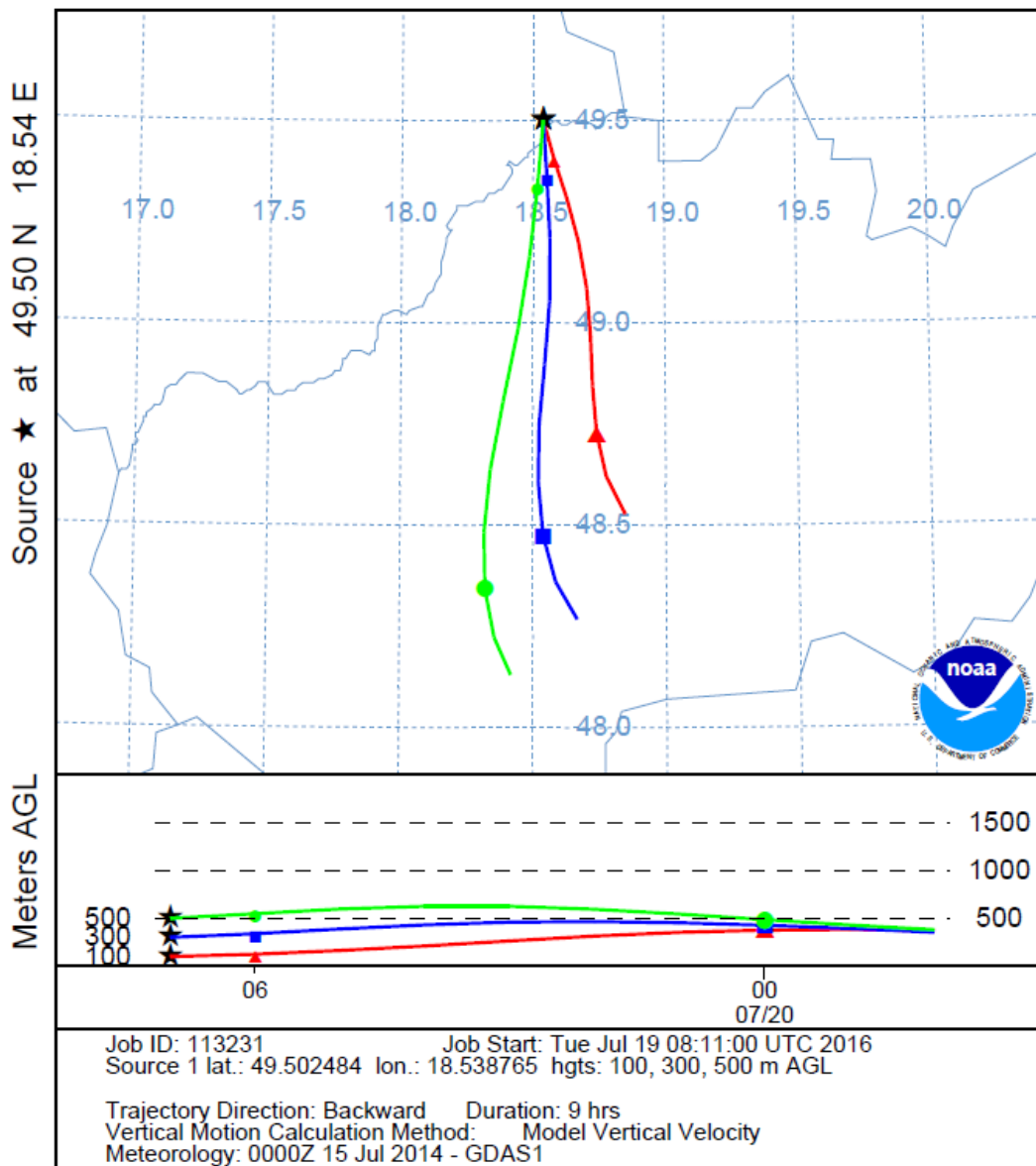
Fig. S1B: Backward trajectories from HYSPLIT model for the Bílý Kříž for the night before lowest toluene flux.